energies

Article

Heat Transfer in Cavities: Configurative Systematic Review

Goutam Saha [1], Ahmed A.Y. Al-Waaly [2], Manosh C. Paul [3] and Suvash C. Saha [4,*]

[1] Department of Mathematics, University of Dhaka, Dhaka 1000, Bangladesh
[2] Department of Mechanical Engineering, Wasit University, Kut 52001, Wasit, Iraq
[3] Systems Power and Energy Research Division, James Watt School of Engineering, University of Glasgow, Glasgow G12 8QQ, UK
[4] School of Mechanical and Mechatronic Engineering, University of Technology Sydney, Sydney, NSW 2006, Australia
* Correspondence: suvash.saha@uts.edu.au

Abstract: This study is a systematic review of research on heat transfer analysis in cavities and aims to provide a comprehensive understanding of flow and heat transfer performance in various kinds of cavities with or without the presence of fins, obstacles, cylinders, and baffles. The study also examines the effects of different forces, such as magnetic force, buoyancy force, and thermophoresis effect on heat transfer in cavities. This study also focuses on different types of fluids, such as air, water, nanofluids, and hybrid nanofluids in cavities. Moreover, this review deals with aspects of flow and heat transfer phenomena for only single-phase flows. It discusses various validation techniques used in numerical studies and the different types and sizes of mesh used by researchers. The study is a comprehensive review of 297 research articles, mostly published since 2000, and covers the current progress in the area of heat transfer analysis in cavities. The literature review in this study shows that cavities with obstacles such as fins and rotating cylinders have a significant impact on enhancing heat transfer. Additionally, it is found that the use of nanofluids and hybrid nanofluids has a greater effect on enhancing heat transfer. Lastly, the study suggests future research directions in the field of heat transfer in cavities. This study's findings have significant implications for a range of areas, including electronic cooling, energy storage systems, solar thermal technologies, and nuclear reactor systems.

Keywords: heat transfer; cavity or enclosure; moving-lid; systematic review; fins; cylinders; blocks; nanofluids; enhancement; degradation; validation; correlations

Citation: Saha, G.; Al-Waaly, A.A.; Paul, M.C.; Saha, S.C. Heat Transfer in Cavities: Configurative Systematic Review. *Energies* **2023**, *16*, 2338. https://doi.org/10.3390/en16052338

Academic Editor: Artur Blaszczuk

Received: 5 February 2023
Revised: 21 February 2023
Accepted: 23 February 2023
Published: 28 February 2023

1. Introduction

The study highlights that enclosed cavities have a broad area of uses, such as electronic cooling, energy storage systems, solar thermal technologies, and nuclear reactor systems. The study has considered various shapes of cavities, including square, rectangular, triangular, trapezoidal, semicircular, hexagonal, U-shaped, etc. Different types of boundary conditions are applied to the walls of the cavities, which affect the flow and thermal behavior inside the cavities. The study considers temperature, heat flux, adiabatic, and isothermal as thermal boundary conditions, such as. On the other hand, the hydraulic boundary conditions considered are fixed, moving, and elastic. Some authors have also applied magnetic field strength to enhance heat transfer or alter buoyancy effects. Different types of fluids have been used in the cavity, including pure water, air, nanofluids, phase change material, porous media, and non-Newtonian fluid.

The main mechanisms of heat transfer in enclosed cavities are natural, forced, or mixed convection. The driving force for natural convection is mainly the buoyancy force (according to Boussinesq approximation), which is caused by the change in fluid density resulting from the applied temperature difference [1,2]. Research has shown that the buoyancy force can destabilize the flow inside the enclosure, but the application of a magnetic field can stabilize it [3]. In addition, the addition of nanoparticles to the liquid inside the cavity can improve its thermal conductivity, heat capacity, and density [4]. Alqaed et al. [5] studied the use of Al_2O_3/H_2O nanofluid with an applied magnetic field. They proved that the presence of nanoparticles contributed to the fluid properties and improved heat transfer. The magnetic field also imposed a specific force (Lorentz force), which opposes the flow inside the cavity and reduces the heat transfer rate. Hatami [6] demonstrated that the presence of fins inside the cavity leads to an increase in vortices (increased mixing) which in turn leads to an enhancement of the rate of heat transfer. The interplay between the magnetic and buoyancy of a hybrid nanofluid Cu-Al_2O_3 inside a cavity leads to a decrease in flow velocity and reduced heat transfer rate [7]. Similar trends in the effect of nanofluid have been observed in different-shaped enclosures such as hexagonal [8], U-shaped [9], and trapezoidal cavities [10].

The moving boundary imposes a shear force on the fluid surface, which can lead to the generation of recirculating eddies that closes the wall of the cavity. The direction of the moving boundary can affect the strength of the shear force and the characteristics of the eddies that are formed. Additionally, for low values of Prandtl numbers, the effects of the moving boundary on the flow can be more pronounced [11]. Adding nanoparticles to a fluid can have a similar effect to that of fixed boundaries in that the fluid's thermal conductivity enhances, and the rate of heat transfer rises. That's because nanoparticles can enhance a fluid's thermal conductivity and improve the rate of heat transfer. Additionally, if the fluid has been subjected to a magnetic field, the presence of the nanoparticles can lead to the generation of Lorentz force that acts in the vertical direction of the magnetic field. This force can suppress circulation and reduce the heat transfer rate. This effect is observed when the nanoparticles are magnetic nanoparticles and the intensity of the magnetic field is raised [12].

The main objective of this work is to conduct a comprehensive literature review of the hydraulic and thermal behaviors inside a cavity. The focus will be on studying the effects of different shapes of the cavity, various applied boundary conditions, and different types of working fluids. The study will compare the effects of using various types of fluids such as air, water, nanofluids, non-Newtonian fluid, etc. The study will also aim to predict correlations for the Nusselt number for different ranges of Rayleigh and Reynolds numbers at different imposed boundary conditions.

The primary conclusion of this literature review is that not many studies have been conducted on phase change materials (PCMs) in cavities, and it is not the focus of our review. Additionally, few studies have considered the use of LES and DNS models to model turbulent flow in cavities. It is also suggested that optimization should be conducted to predict the optimum shape of the cavity. Finally, more studies are needed to investigate the behavior of cavities filled with different types of fluids, such as two immiscible fluids, which can include the interaction between two different regions inside the same enclosure, such as the development of a couple of thermal boundary layer with different fluids separated by different types of partition.

Aim of the Study

A configurative systematic review process is adopted for this study to review the following:

a. Model geometry, flow domain, type, CFD modeling, parameters, and meshing.
b. Different types of validations are used by researchers.
c. Heat transfer behavior for different flow conditions, geometries, boundary conditions, and the presence of different obstacles inside cavities.

2. Methodology

The present review employs a configurative systematic review approach to report on the heat transfer analysis inside different shapes of cavities. A flow chart of the process is provided in Figure 1. The study used various databases such as ScienceDirect, SAGE, ResearchGate, Google Scholar, and Web of Science to conduct the literature search. The search was conducted using key terms such as “Heat transfer”, “Rectangular cavity”, “Square cavity”, “Trapezoidal cavity”, “Triangular cavity”, “Hexagonal cavity”, “Octagonal cavity”, “T-shaped cavity”, “U-shaped cavity”, “C-shaped cavity”, “V-shaped cavity”, “H-shaped cavity”, “Arc-shaped cavity”, “L-shaped cavity”, “M-shaped cavity”, and “Cavity or enclosure”. The article-searching process began on 1 March 2022 and ended on 30 November 2022. One restriction was imposed during the search process, which was that the articles must be written in English.

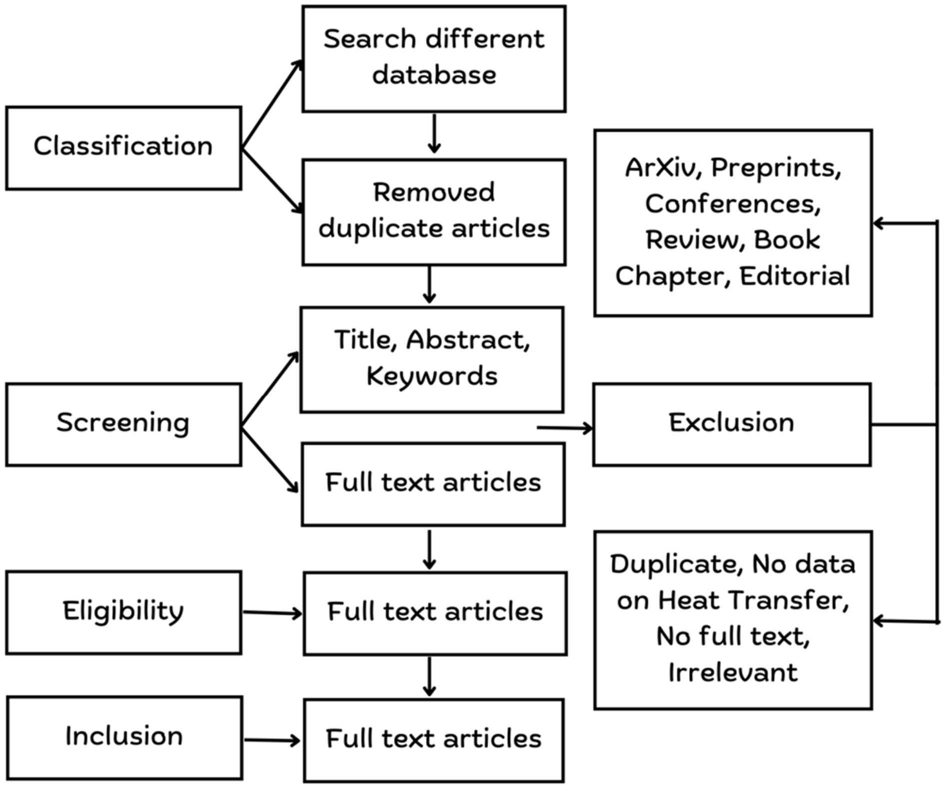

Figure 1. Flow chart of the study selection process.

In addition to the language restriction, the review also excluded articles that were published in ArXiv and Preprints, including conference and review articles. Book chapters, editorials, duplicate articles, articles with no data on heat transfer, articles with no full text available, and other irrelevant articles were also excluded. The authors also reviewed all the references that are connected to their research. Eligible articles were selected by two authors (G.S. & A.A.) who worked independently, screened all the articles, checked the title and abstract as well as assessed the full text. If there was any disagreement regarding the selection, a third author (S.C.S.) discussed the issues that occurred between the first two authors and then resolved the problem. Two authors (G.S. & A.A.) collected some information from the appropriate studies: author’s last name, published year, CFD tools, flow domain or shape of the domain, dimension of the study, algorithms used to solve the problem, parameters and their ranges, type of flow, name of nanofluids or hybrid nanofluids, nanofluids thermo-physical properties, validation data, and results on heat transfer analysis. A total of 2732 articles were considered, 1257 articles were removed because of duplication, 905 articles were removed for other exclusion criteria, and 570 articles were considered which were related to heat transfer analysis inside cavities. After careful screening of the title and abstract, a total of 315 articles were considered for screening of the full text. Finally, 297 articles were selected for the present review study.

The word cloud map in Figure 2 shows the most frequently used words in the abstracts of the selected articles. It appears that the main topics of these articles are natural convection and mixed convection, steady flow, and heat transfer. These articles also focus on numerical experiments, using air and nanofluids as working fluids and utilizing FVM and FEM as numerical methods. The average rate of heat transfer is often presented as a function of the Nusselt number in relation to the Richardson number and Rayleigh number.

Figure 2. Word Cloud Map.

Figure 3 shows that square cavities are the most studied among the different types of cavities, accounting for 47.5% of the total number of articles. The second most studied are triangular cavities, with 14.1% of the articles. Rectangular cavities (12.5%), trapezoidal cavities (7.4%), and cubical cavities (6.1%) are also studied in a significant number of articles. The other types of cavities are studied at much lower percentages, with T-shaped (0.7%) and U-shaped (1%) cavities being the least studied. 2.5% of articles deal with other types of cavities. Square cavities have a wide range of practical applications in various fields, such as aerospace, mechanical engineering, energy, and electronics. They have many advantages, for example, in heat transfer, fluid flow, and electromagnetic waves, and therefore are widely used in many engineering systems and devices. The high percentage of research articles focused on square cavities suggests that they are an important area of study in the field.

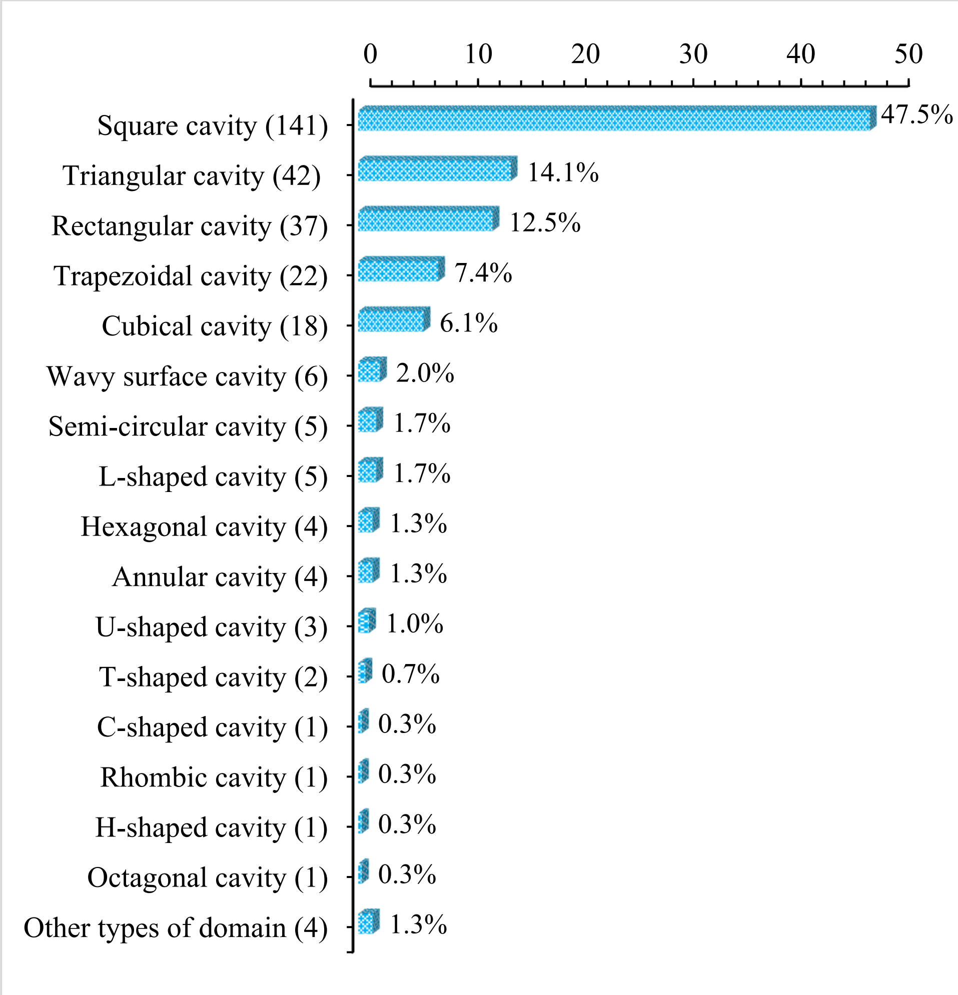

Figure 3. Percentage of different types of cavities.

3. Physical Domain and Mathematical Modelling

3.1. Physical Domain

Many researchers have published a large number of articles over the years to study the hydraulic and thermal performances inside enclosures with various shapes such as square, rectangular, triangular, hexagonal, octagonal, trapezoidal, T-shaped, U-shaped, L-shaped, M-shaped, V-shaped, H-shaped, I-shaped, C-shaped, arc-shaped, and other modified geometries. These studies often introduce obstacles such as fins, cylinders, blocks, rotating blades, etc., inside these physical domains to further complicate the flow patterns and potentially enhance or degrade heat transfer rates Table 1 provides more information about this research.

3.2. Governing Equations

The Navier-Stokes equations describe the motion of a fluid and are widely used in engineering and physics to model different fluid flow phenomena. The equations consist of three main components: the continuity equation, which describes the conservation of mass, the momentum equation, which describes the forces that were applied to the fluid; and the energy equation, which describes the transfer of thermal energy. These equations can be applied to a wide range of fluid types and flow conditions, including incompressible, steady and unsteady flows, Newtonian and non-Newtonian fluids, laminar and turbulent flows, and fluids with different physical properties, such as air, water, and nanofluids. The geometry of the system can also be two or three-dimensional. Solving the Navier-Stokes equations is a challenging task and requires advanced mathematical techniques. In addition to the commonly studied body forces such as gravity and electromagnetic forces, other types of body forces can also play a role in various physical systems. These can include buoyancy forces, Brownian motion of particles, thermophoresis effect, heat generation or absorption, radiation, and the porous medium effect described by the Forchheimer-Brinkman model. These forces can have significant effects on the behavior of the system and must be taken into account when studying and modeling the system. Considering all the assumptions, the three-dimensional Navier-Stokes equation can be presented in the dimensional form (Versteeg [13]):

Continuity equation:

$$\frac{\partial u}{\partial x} + \frac{\partial v}{\partial y} + \frac{\partial w}{\partial z} = 0 \tag{1}$$

u-momentum equation:

$$\frac{\partial u}{\partial t} + u\frac{\partial u}{\partial x} + v\frac{\partial u}{\partial y} + w\frac{\partial u}{\partial z} = -\frac{1}{\rho}\frac{\partial p}{\partial x} + \frac{\mu}{\rho}\left(\frac{\partial^2 u}{\partial x^2} + \frac{\partial^2 u}{\partial y^2} + \frac{\partial^2 u}{\partial z^2}\right) + \text{other terms} \tag{2}$$

v-momentum equation:

$$\frac{\partial v}{\partial t} + u\frac{\partial v}{\partial x} + v\frac{\partial v}{\partial y} + w\frac{\partial v}{\partial z} = -\frac{1}{\rho}\frac{\partial p}{\partial y} + \frac{\mu}{\rho}\left(\frac{\partial^2 v}{\partial x^2} + \frac{\partial^2 v}{\partial y^2} + \frac{\partial^2 v}{\partial z^2}\right) + g\beta(T - T_c)\ \sin\alpha + \text{other terms} \tag{3}$$

w-momentum equation:

$$\frac{\partial w}{\partial t} + u\frac{\partial w}{\partial x} + v\frac{\partial w}{\partial y} + w\frac{\partial w}{\partial z} = -\frac{1}{\rho}\frac{\partial p}{\partial z} + \frac{\mu}{\rho}\left(\frac{\partial^2 w}{\partial x^2} + \frac{\partial^2 w}{\partial y^2} + \frac{\partial^2 w}{\partial z^2}\right) + g\beta(T - T_c)\ \cos\alpha + \text{other terms} \tag{4}$$

Energy equation:

$$\frac{\partial T}{\partial t} + u\frac{\partial T}{\partial x} + v\frac{\partial T}{\partial y} + w\frac{\partial T}{\partial z} = \frac{\kappa}{\rho C_p}\left(\frac{\partial^2 T}{\partial x^2} + \frac{\partial^2 T}{\partial y^2} + \frac{\partial^2 T}{\partial z^2}\right) + \frac{Q}{\rho C_p}(T - T_c) + \text{other terms} \tag{5}$$

Here, $u,\ v,\ w$ are the velocities, p is the pressure, and t is the time. $x,\ y,\ z$ are the Cartesian coordinate systems, T is the temperature, ρ is density, μ is dynamic viscosity, g is gravitational acceleration, α is the angle, and β is the thermal expansion coefficient respectively.

Complex geometries are often encountered in physical systems, and numerical methods are often used to solve the system of equations that govern these systems. Some common numerical techniques used include the finite difference method, finite volume method, finite element method, lattice Boltzmann method, wavelet-based methods such as Coiflet wavelet-homotopy method, fourth-order compact formulation, dual reciprocity boundary element method, spectral element method, large eddy simulation, direct numerical simulation, radial basis function-based partition of unity method, and Improved element-free Galerkin–reduced integration penalty method. These methods can be used to solve a wide range of problems and have been applied in various fields, such as fluid dynamics, heat transfer, and solid mechanics. The problem of heat transfer analysis inside cavities can also be solved using commercial and open-source computational fluid dynamics (CFD) codes or software. Some examples of commonly used commercial CFD codes include COMSOL Multiphysics, ANSYS Fluent, and ADINA Multiphysics. There are also open-source options, such as FlexPDE and OpenFOAM that can be used to solve such problems. These codes and software can be used to perform a wide range of simulations, including heat transfer, fluid flow, and solid mechanics. They are widely used in various fields such as aerospace, automotive, and mechanical engineering and often include a range of features and capabilities such as pre-processing, solving, and post-processing.

3.3. Meshing

In order to solve the system of equations that govern a physical system, the physical domain must be discretized into a smaller number of elements or cells. This process is known as meshing. The Navier-Stokes equations are then solved on these elements or cells to determine the complex flow and thermal field nature. The accuracy of the results largely relies on the number of cells used in the mesh, and smaller cells are preferred to obtain higher accuracy. However, there is a trade-off between the accuracy and computational resources required. It is necessary to find a balance between the computational time and cost and the desired accuracy of the solution.

Researchers have used a variety of meshing techniques to discretize the physical domain and solve the Navier-Stokes equations. These include uniform or non-uniform meshing with rectangular or orthogonal grids, tetrahedral meshing, and non-uniform meshing with triangular grids or clustered grids. The choice of meshing technique depends on the complexity of the geometry, the level of accuracy required, and the computational resources available. It is observed that many researchers have used structured meshes as opposed to unstructured meshes. This is because structured meshes are typically less computationally expensive and require less time for simulation. Additionally, most of the researchers carry out grid-independent tests (GIT) to ensure that the solution does not depend on the grid size. GIT is a vital part of numerical simulations, and it is important that researchers present a clear and detailed discussion of GIT. However, it is also seen that some researchers did not present a clear and detailed discussion on GIT.

A lack of comparison between the performance of uniform meshes and dense non-uniform or fine meshes on flow and temperature fields is often missing in the literature. This can make it difficult for readers to understand the effects of mesh resolution on the solution and the accuracy of the simulation. Comparing the results of simulations using different meshes is an important part of any numerical study, and it is known as a mesh independence study. This is particularly important for complex flow features and can help readers to understand or revisit the study. By comparing the performance of uniform meshes and dense non-uniform or fine meshes, one can determine the optimal mesh resolution for a specific problem and also identify the errors and uncertainties associated with the simulation. Therefore, a clear presentation of the mesh independence study is important for future readers to understand the study and to replicate the simulations.

Table 1. (a): Research performed from 1989 to 2013. (b) The research was performed from 2014 to 2019. (c): Research performed from 2020 to 2023.

(a)					
Ref.	**CFD Methods and Algorithms**	**Flow Domain**	**Dimension, Type of Flow**	**Parameters and Ranges**	**Meshing**
Wee et al. [2]	Experimental, FDM, DADI	Rectangular cavity	2D, unsteady, laminar	$2 \times 10^5 \leq Gr_T \leq 2 \times 10^6$, $10 \leq Gr_C \leq 2 \times 10^5$, $2 \times 10^4 \leq Ra \leq 1.47 \times 10^6$	-
Moallemi & Jjang [11]	FVM, SIMPLIER	Lid-driven square cavity	2D, steady, laminar, non-Newtonian	$10^2 \leq Re \leq 2200$, $0.01 \leq Pr \leq 50$, $0.01 \leq Ri \leq 10$	Non-uniform grid, 42×42
Sasaguchi et al. [14]	Grid generation	Rectangular cavity with cylinders	2D, unsteady, laminar	N/A	Uniform mesh, 31×101, 31×121
Al-Amiri et al. [15]	FEM	Lid-driven cavity with wavy wall	2D, steady, laminar, mixed convection	Pr = 0.71, 1, Gr = 10^4, $0.1 \leq Ri \leq 10$, $0 \leq Am \leq 0.075$, $0 \leq \lambda \leq 3$, Re = 500	-
Saha et al. [16]	FEM	Inclined rectangular enclosure	2D, natural convection, steady, laminar	Pr = 0.71, $10^3 \leq Gr \leq 10^6$, $0.5 \leq A \leq 1.0$, $0 \leq \phi \leq 30$	Non-uniform, six nodded 6394 elements

Table 1. *Cont.*

Saha et al. [17]	FVM	Triangular cavity	2D, natural convection	Pr = 0.71, Gr = 1.33 $\times$ 10^6, 0.5 $\leq$ A $\leq$ 1.0	360 $\times$ 90, 720 $\times$ 160, 270 $\times$ 90 for A = 0.2, 0.5, 1.0
Tiwari & Das [18]	FVM, SIMPLE, QUICK, TDMA	Double lid-driven square cavity	2D, unsteady	Pr = 6.2, 0.1 $\leq$ Ri $\leq$ 10, 10^3 $\leq$ Ra $\leq$ 106, 0 $\leq \chi \leq$ 0.2, Cu-water nanofluid	Uniform grid, 61 $\times$ 61
Saha et al. [19]	FEM	Inclined sinusoidal enclosure	2D, steady, natural convection, laminar	Pr = 0.71, 10^3 $\leq$ Gr $\leq$ 10^6, 0 $\leq \phi \leq$ 45	Non-uniform grid, 5240 elements
Varol et al. [20]	FDM	Triangular cavity	2D, natural convection	0.25 $\leq$ A $\leq$ 1.0, 10^2 $\leq$ Ra $\leq$ 10^3	Uniform grid, 61 $\times$ 61
Chen & Cheng [21]	FVM, SOR	Lid-driven triangular cavity	2D, mixed convection, unsteady, laminar	Pr = 0.71, Re = 100, Gr = 5 $\times$ 10^5	41 $\times$ 41
Noor et al. [22]	FDM, QUICK, RK-4, SOLA	Double lid-driven square cavity	2D, unsteady, laminar	Pr = 0.71, 10 $\leq$ Re $\leq$ 10^3, 1 $\leq \varpi \leq$ 5	Clustered grid, 125 $\times$ 125
Ouertatani et al. [23]	FVM, QUICK. CDS, RBSOR	Double lid-driven cubic cavity	3D, mixed convection, unsteady, laminar	Pr = 0.71, 102 $\leq$ Re $\leq$ 103, 10^{-3} $\leq$ Ri $\leq$ 10	64 $\times$ 64 $\times$ 64
Basak et al. [24]	FEM	Triangular porous cavities	2D, natural convection, steady	10^{-5} $\leq$ Da $\leq$ 10^{-1}, 0.015 $\leq$ Pr $\leq$ 10^3, 10^3 $\leq$ Ra $\leq$ 510^5	20 $\times$ 20–28 $\times$ 28 bi-quadratic elements
Lei & O'Neill [25]	FVM, SIMPLE, CDS, SUR	Square cavity with different corners	2D, unsteady, natural convection	Pr = 6.62, 0 $\leq$ Ra $\leq$ 10^8	16,000 cells
Saha [26]	FEM	Sinusoidal corrugated enclosure	2D, steady	Pr = 0.71, 10^3 $\leq$ Gr $\leq$ 10^6, 0 $\leq$ Ha $\leq$ 10^2	Non-uniform grid, 4928 elements
Saha et al. [27]	FEM	Octagonal enclosure	2D, natural convection, steady, laminar	Pr = 0.71, 7, 20, 50, 10^3 $\leq$ Ra $\leq$ 10^6	Non-uniform, 10,466 elements
Saha et al. [28]	FVM, QUICK, SIMPLE	Triangular enclosure	2D, natural convection, unsteady	Pr = 0.72, 10^4 $\leq$ Ra $\leq$ 7.2 $\times$ 10^6, A = 0.2, 0.5, 1.0	270 $\times$ 90, 320 $\times$ 80, 360 $\times$ 90 for A = 1, 0.5 & 0.2
Saha et al. [29]	FVM, QUICK, SIMPLE	Triangular enclosure	2D, natural convection, unsteady	Pr = 0.72, 7.2 $\times$ 10^3 $\leq$ Ra $\leq$ 1.5 $\times$ 10^6, A = 0.2, 0.5, 1.0	270 $\times$ 90, 320 $\times$ 80, 360 $\times$ 90 for A = 1, 0.5 & 0.2
Saha et al. [30]	FVM, QUICK, SIMPLE	Triangular enclosure	2D, natural convection, unsteady	Pr = 0.72, 5 $\leq$ Ra $\leq$ 1.5 $\times$ 10^7, A = 0.2, 0.5, 1.0	360 $\times$ 120, 320 $\times$ 90, 360 $\times$ 90 for A = 1, 0.5 & 0.2
Sivasankaran et al. [31]	FVM, UDS, CDS, SOR	Lid-driven square cavity	2D, unsteady, laminar, mixed convection	Pr = 0.71, 0 $\leq$ Am $\leq$ 1, 0 $\leq \phi \leq \pi$, 0.1 $\leq$ Ri $\leq$ 102, 102 $\leq$ Re $\leq$ 103	Uniform grid, 81 $\times$ 81
Sivakumar et al. [32]	FVM, SIMPLE, QUICK. CDS	Lid-driven square cavity	2D, mixed convection, unsteady, laminar	Pr = 0.71, 10^2 $\leq$ Re $\leq$ 10^3, 10^2 $\leq$ Gr $\leq$ 10^6, 10^{-2} $\leq$ Ri $\leq$ 10^2	Uniform grid, 81 $\times$ 81
Al-Amiri & Khanafer [33]	ADINA, FSI, FEM, ALE	Lid-driven square cavity	2D, steady, laminar	Pr = 0.71, 10^2 $\leq$ Re, Gr $\leq$ 10^3	Non-uniform mesh, 120 $\times$ 120
Cheng [34]	Compact formulation, SOR, ADI	Lid-driven square cavity	2D, mixed convection	10 $\leq$ Re $\leq$ 2200, 100 $\leq$ Gr $\leq$ 4.86 $\times$ 10^6, 10^{-2} $\leq$ Pr $\leq$ 50, 10^{-2} $\leq$ Ri $\leq$ 10^2	256 $\times$ 256
Nasrin & Parvin [35]	FEM, TFM	Lid-driven square cavity with wavy wall	2D, laminar, steady, mixed convection	30 $\leq$ Re $\leq$ 300, 0 $\leq$ Ha $\leq$ 50, Pr = 0.71, Ra = 10^4	Non-uniform, 37,123 nodes, 5604 elements

Table 1. *Cont.*

Saha [36]	FVM, QUICK	Triangular cavity	2D, unsteady, natural convection	$0.2 \le A \le 1.0$, $5 \le Pr \le 100$, Ra = 10^7	-
Saha [37]	FVM, SIMPLE, QUICK	Triangular cavity	2D, unsteady, natural convection	$0.2 \le A \le 1.0$, $5 \le Pr \le 100$, $5 \times 10^6 \le Ra \le 10^8$	-
Yu et al. [38]	Fluent, FVM, QUICK, SIMPLE	Square cavity	2D, unsteady, natural convection	$10^4 \le Ra \le 10^6$, $0 \le \chi \le 0.04$, CuO–H_2O nanofluid	100 × 100
Al-Farhany & Turan [39]	FVM, SIMPLER	Inclined rectangular porous cavity	2D, unsteady, natural convection	$0 \le \phi \le 85$, $0.1 \le Le \le 10$, $-5 \le N \le 5$, Pr = 4.5, Ra = 5×10^6	-
Arani et al. [40]	FVM, SIMPLIER, TDMA, CDS, UDS	Lid-driven square cavity	2D, mixed convection, laminar, steady	$10^{-3} \le Ri \le 10$, $0 \le \chi \le 0.1$, Gr = 10^2, Re = 10^2 Cu–H_2O nanofluid	Uniform grid. 80 × 80
Basak et al. [41]	FEM	Porous triangular cavities	2D, natural convection, steady	Pr = 0.025, 1000, $10^{-5} \le Da \le 10^{-3}$, Ra = 5×10^5	28 × 28 bi-quadratic elements
Chamkha & Abu-Nada [42]	FVM, CDS, UDS, SOR, SUR	Double lid-driven square cavity	2D, mixed convection, steady, laminar	$0.001 \le Ri \le 10$, $0 \le \chi \le 0.1$, H_2O-Al_2O_3 nanofluid	Uniform grid, 81 × 81
Nasrin & Parvin [43]	FEM	Trapezoidal cavity	2D, free convection, steady, laminar	Ra = 10^5, χ = 0.05, $0.65 \le A \le 2$, $1.47 \le Pr \le 8.81$, Cu–H_2O nanofluid	40,295 nodes, 10,936 elements
Raji et al. [44]	FVM, SIMPLIER	Square cavity with blocks	2D, natural convection, laminar, steady	$10^3 \le Ra \le 10^8$, Pr = 0.71	254 × 254
Saha & Gu [45]	FVM	Triangular enclosure	2D, natural convection, unsteady	Pr = 0.7, Ra = 10^5, A = 0.5	Triangular grid, 8143 nodes
Saha & Gu [46]	FVM	Triangular enclosure	2D, natural convection, unsteady	Pr = 0.72, $5.0 \times 10^4 \le Ra \le 10^6$, A = 0.5	-
Teamah & El-Maghlany [47]	FVM, CDS, GS, TDMA	Square cavity	2D, steady, laminar	$10^3 \le Ra \le 10^7$, $0 \le Ha \le 60$, $0 \le \chi \le 0.06$, $-10 \le q \le 10$, Pr = 6.2, H_2O based Al_2O, Cu, TiO_2 nanofluids	60 × 60
Ahmed et al. [48]	Collocated FVM, UDS, CDS, TDMA	Inclined lid-driven square cavity	2D, mixed convection, laminar, steady	$10^{-2} \le Ri \le 10^2$, $0 \le Am \le 1.0$, $0 \le Ha \le 100$, $0 \le \varphi \le 90$	Uniform grid. 81 × 81
Bhardwaj & Dalal [49]	FDM, QUICK, SOR, CDS	Porous triangular cavity	2D, natural convection, laminar	$10^3 \le Ra \le 10^6$, $10^{-4} \le Da \le 10^{-2}$, Am = 0.05	Orthogonal mesh, 41 × 41
Cho et al. [50]	FVM, SIMPLEC, TDMA	Lid-driven cavity with wavy surfaces	2D, mixed convection, laminar, steady	$0 \le \chi \le 0.1$, $10^{-2} \le Ri \le 10^3$, $10^1 \le Gr \le 10^4$, $0 \le Am \le 0.2$, Pr = 6.2, H_2O based Cu, Al_2O_3, TiO_2 nanofluids	101 × 201
Elsherbiny & Ragab [51]	-	Inclined rectangular cavities	2D, laminar, natural convection	$10^2 \le Ra \le 10^6$, $0.5 \le A \le 5$, $0 \le \varphi \le 180$	Uniform mesh, 42 × 42
Huelsz & Rechtman [52]	LBM	Inclined square cavity	2D, natural convection, laminar, unsteady	Pr = 0.71, $-180 \le \varphi \le 180$, $10^3 \le Ra \le 10^6$	103 × 103

Table 1. *Cont.*

Khanafer & Aithal [53]	ADINA, FEM, NR	Lid-driven square cavity with cylinder	2D, steady, laminar, mixed convection	Pr = 0.7, $10^4 \leq Gr \leq 10^6$, $0.01 \leq Ri \leq 10$, Re = 10^2	Non-uniform grid, 19,520 nodes
Ramakrishna et al. [54]	FEM	Trapezoidal cavities	2D, free convection, laminar	$30 \leq \varphi \leq 90$, Pr = 0.015, 7.2, $10^3 \leq Ra \leq 10^5$	28 × 28 bi-quadratic elements
Sivasankaran et al. [55]	FVM, UDS, CDS	Inclined lid-driven square cavity	2D, unsteady, laminar, mixed convection	Pr = 0.71, $0.01 \leq Ri \leq 10^2$, $0 \leq \varphi \leq 90$	81 × 81
(b)					
Ref.	**CFD Methods and Algorithms**	**Flow Domain**	**Dimension, Type of Flow**	**Parameters and Ranges**	**Meshing**
Sathitamoorthy & Chamkha [56]	FEM	Square cavity with thin partition	2D, natural convection, steady	Pr = 0.7, 100, $10^3 \leq Ra_h \leq 10^5$	20 × 20 elements, 41 × 41 grid points
Abu-Nada & Chamkha [57]	FVM, SOR, SUR, UDS	Lid-driven square cavity with wavy wall	2D, mixed convection, laminar, steady	Pr = 6.57, $0.01 \leq Ri \leq 10^2$, $0 \leq \chi \leq 0.09$, H_2O-CuO nanofluid	Uniform grid, 81 × 81
Ait-Taleb et al. [58]	FDM, SIMPLE, TDMA	Rectangular cavities with tiles	2D, steady, laminar	$8.7 \times 10^3 \leq Ra_h \leq 1.8 \times 10^5$, $4.1 \times 10^5 \leq Ra_H \leq 1.23 \times 10^7$, Pr = 0.71	Non-uniform mesh, 80 × 40
Cheng & Liu [59]	Ansys Fluent, FVM, SOR, ADI	Lid-driven square and rectangular cavities	2D, unsteady	Pr = 0.71, $10^{-2} \leq Ri \leq 10^2$, $0.2 \leq A \leq 5$, $0 \leq \varphi \leq 90$, Re = 10^2	Uniform grid, 640 × 128, 128 × 128, 128 × 640
Cho [60]	FVM, SIMPLE, TDMA	Square cavity with wavy wall	2D, natural convection, laminar, steady	$10^3 \leq Ra \leq 10^6$, $0 \leq \chi \leq 0.04$, Pr = 6.2, H_2O-Al_2O_3 nanofluid	101 × 201
Kalteh et al. [61]	FDM, CDS, SUR	Lid-driven square cavity with block	2D, steady, mixed convection	Gr = 10^2, $0.000625 \leq Ri \leq 4$, $0 \leq \chi \leq 0.05$, H_2O based Al_2O_3, TiO_2, Ag, CuO nanofluids	Regular grid, 80 × 80
Khanafer [62]	ADINA, FEM, FSI, ALE	Lid-driven square cavity	2D, steady, laminar, mixed convection	Pr = 0.7, $10^2 \leq Gr \leq 10^4$, $10^{-4} \leq Ri \leq 1.0$, $10^2 \leq Re \leq 10^3$	Non-uniform, 120 × 120
Muthtamilselvan & Doh [63]	FVM, SIMPLE, QUICK, TDMA	Lid-driven square cavity	2D, steady, mixed convection	$0 \leq Ra_i \leq 10^5$, Pr = 6.2, $10^{-2} \leq Ri \leq 10$, $0 \leq \chi \leq 0.06$, Cu-H_2O nanofluid	Uniform grid, 41 × 41
Ramakrishna et al. [64]	FEM	Porous trapezoidal cavity	2D, natural convection, laminar, steady	$10^{-5} \leq Da \leq 10^{-3}$, $30 \leq \varphi \leq 90$, Pr = 0.015, 10^3	28 × 28 bi-quadratic elements
Ray & Chatterjee [65]	Fluent, FVM	Lid-driven square cavity	2D, steady, mixed convection	$0.1 \leq Ri \leq 10$, $0 \leq Ha \leq 50$, $0 \leq J \leq 5$, Re = 10^2, Pr = 0.71	Non-uniform, 56,126 mixed elements
Saha & Gu [66]	Fluent, FVM	Triangular cavity	2D, unsteady, natural convection	Pr = 0.72, $10^5 \leq Ra \leq 10^8$, A = 0.2, 0.5, 1.0	Non-uniform grid, 400 × 100
Xu & Saha [67]	FVM, SIMPLE, QUICK	Square cavity with fin	2D, unsteady, natural convection	Pr = 0.71, $10^5 \leq Ra \leq 10^9$	Non-uniform grid, 198 × 198
Cui et al. [68]	Fluent, FVM, SIMPLE, QUICK	Triangular cavity	3D, natural convection, unsteady	A = 0.5, Pr = 6.98, Ra = 2.08×10^6	Non-uniform grid, 100 × 66× 45
Elsherbiny & Ismail [69]	FDM, TDMA, CDS	Inclined rectangular cavities	2D, laminar, steady	Pr = 0.71, $0 \leq \varphi \leq 180$, $10^3 \leq Ra \leq 10^6$, A = 1, 5, 10	Uniform grid, 42 × 42
Elsherbiny & Ragab [51]	-	Inclined rectangular cavities	2D, laminar, natural convection	Pr = 0.71, $0 \leq \varphi \leq 180$, $10^2 \leq Ra \leq 10^6$	Uniform mesh, 42 × 42

Table 1. *Cont.*

Groşan et al. [70]	FDM, CDS	Porous square cavity	2D, steady, natural convection	Ra = 10, 100, Le = 1, 10, H_2O, aluminum foam, carbon nanotubes	227 × 227
Moumni et al. [71]	FVM, AB, QUICK, CDS, Euler, RBSOR	Double lid-driven square cavity	2D, unsteady, laminar	$1 \leq Re \leq 10^2$, Pr = 6.2, $10^{-2} \leq Ri \leq 20$, $0 \leq \chi \leq 0.2$, H_2O based Cu, Ag, Al_2O_3, TiO_2 nanofluids	Uniform grid, 120 × 120
Saha & Gu [72]	Fluent, FVM, QUICK	Triangular enclosure	2D, natural convection, steady, unsteady	$10^5 \leq Ra \leq 10^6$, Pr = 0.72, A = 0.2, 0.5, 1.0	Non-uniform grid
Sheremet & Pop [73]	FDM, CDS, SOR	Lid-driven square cavity	2D, unsteady, laminar, mixed convection	Re = 10^2, Pr = 6.26, $10 \leq Gr \leq 10^5$, $10 \leq Le \leq 10^4$, N, N_b, N_t = 0.1 to 0.4	Uniform grid, 400 × 400
Sojoudi et al. [74]	Fluent, FVM	Triangular cavity	2D, natural convection, unsteady	$10^3 \leq Ra \leq 10^6$, $0.2 \leq A \leq 1$, Pr = 0.72	15,700 triangular elements
Armaghani et al. [75]	FVM, SIMPLE	L-shaped cavity with baffle	2D, steady, natural convection	Pr = 0.71, $10^4 \leq Ra \leq 10^6$, $0.1 \leq A \leq 0.7$, $0 \leq B_f \leq 0.3$, $0 \leq \chi \leq 0.04$, Al_2O_3-H_2O nanofluid	Uniform grid, 100 × 100
Jmai et al. [76]	FVM, QUICK, SOR, multigrid	Double lid-driven square cavity	2D, unsteady, laminar, mixed convection	$10^{-2} \leq Ri \leq 10^2$, $0 \leq \chi \leq 0.1$, Cu–H_2O nanofluid	Non-uniform grid, 64 × 64
Kareem et al. [77]	Fluent, URANS, LES, FVM, SIMPLE	Cubic lid-driven cavity	3D, unsteady, mixed convection, turbulent	Re = 5000, 10,000, 15,000 and 30,000	Structured, non-uniform, 1,699,200 grids
Kareem et al. [78]	FVM, UDS, SIMPLE	Lid-driven trapezoidal cavity	2D, mixed convection	$0 \leq \chi \leq 0.04$, $0.1 \leq Ri \leq 10$, $10^2 \leq Re \leq 1200$, $0 \leq \varphi \leq 60$, $0.5 \leq A \leq 2$, H_2O based Al_2O_3, CuO, SiO_2, TiO_2 nanofluids	Unstructured, non-uniform 5470 grids
Mamourian et al. [79]	FVM, SIMPLE	Lid-driven square cavity	2D, steady, laminar, Mixed convection	$10^{-2} \leq Ri \leq 10^2$, $0 \leq \chi \leq 0.1$, Gr = 10^2, Am = 0.25, Cu–H_2O nanofluid	Structured non-uniform, 101 × 201
Mejri et al. [80]	LBM	Triangular cavity	2D, natural convection, laminar	$10^3 \leq Ra \leq 10^6$, $0 \leq \varphi \leq 315$, Ma = 0.1	-
Rahmati et al. [81]	LBM	Double lid-driven cavity	2D, mixed convection, laminar, steady	Gr = 100, Pr = 6.57, $10^{-2} \leq Ri \leq 10^2$, $0 \leq \chi \leq 0.06$, Cu-H_2O nanofluid	100 × 100
Rashad et al. [12]	FVM, ADI, SIMPLE, UDS, CDS	Lid-driven square cavity	2D, mixed convection, laminar	$0 \leq Ha \leq 100$, $10^{-3} \leq Ri \leq 10$, $0 \leq \chi \leq 0.01$, Cu-H_2O nanofluid	Uniform grid, 81 × 81
Selimefendigil & Öztop [82]	FEM, ALE	Lid-driven inclined square cavity	2D, steady	$10^{-2} \leq Ri \leq 10^2$, $0 \leq \chi \leq 0.05$, $10^3 \leq Ra_i \leq 10^6$, $0 \leq Ha \leq 50$, $0 \leq \varphi \leq 90$, $5\times 10^2 \leq E \leq 10^6$, CuO-$H_2O$ nanofluid	Non-uniform mesh, 10,916 nodes
Selimefendigil & Öztop [83]	FEM, FSI, ALE	Triangular cavity	2D, natural convection, steady	$10^4 \leq Ra \leq 10^6$, $10^4 \leq Ra_i \leq 10^7$, $0 \leq Ha \leq 40$, $0 \leq \varphi \leq 90$, Pr = 7.1, $5 \times 10^2 \leq E \leq 10^5$	-

Table 1. *Cont.*

Selimefendigil et al. [84]	FEM, NR	Lid-driven square cavity	2D, Mixed convection	$10^{-2} \leq Ri \leq 10^2$, $0 \leq Ha \leq 50$, $0 \leq \varphi \leq 90$, $0 \leq \chi \leq 0.05$, CuO-H_2O nanofluid	Non-uniform,. 17,408 elements
Sojoudi et al. [85]	FVM, QUICK, SIMPLE	Triangular cavity	2D, unsteady, natural convection	$10^3 \leq Ra \leq 10^6$, $0.2 \leq A \leq 1.0$, Pr = 0.72	15,600 triangular elements
Sojoudi et al. [86]	FVM, QUICK, SIMPLE	Triangular cavity	2D, unsteady, natural convection	$10^3 \leq Ra \leq 10^6$, $0.2 \leq A \leq 1.0$, Pr = 0.71	360×75, 360×90, 360×120 for A = 0.2, 0.5, 1
Aparna & Seetharamu [87]	FEM	Porous trapezoidal cavity	2D, natural convection	$10^0 \leq Ra \leq 2000$	41×41
Alsabery et al. [88]	COMSOL, FEM	Trapezoidal cavity	2D, unsteady, non-Newtonian, laminar	$10^4 \leq Ra \leq 10^6$, $0 \leq \chi \leq 0.2$, $0.1 \leq Pr \leq 10^3$, $0 \leq \varphi \leq 21.8$, H_2O based TiO_2, Cu, Al_2O_3, Ag nanofluids	Non-uniform, 4690 elements
Al-Weheibi et al. [89]	COMSOL, FEM	Trapezoidal enclosure	2D, natural convection, unsteady, laminar	$10^3 \leq Ra \leq 10^6$, $0 \leq \chi \leq 0.1$, $0.25 \leq A \leq 1.0$	6-noded 403,388 elements, 204,436 grids
Balla et al. [90]	FEM	Inclined porous square cavity	2D, free convection, laminar	$0.01 \leq \chi \leq 0.3$, $10^1 \leq Ra \leq 10^3$, $0 \leq M \leq 10$, $0 \leq \varphi \leq 90$, H_2O based TiO_2, Cu, Al_2O_3, SiO_2 nanofluids	6-noded triangular grid, 5000 elements, 2601 nodes
Cui et al. [91]	FVM	Prismatic enclosure	3D, unsteady, natural convection	$10^0 \leq Ra \leq 10^6$, Pr = 0.71	Non-uniform grid, $100 \times 66 \times 45$
Das et al. [92]	FEM	Square & triangular cavities	2D, steady, laminar	Pr = 0.7, $10^3 \leq Ra \leq 10^5$	34×34 biquadratic elements
Gangawane [93]	Fluent, FVM, SIMPLE, QUICK	Lid-driven cavity with triangular block	2D, steady, laminar, mixed convection	$1 \leq Re \leq 10^3$, $0 \leq Gr \leq 10^5$, Pr = 1, 50, 10^2, b = 10%, 20%, 30%	Unstructured, non-uniform, 26,318 nodes, 9126 elements
Ghalambaz et al. [94]	FEM, FSI, ALE	Square cavity with oscillating elastic fin	2D, natural convection, laminar, unsteady	Pr = 0.7, $10^4 \leq Ra \leq 10^7$, $10^{-3} \leq Am \leq 0.1$, $1 \leq Tr \leq 10^3$, $10^8 \leq E \leq 10^{13}$	27,131 domain elements, 1022 boundary elements
Gibanov et al. [95]	FDM	Lid-driven square cavity with block	2D, steady, laminar, mixed convection	$10^{-2} \leq Ri \leq 10$, $0 \leq \chi \leq 0.05$, Re = 10^2, Pr = 6.82, Al_2O_3-H_2O nanofluid	Uniform grid, 200×200
Gibanov et al. [96]	FDM	Lid-driven inclined square cavity	2D, unsteady, mixed convection	Ri =1, Re = 10^2, Pr = 6.26, Da = 10^{-7}, 10^{-3}, $0 \leq Ha \leq 10^2$, $0 \leq \chi \leq 0.05$, $0 \leq \varphi \leq \pi$, ferrofluid	Uniform grid, 200×200
Hammami et al. [97]	FVM, QUICK, RBSOR	Double lid-driven cubic cavity with cylinder	3D, unsteady	$10^2 \leq Re \leq 1500$, Pr	Staggered grid non-uniform, $80 \times 80 \times 80$
Hatami [6]	FEM, FlexPDE	Rectangular cavity with heated fins	2D, steady	$0.03 \leq \chi \leq 0.09$, H_2O based TiO_2, Al_2O_3 nanofluids	-
Hatami et al. [98]	FEM, RSM, FlexPDE	Lid-driven T-shaped porous cavity	2D, steady, mixed convection	Ri = 0.1, Re = 50, Da = 0.001, H_2O based TiO_2, Cu, Al_2O_3 nanofluids	-
Hussain et al. [99]	FEM, GE, CN	Double lid-driven square cavity	2D, steady, mixed convection	$1 \leq Re10^2$, $0 \leq \varphi \leq 45$, $0.01 \leq Ri \leq 10$, $0 \leq \chi \leq 0.04$, Al_2O_3-H_2O nanofluid	Uniform grid, 65,536 elements

Table 1. *Cont.*

Javed et al. [100]	FEM	Trapezoidal porous cavities	2D, free convection, steady	Pr = 6.2, $10^{-5} \leq$ Da $\leq 10^{-3}$, $10^5 \leq$ Ra $\leq 10^7$, $0 \leq$ Ha ≤ 60, $0 \leq \chi \leq 0.03$, Cu-H_2O nanofluid	6 noded 704 elements, 1000 grids
Kareem & Gao [101]	Fluent, LES, URANS, SIMPLEC, QUICK	Lid-driven cubic cavity with cylinder	3D, unsteady, mixed convection, turbulent	Pr, Re = 5000, 10,000, 15,000, 30,000, $0 \leq \Omega \leq 10$	Structured, non-uniform cells, 929,160 elements
Khanafer & Aithal [102]	ADINA, FEM	Lid-driven square cavity with cylinder	2D, steady, laminar, mixed convection	$0.01 \leq$ Ri ≤ 10, Re = 100, $-10 \leq \omega \leq 10$	150 × 150
Khatamifar et al. [103]	DNS, SIMPLE, QUICK	Rectangular cavity with partition	2D, natural convection, unsteady	$10^5 \leq$ Ra $\leq 10^9$, Pr = 0.71, $0.05 \leq$ Tp ≤ 0.2	Non-uniform mesh, 300 × 250
Mojumder et al. [104]	FEM	Lid-driven L-shaped cavity	2D, mixed convection, laminar, steady	$1 \leq$ Re ≤ 100, $10^3 \leq$ Gr $\leq 10^5$, $10^{-5} \leq$ Da $\leq 10^{-3}$, Pr = 6.2	Triangular mesh, 4452 elements
Selimefendigil et al. [105]	FEM, ALE, FSI	Lid-driven square cavity	2D, steady	$0.01 \leq$ Ri ≤ 5, $0 \leq$ Ha ≤ 50, $10^2 \leq$ Re $\leq 10^3$, CuO-H_2O nanofluid	Triangular elements, 17,224 grids
Selimefendigil et al. [106]	FEM, ALE, NR	Lid-driven Trapezoidal cavity with cylinder	3D, steady, laminar, mixed convection	$0.5 \leq$ Ri ≤ 50, $0 \leq \varphi \leq 20$, $0 \leq \chi \leq 0.04$, $10^3 \leq$ E $\leq 10^5$, CuO-H_2O nanofluid	Tetrahedral elements
Selimefendigil & Öztop [107]	FEM, FSI, ALE	Lid-driven triangular cavity	2D, mixed convection, steady	$0.05 \leq$ Ri ≤ 50, $0 \leq \chi \leq 0.04$, Pr = 6.8, $10^4 \leq Ra_I \leq 10^8$, $500 \leq$ E $\leq 10^5$, H_2O–CuO nanofluid	Non-uniform grid, 26,306 elements
Sheremet et al. [108]	FDM	Triangular cavities	2D, natural convection	Pr = 0.7, $10^4 \leq$ Ra $\leq 2 \times 10^5$, $10^2 \leq$ Le $\leq 10^4$, $0 \leq$ N ≤ 5, $N_b = N_t = 0.1$	Uniform grid, 300 × 150
Yu et al. [3]	FDM, UCS, TVD, RK	Rectangular cavity	2D, unsteady, laminar	Pr = 0.025, A = 2, $0 \leq$ Ha ≤ 50, $0 \leq$ Le ≤ 20	Uniform grid, 41 × 81
Aghakhani et al. [109]	FDLBM	C-shaped cavity	2D, laminar, non-Newtonian	$10^3 \leq$ Ra $\leq 10^5$, $0 \leq$ Ha ≤ 40, $0.2 \leq$ A ≤ 0.6	160 × 160
Astanina et al. [110]	FDM	Lid-driven square porous cavity	2D, steady, mixed convection	$0.01 \leq$ Ri ≤ 10, $0 \leq \chi \leq 0.04$, $10^{-7} \leq$ Da $\leq 10^{-3}$, $Da_2 = 10^{-5}$, Re = 102, Pr = 6.82, H_2O–Al_2O_3 nanofluid	Uniform grid, 200 × 200
Alsabery et al. [111]	FEM, FEA, NR	Double lid-driven square cavity with block	2D, steady, laminar, mixed convection	$1 \leq$ Re ≤ 500, $10^{-2} \leq$ Ri $\leq 10^2$, $0 \leq \chi \leq 0.04$, Pr = 4.623, Le = 3.5×10^5, Sc = 3.55×10^4, H_2O–Al_2O_3 nanofluid	Uniform triangular grid, 12,232 grids
Balootaki et al. [112]	LBM-BGK	Lid-driven rectangular cavity with block	2D, mixed convection	$10^{-2} \leq$ Ri ≤ 50, Re = 100, Pr = 0.7	450 × 150
Bhowmick et al. [113]	FEM, SIMPLE, QUICK	V-shaped cavity	2D, natural convection	$2.26 \times 10^5 \leq$ Ra $\leq 2.26 \times 10^9$, $0.1 \leq$ A ≤ 1.0, Pr = 6.63	Non-uniform, 800 × 150
Cho [114]	FVM, TDMA, SIMPLE	Lid-driven cavity with wavy surface	2D, steady, laminar, mixed convection	$10^{-2} \leq$ Ri $\leq 10^2$, $0 \leq \chi \leq 0.04$, $1 \leq$ Re ≤ 200, Pr = 6.2, $0 \leq$ Am ≤ 0.6, H_2O–Cu nanofluid	101 × 1001

Table 1. *Cont.*

Gangawane et al. [115]	Fluent, FVM, SIMPLE, QUICK	Lid-driven square cavity with block	2D, steady, laminar, mixed convection	Ri= 0.01, 1, 10, Pr= 1, $1 \leq Re \leq 10^3$	Unstructured, 17,874 nodes, 17,598 elements
Gibanov et al. [116]	FDM	Lid-driven square cavity	2D, mixed convection, laminar, unsteady	$10^{-2} \leq Ri \leq 10$, $0 \leq \chi \leq 0.05$, $1.0 \leq K \leq 20.0$, Re = 100, Pr = 6.82, $H_2O–Al_2O_3$ nanofluid	Uniform grid, 100 × 100
Hussain et al. [117]	FEM, CN, GE	Double lid-driven square cavity	2D, laminar, unsteady, mixed convection	$0 \leq \chi \leq 0.04$, $10^{-2} \leq Ri \leq 10$, $0 \leq Ha \leq 10^2$, $0 \leq \varphi \leq 90$, $H_2O–Al_2O_3$ nanofluid	Non-uniform triangular grid, 65,536 elements
Javed & Siddiqui [118]	FEM	Square cavity with square blockage	2D, free convection, steady, laminar	$10^5 \leq Ra \leq 10^7$, Pr = 0.062, $0 \leq \chi \leq 0.06$, $0 \leq Ha \leq 60$, H_2O–Cobalt ferrofluid	Non-uniform, 6-noded 1776 elements
Karbasifar et al. [119]	SIMPLEC	Lid-driven cubic cavity with cylinder	3D, laminar, steady, mixed convection	$10^{-2} \leq Ri \leq 10^2$, χ = 0, 0.1%, 0.2%, φ = 0, 15, 45, $H_2O–Al_2O_3$ nanofluid	-
Kareem & Gao [120]	Fluent, URANS, SIMPLEC, QUICK	Lid-driven Cubical cavity with cylinder	3D, mixed convection, unsteady, turbulent	$5000 \leq Re \leq 10^4$, $-5 \leq \Omega \leq 5$, SiO_2-H_2O nanofluid	929,160 grids
Mikhailenko et al. [121]	FDM, CDS, Thomas, SOR	Rotating square cavity with obstacle	2D, laminar, unsteady	Pr = 0.7, Ra = 10^5, $0 \leq \varphi \leq 180$, $0 \leq Ta \leq 10^6$, $0.1 \leq Os \leq 1.0$, $0.0 \leq \varepsilon \leq 0.9$	101 × 101
Oglakkaya & Bozkaya [122]	DRBEM	Lid-driven square cavity	2D, mixed convection, unsteady, laminar	Pr = 0.71, Re = 10^2, Am = 0.05, Ha = 0, 25, 50, $0 \leq \varphi \leq 90$, J = 0, 1, 3, 5, $10^3 \leq Ra \leq 10^5$	400 grids
Razera et al. [123]	Fluent, FVM, SIMPLEC	Lid-driven square cavity	2D, steady, laminar, mixed convection	$10^1 \leq Re \leq 10^3$, $10^3 \leq Ra \leq 10^6$, Pr = 0.71	Non-uniform, 33,248 volumes
Selimefendigil & Öztop [124]	FEM, COBYLA	Lid-driven trapezoidal cavity	2D, mixed convection	$0.01 \leq Ri \leq 25$, $0 \leq Ha \leq 40$, $0 \leq \varphi \leq 90$, $0 \leq \chi \leq 0.03$, $H_2O–Al_2O_3$ nanofluid	6282, 4685 and 3691 elements for different φ
Sheikholeslami [125]	LBM	Lid-driven square cavity with hot sphere	3D, forced convection	$10^{-3} \leq Da \leq 10^2$, $30 \leq Re \leq 180$, $0 \leq Ha \leq 40$, $H_2O–Al_2O_3$ nanofluid	81 × 81 × 81
Sheremet et al. [126]	FDM	Porous square vented cavity	2D, mixed convection, unsteady	$10^4 \leq Ra \leq 10^6$, Nb = Nt = 10^{-6}, $10^{-5} \leq Da \leq 10^{-2}$, $50 \leq Re \leq 300$, Pr = 6.82, Le = 10^3, N = 1, $H_2O–Al_2O_3$ nanofluid	Uniform grid, 201 × 201
Taghizadeh & Asaditaheri [127]	OpenFOAM, FVM. SIMPLE	Lid-driven square cavity with cylinder	2D, laminar, mixed convection	$0.01 \leq Ri \leq 10$, $10^{-5} \leq Da \leq 10^{-2}$, $0 \leq \varphi \leq 90$, Re = 100, Pr = 0.7	Non-uniform, 11,200
Zhai et al. [128]	FVM, SIMPLE, QUICK	Triangular Roof	2D, unsteady, natural convection	$10^4 \leq Ra \leq 10^7$, $0.1 \leq A \leq 1.0$, Pr = 0.71	Non-uniform mesh, 600 × 600
Zhou et al. [129]	LBM, OpenMP	Double lid-driven cubic cavity	3D, mixed convection, laminar, unsteady	$0.1 \leq Ri \leq 10^2$, $0 \leq \chi \leq 0.04$, $H_2O–Al_2O_3$ nanofluid	101 × 101 × 101
Alnaqi et al. [130]	FDM	Square cavity with a fin	2D, laminar, steady	$0 \leq Ha \leq 60$, $10^3 \leq Ra \leq 10^6$, $0 \leq Rd \leq 3$, $0 \leq \chi \leq 0.06$, $H_2O–Al_2O_3$ nanofluid	Uniform grid. 120 × 120

Table 1. *Cont.*

Al-Rashed et al. [131]	FVM, SIMPLEC	Inclined lid-driven cubical cavity	3D, steady, mixed convection, laminar	Re, Gr, Pr, $1 \leq Ri \leq 10^2$, $0 \leq \varphi \leq 45$, H_2O–Al_2O_3 nanofluid	-
Barnoon et al. [132]	FVM, SIMPLE	Lid-driven square cavity with cylinders	2D, steady, laminar, mixed convection	$0 \leq Ha \leq 30$, $1 \leq Ri \leq 10^2$, $0 \leq \varphi \leq 90$, $0.01 \leq \chi \leq 0.03$, H_2O–Al_2O_3 nanofluid	Non-uniform grid, 19,297 elements
Bhowmick et al. [133]	Fluent, FVM, SIMPLE	V-shaped triangular cavity	2D, natural convection, unsteady	$1 \leq Ra \leq 10^8$, A = 0.5, Pr = 0.71	800 × 150
Cho [134]	FVM, SIMPLE, TDMA	Lid-driven cavity with wavy wall	2D, laminar, mixed convection	$1 \leq Re \leq 300$, $0 \leq Ha \leq 50$, $10^{-2} \leq Re \leq 10^2$, $0 \leq Am \leq 0.7$, $0 \leq \chi \leq 0.04$, $0 \leq \varphi \leq 360$, Cu-H_2O nanofluid	Non-uniform grid, 101 × 1001
Cui et al. [135]	FVM	Prismatic enclosure	3D, unsteady, natural convection	$10^0 \leq Ra \leq 10^7$, Pr = 0.71, $0.1 \leq A \leq 1.5$	Non-uniform mesh, 138 × 42 × 51
Hadavand et al. [136]	FVM, SIMPLEC	Lid-driven sim-circular cavity	2D, mixed convection, laminar, steady	$1 \leq Ri \leq 10$, $\varphi = -90$ to 90, $0 \leq \chi \leq 0.06$, Ag-H_2O nanofluid	Unorganized triangular grid, 44,896 grids
Hamid et al. [137]	FEM	Trapezoidal cavity	2D, steady, non-Newtonian, natural convection, laminar	$10^4 \leq Ra \leq 10^{5.5}$, Pr = 20	-
Jiang & Zhou [4]	FVM, QUICK, CDS, PISO	Rectangular cavity	2D, steady, laminar	$0 \leq \chi \leq 0.25$, d_p = 13, 36, 50 nm, distilled H_2O-Al_2O_3, PGW-ZnO nanofluids	Non-uniform orthogonal grid, 200 × 50
Karatas & Derbentli [138]	Experimental research	Rectangular cavity	3D, unsteady	$4.5 \times 10^3 \leq Rai \leq 1.13 \times 10^8$, A = 1, 2.09, 3, 4, 5, 6	-
Lamarti et al. [139]	LBM	Lid-driven square cavity	2D, mixed convection, laminar	Pr = 0.71, $10^2 \leq Re \leq 10^3$, $10^2 \leq Gr \leq 10^6$, $1 \leq \omega \leq 5$	100 × 100
Louaraychi et al. [140]	FVM, SIMPLER, TDMA	Double lid-driven rectangular cavity	2D, unsteady, mixed convection	$1 \leq Ra \leq 10^7$, $0.1 \leq Pe \leq 500$, A = 24	Uniform grid, 381 × 121
Mohebbi et al. [141]	LBM	Γ-shaped enclosure with obstacle	2D, natural convection, steady, laminar	$10^3 \leq Ra \leq 10^6$, $0 \leq \chi \leq 0.05$, $0.2 \leq A \leq 0.6$, Al_2O_3-H_2O nanofluid	100 × 100
Selimefendigil & Öztop [142]	FEM, ALE, NR	Lid-driven L-shaped cavity	2D, steady, mixed convection	$0.03 \leq Ri \leq 30$, $0 \leq \chi \leq 180$, $10^4 \leq Ra_I \leq 10^6$, $0 \leq Ha \leq 50$, CuO-H_2O nanofluid	Non-uniform, 19,112 elements
			(c)		
Ref.	**CFD Methods and Algorithms**	**Flow Domain**	**Dimension, Type of Flow**	**Parameters and Ranges**	**Meshing**
Abu-Hamdeh et al. [143]	FVM, SIMPLE, CDS, UDS, TDMA	Lid-driven porous square open cavity	2D, mixed convection, steady	$10^2 \leq Re \leq 10^3$, $10^{-3} \leq Da \leq 0.1$, $10^3 \leq Gr \leq 10^5$	Staggered grid, 48 × 48
Afrand et al. [144]	SIMPLE	Triangular cavity	2D, free convection, laminar, steady	$10^4 \leq Ra \leq 10^6$, $0 \leq Ha \leq 40$, $0 \leq \varphi \leq 90$, $0 \leq \chi \leq 0.06$, Al_2O_3-H_2O nanofluid	Staggered grid
Alsabery et al. [145]	FEM	Lid-driven square cavity	2D, mixed convection, steady, laminar	$1 \leq Re \leq 500$, $0.01 \leq Ri \leq 100$, $0 \leq Ha \leq 50$, $0 \leq \phi \leq 0.04$, Al_2O_3-H_2O nanofluid	Triangular grid, 6402 elements

Table 1. *Cont.*

Alsabery et al. [146]	FEM	Lid-driven cubic cavity with cylinder	3D, mixed convection, steady	Re = 10, 100, Pr = 4.623, $10^{-2} \leq Ri \leq 10^2$, $0 \leq \chi \leq 0.04$, Le = 3.5×10^5, Sc = 3.55×10^4, Al_2O_3-H_2O nanofluid	Non-uniform triangular grid, 175,778 elements
Bilal et al. [147]	FEM	Triangular cavity with cylinder	2D, laminar, steady, free convection	$10^3 \leq Ra \leq 10^6$, $0.2 \leq Pr \leq 7$	Hybrid grid
Cho [148]	FVM, SIMPLE, TDMA	Square cavity with wavy walls	2D, natural convection, steady, laminar	Pr = 6.2, $10^2 \leq Ra \leq 10^6$, $10^{-6} \leq Da \leq 10^{-2}$, $0 \leq \chi \leq 0.04$, Cu-H_2O nanofluid	101×1001
Ganesh et al. [149]	FEM	Square Cavity with different obstacles	2D, steady, laminar	$10^3 \leq Ra \leq 10^6$, $0 \leq \chi \leq 0.08$, $10^3 \leq Ra_E \leq 10^6$, $10^3 \leq Ra_I \leq 10^5$ Al_2O_3-H_2O/Ethylene Glycol nanofluid	Circular: 6979 elements, Square: 21,916 elements, Triangular: 19,431 elements
Haq et al. [150]	FEM	Lid-driven hexagonal cavity with obstacle	2D, steady	$200 \leq Re \leq 500$, Pr = 6.2, $10^{-6} \leq Ri \leq 1$, $0 \leq Ha \leq 20$, SWCNT-H_2O nanofluid	Non-uniform triangular elements
Khan et al. [151]	FEM	Porous trapezoidal cavity	2D	Pr = 6.2, $10^2 \leq Ha \leq 10^4$, $10^4 \leq Ra \leq 10^5$, $0 \leq \chi \leq 0.2\%$, Fe_3O_4-H_2O ferrofluid	-
Li et al. [152]	FDLBM	Triangular enclosure	2D, laminar, non-Newtonian, steady	$10^3 \leq Ra \leq 10^5$, $0 \leq Ha \leq 60$, $0 \leq \varphi \leq 90$	160×160 or 19,600 nodes
Liu & Huang [153]	DNS, QUICK, SIMPLE, CDS	Rectangular cavities with or without fins	2D, unsteady, turbulent	$1.15 \times 108 \leq Ra \leq 3.68 \times 10^9$	Non-uniform grid, 400×360 cells
Rammane et al. [154]	TS, MLS, NR, HO-MFA	Lid-driven square cavity	2D, steady	$10^2 \leq Re \leq 2 \times 10^4$	Mesh free
Saha et al. [155]	FVM, SIMPLE, QUICK	Triangular enclosure	2D, unsteady, natural convection	Pr = 0.72, $10^5 \leq Ra \leq 10^9$, $0.2 \leq A \leq 1.0$	380×80, 380×100, 380×160 for A = 0.2, 0.5, 1
Selimefendigil & Öztop [156]	FVM, QUICK, SIMPLE	U-shaped corrugated cavity	2D, forced convection, laminar, steady	$10^2 \leq Re \leq 10^3$, $0 \leq Ha \leq 50$, $10^{-4} \leq Da \leq 5 \times 10^{-2}$, CNT-$H_2O$ nanofluid	Non-uniform grid, 38,874 grids
Soomro et al. [157]	FEM	Lid-driven Triangular cavity with obstacle	2D, mixed convection, laminar, steady	$200 \leq Re \leq 600$, $0.01 \leq Ri \leq 1$, $0 \leq Ha \leq 20$, Pr = 6.2	Around 5000 nodes
Thiers et al. [158]	SEM, NeK5000, GMRES	Rectangular cavity	2D, unsteady	A = 4, Pr = 0.71, Ra = 9×10^7	183×169
Aljabair et al. [159]	FDM, CDS, UDS, SOR	Sinusoidal lid-driven cavity	2D, mixed convection, laminar	$1 \leq Re \leq 1000$, $0 \leq Ra \leq 10^7$, $0 \leq \chi \leq 0.07$, Cu-H_2O nanofluid	41×41
Alsabery et al. [160]	FEM	Wavy lid-driven square cavity	2D, laminar, steady, mixed convection	$0.01 \leq Ri \leq 10$, Re = 100, $0 \leq \phi \leq 0.04$, H_2O/Cu-Al_2O_3 hybrid nanofluid	-
Çolak et al. [161]	OpenFOAM, FVM, SIMPLE	Lid-driven cavity with porous block	2D, mixed convection, steady	$10^{-1} \leq Ri \leq 10$, Gr = 105, $10^{-7} \leq Da \leq 10^{-1}$, Pr = 6.2	Uniform grid, 201×201

Table 1. *Cont.*

Eshaghi et al. [162]	FEM	H-shaped cavity with a baffle inside	2D, natural convection, laminar	$10^4 \leq Ra \leq 10^6$, $2 \leq Le \leq 8$, $1 \leq N \leq 3$, $-60 \leq \varphi. \leq 60$, Cu-$Al_2O_3$-$H_2O$ hybrid nanofluid	-
Fayz-Al-Asad et al. [163]	FEM	Triangular cavity	2D, natural convection, steady	Pr = 0.71, $10^4 \leq Ra \leq 10^6$	6718 elements, 13,112 nodes
Hasnaoui et al. [164]	LBM, MRT, BGK	Rectangular cavity	2D, biry mixture	Sr = −0.5, 0, 0.5, $0 \leq Ra \leq 80$, Pr = 0.71, A = 2, Le = 2	120 × 240
Hussain et al. [165]	FEM	Double lid-driven cavity with fins	2D, laminar, steady	$0 \leq Ha \leq 100$, $0 \leq \varphi \leq 90$, $0.01 \leq Ri \leq 1$, Pr = 6.2, Re = 100, χ = 0.02, Cu-H_2O nanofluid	33,177 grids
Hoston et al. [166]	IEFG–RIPM	Lid-driven square cavity	2D, steady	Re = 10,000, 15,000, 20,000, 25,000, 30,000 and 35,000	150 × 150 (Refined at cavity walls)
Ibrahim & Hirpho [167]	COMSOL, FEM	Trapezoidal cavity	2D, mixed convection, laminar	Ha = 0, 50, Ri = 0.1, 1, 10, Re = 100, Am = 0.25, 0.5, 1	91 × 91
Ikram et al. [168]	FEM, ALE	Hexagonal cavity with rotating modulator	2D, forced convection, unsteady, laminar	Pr = 0.71, $10^2 \leq Re \leq 10^3$, $10^3 \leq Bi \leq 10^4$, $10^3 \leq Ra \leq 10^7$	Non-uniform, 48,548 elements
Joe & Perumal [169]	OpenFOAM, FVM	Rectangular cavity containing cylinders	2D, unsteady	Pr = 0.72, Re = 1600	Unstructured triangular cells
Mondal & Mahapatra [170]	FDM, BiCGStab	Trapezoidal cavity	2D, mixed convection, steady, laminar	Pr = 6.2, N = 5, $0.5 \leq A \leq 2$, $10^{-2} \leq Ri \leq 10^2$, $10^2 \leq Re \leq 10^3$, $45 \leq \varphi \leq 90$, $0 \leq \chi \leq 0.5$, $20 \leq Ha \leq 40$, $1 \leq Le \leq 2$, Al_2O_3-H_2O nanofluid	81 × 81
Mebarek-Oudina et al. [171]	FEM	Trapezoidal porous cavity with zigzag wall	2D, laminar, steady	$0 \leq Ha \leq 100$, $0 \leq \varphi \leq 90$, $10^3 \leq Ra \leq 10^5$, $0 \leq \chi \leq 0.08$, Cu-Al_2O_3/H_2O hybrid nanofluid	Triangular grid, 20,296 elements
Saha et al. [172]	FVM	Rectangular cavity with baffles	2D, laminar, steady	$50 \leq Re \leq 250$ Ri = 0, 2, 4	45 × 51
Saha et al. [173]	FVM, SIMPLE, QUICK	Triangular cavity	2D, natural convection	Pr = 0.72, $10^3 \leq Ra \leq 10^6$, A = 0.2, 0.5, 1.0	360 × 75, 360 × 90, 360 × 120 for A = 0.2, 0.5, 1
Shah et al. [174]	FEM, NR	Lid-driven trapezoidal cavity with obstacle	2D, mixed convection, steady, laminar	$10^{-2} \leq Ri \leq 10$, $0.1 \leq Le \leq 10$, $300 \leq Re \leq 500$, $-10 \leq N \leq 10$, Pr = 0.71	Non-uniform, approx. 3200 elements
Shahid et al. [175]	MRT-LBM	Triangular lid driven cavity	2D, mixed convection, unsteady	Pr = 0.71, 1, 7, $10^{-2} \leq Ri \leq 10^2$, $10^4 \leq Gr \leq 10^7$	-
Shahid et al. [176]	MRT-LBM	Lid-driven rectangular cavity with obtacles	2D, mixed convection, laminar	Pr = 0.71, 1, 7, $10^{-2} \leq Ri \leq 10^2$, $10^3 \leq Gr \leq 10^6$, A = 0.2, 0.5, 2, 5	Not clearly mentioned for different A
Shekaramiz et al. [177]	OpenFOAM, FVM, SIMPLE	Wavy triangular cavity	2D, free convection, steady	$5 \times 10^3 \leq Ra \leq 2 \times 10^5$, Pr = 4.6, $0 \leq Ha \leq 50$, $0 \leq \varphi \leq 90$, χ = 2%, H_2O-Fe3O4 nanofluid	16,000 and 12,000 nodes
Tizakast et al. [178]	FVM, SIMPLER	Lid-driven rectangular cavity	2D, laminar, unsteady, non-Newtonian	$Ra_T \leq 5 \times 10^6$, $Pe \leq 10^3$, $10^{-3} \leq Le \leq 10^3$, $10^{-3} \leq N \leq 10^3$, $0.6 \leq n \leq 1.4$	Uniform grid, A = 24:381 × 121

Table 1. *Cont.*

Velkennedy et al. [179]	FDM, ADI, CDS	Rectangular vented cavity	2D, laminar, unsteady	$10^3 \leq Ra \leq 10^6$, Pr = 0.71	181 × 121
Xiong et al. [180]	FEM	Lid-driven triangular cavity	2D, mixed convection	Pr = 6.2, $0 \leq Ha \leq 40$, $0 \leq Re \leq 10^3$, $0.01 \leq Ri \leq 2$	Uniform triangular mesh
Abbas et al. [181]	FEM	Square cavity with obstacles	2D, steady, laminar	$0 \leq \chi \leq 0.04$, $10 \leq Ha \leq 40$, $10^3 \leq Ra \leq 10^7$, Cu-H_2O nanofluid	59,173 elements
Ahmed et al. [182]	Coiflet wavelet-homotopy method	Lid-driven square porous cavity	2D, unsteady	Pr = 6.2, $10 \leq Ri \leq 10^2$, $10^{-4} \leq Da \leq 10^{-1}$, $3 \leq Le \leq 10^6$, Al_2O_3-Cu/H_2O hybrid nanofluid	-
Alam et al. [8]	FEM	Semi-circular cavity	2D, unsteady, semi-circular cavity, free convection	Pr = 23.0, 6.84, $1 \leq dp \leq 10$, $0 \leq \chi \leq 0.05$, $0 \leq Ha \leq 100$, $10^4 \leq Ra_T \leq 10^6$, ZnO, Fe_3O_4, Co, Al_2O_3, Ag nanoparticles, H_2O & kerosene as base fluids	15,817 elements
Ali et al. [183]	Comsol, FEM	Lid-driven square cavity	2D, mixed convection, steady	Re = 1, 10, 10^2, Ha = 0, 10, 25, χ = 0, 1%, 5%, Pr = 6.2, Gr = 10^2, Al_2O_3-H_2O nanofluid	Non-uniform, 30,550 nodes, 60,036 elements
Alqaed et al. [5]	FVM, SIMPLE	Rectangular cavity with triangular blades	2D, steady, laminar	$10^3 \leq Ra \leq 10^5$, $0 \leq Ha \leq 30$, χ = 0.3, Al_2O_3-H_2O nanofluid	150 × 450
Acharya & Chamkha [184]	FEM	Hexagonal cavity with parallel fins	2D, laminar, steady	$10^3 \leq Ra \leq 10^5$, $0 \leq Ha \leq 100$, $0 \leq \chi \leq 0.04$, Pr = 6.2, Al_2O_3-H_2O nanofluid	Non-uniform, 34,502 elements
Batool et al. [185]	FVM, SIMPLE	Lid-driven square cavity	2D, steady, laminar	$100 \leq Re \leq 400$, micropolar nanofluids	Staggered grid
Charqui et al. [186]	FVM, SIMPLE, TDMA	Tall partitioned cavity	2D, natural convection, laminar	Pr = 0.71, 7, A = 40	Uniform mesh, 80 × 200
Cui et al. [187]	FVM, SIMPLE	Triangular cavity	3D, natural convection, unsteady	Pr = 0.7, $10^2 \leq Ra \leq 10^7$, $0.1 \leq A \leq 1.5$	Non-uniform mesh, 141 × 41 × 51
Dahani et al. [188]	LBM, MRT, BGK operator	Double lid-driven square cavity	2D, unsteady	$0 \leq \varphi \leq 180$, Re = 10^2, $10^{-2} \leq Ri \leq 10^2$, $10^2 \leq Gr \leq 10^6$, Pr = 0.71	Uniform grid, 160 × 160
Esfe et al. [9]	Fluent, FVM, SIMPLE	U-shaped porous enclosure	2D, steady	$10^3 \leq Ra \leq 10^5$, $0 \leq \chi \leq 0.03$, Al_2O_3-H_2O nanofluid	Approx 1600 cells
Geridonmez & Oztop [10]	Rbf-Pum	Right Isosceles triangular cavity	2D, natural convection, steady, laminar	$0 \leq Ha \leq 100$, $0.25 \leq A \leq 1$, Pr = 6.07, Ra = 10^5, $0 \leq \chi \leq 0.02$, Al_2O_3-Cu/H_2O nanofluid	1,842,025 & 1,741,596 nodes
Hirpho & Ibrahim [189]	FEM	Trapezoidal enclosure	2D, mixed convection, non-Newtonian, steady, laminar	$10^{-1} \leq Ri \leq 10^2$, Re = 100, Pr = 20, $0 \leq \chi \leq 0.02$, Al_2O_3-Cu/H_2O hybrid nanofluid	201 × 201
Khalil et al. [190]	Fluent, FVM, RSM	Porous trapezoidal cavity with wavy wall	2D, steady	$0 \leq Ha \leq 40$, $0 \leq Am \leq 20$, $5 \times 10^2 \leq Ra \leq 2.4 \times 10^4$	320 × 320
Liu [191]	CDS, SIMPLE, QUICK	Rectangular cavity with fins	2D, free convection, unsteady	$0 \leq \varphi \leq 40$, Ra = 1.84×10^9	360 × 400

Table 1. *Cont.*

Noor et al. [192]	FEM	Lid-driven trapezoidal cavity with obstacle	2D, forced convection, steady	$10^2 \leq Re \leq 700$, $10^{-3} \leq Ri \leq 10$, $0 \leq Ha \leq 10^2$	Trangular grid, 4622 nodes. 8929 elements
Nouraei et al. [193]	FVM, SIMPLE	Semi-circular vented cavity	2D, mixed convection, laminar, steady	$10 \leq Re \leq 100$, $0 \leq \chi \leq 0.06$, Cu-H_2O nanofluid	52,000 grids
Polasanapalli & Anupindi [194]	LBM	Concentric circular annular cavity	2D, mixed convection, unsteady	$10^4 \leq Ra \leq 10^6$, $0 \leq Re \leq 10^4$, Pr = 0.71, $0 \leq \varphi \leq 360$, $10^{-3} \leq Ri \leq 10^3$	120 × 120, 180 × 180
Prince et al. [195]	COMSOL, FEM	Trapezoidal cavity with different surface	2D, natural convection	Pr = 0.716, $10^3 \leq Ra \leq 10^6$, *Materials*: Pinewood, plexiglas, dry concrete, glass fiber	Rectangle: 6112, Triangle: 10,191, Sinusoidal: 5993 elements
Rahaman et al. [196]	Fluent, FVM, CDS, SIMPLE	Trapezoidal cavity	2D, unsteady, natural convection	Pr = 0.71, $10^0 \leq Ra \leq 10^8$, A = 0.5	Non-uniform, 300 × 100
Roy et al. [197]	FEM	Square enclosure with blocks	2D, unsteady, natural convection	Pr = 6.2, $0 \leq Rd \leq 3$, $0 \leq \chi \leq 0.09$, $10^4 \leq Ra \leq 10^6$, $0 \leq Ha \leq 60$, Cu- Al_2O_3/H_2O hybrid nanofluid	Triangular 65,740 elements
Shah et al. [198]	FEM, NR	Lid-driven corrugated porous cavity	2D, mixed convection, laminar, steady	$10^2 \leq Re \leq 400$, $0 \leq \chi \leq 0.05$, $10^{-5} \leq Da \leq 10^{-1}$, Pr = 6.2, $10^{-2} \leq Ri \leq 100$, CuO-H_2O nanofluid	Approx 8000 elements
Tizakast et al. [199]	FVM, SIMPLE	Lid-driven Rectangular cavity	2D, unsteady non-Newtonian, laminar	$2 \leq A \leq 30$, $10^2 \leq Ra_T \leq 10^7$, $10^{-3} \leq Le \leq 10^3$, $0.1 \leq Pe \leq 10^4$	-
Xia et al. [200]	UPWIND	T-shaped lid-driven cavity	2D, mixed convection	$0 \leq \chi \leq 0.03$, $0.1 \leq Re \leq 10$, $0.2 \leq A \leq 0.4$, Al_2O_3-H_2O nanofluid	Uniform mesh, 250,000 cells
Zarei et al. [201]	FVM, SIMPLE	Square cavity with wavy walls	2D, steady	Ra = 10^4, $0 \leq Am \leq 0.15$, $0 \leq \chi \leq 0.04$, Cu-H_2O nanofluid	135,008 triangular cells
Zhang et al. [202]	FVM, SIMPLE	Semi-elliptic lid-driven cavity	2D, mixed convection, steady, laminar	$0 \leq \chi \leq 0.06$, Gr = 5 × 10^4, 15 × 10^4, 25 × 10^4, 4 × 10^5, $10^{-1} \leq Ri \leq 10$, Pr = 6.2, Ag-H_2O nanofluid	43,905 triangular grids
Akhter et al. [7]	FEM	square cavity with cylinder	2D, steady	$10^4 \leq Ra \leq 5 \times 10^6$, Pr = 6.2, $0 \leq \chi \leq 0.05$, $0 \leq Ha \leq 10^2$, Cu-Al_2O_3/H_2O hybrid nanofluid	24,961 nodes, 49,188 elements
He et al. [203]	Experimental, FVM, SIMPLE	Cubic cavity	3D	$0 \leq B \leq 133$, $0 \leq \chi \leq 0.03$, $6.9 \times 10^5 \leq Ra_m \leq 11.6 \times 10^5$, Fe_3O_4-Paraffin nanofluid	50 × 50 × 50
Ikram et al. [204]	FEM, ALE	Hexagonal cavity with rotating modulator	2D, forced convection, unsteady, laminar	Pr = 0.71, $10^2 \leq Re \leq 10^3$, $10^4 \leq Ra \leq 10^6$, Bi = 10^4	49,874, 50,672 and 52,601 elements
Ouri et al. [205]	Comsol, FEM, ANFIS	L-shaped cavity with rotating cylinder	2D, unsteady	$200 \leq Re \leq 10^3$, $10^2 \leq Re_w \leq 10^3$, $0 \leq Ha \leq 40$, $0 \leq \chi \leq 0.02$, Ag-MgO/H_2O hybrid nanofluid	Non-uniform triangular 65,216 elements
Sayed et al. [206]	FVM, LES, URANS	Cubical cavity	3D, unsteady	Ra = 10^9, Pr = 0.71, Pr_t = 0.9	166,375 cells

4. Validations

In computational fluid dynamics (CFD), validation is an important aspect of research. It is the process of comparing the numerical results with experimental, benchmark, or numerical results to assess the accuracy of the simulation. Validation is important for several reasons: it helps to ensure that the numerical model is implemented correctly and that the solution is not affected by any errors or bugs in the code; it also allows researchers to compare their results with other studies, and it gives an idea about the accuracy of the numerical model compared with real-world data. One common way to validate CFD simulations is to compare the numerical results with experimental data. This can be conducted by comparing the velocity, temperature, and pressure fields obtained from the simulation with measurements taken in a laboratory experiment. The percentage difference between the numerical and experimental results is used as a measure of the accuracy of the simulation. A percentage difference of less than 5% is generally considered to be a good match between the numerical and experimental results. The above-mentioned studies used different types of validations, and details of some of these are presented below. Providing detailed information about the validation process in a study is important for ensuring the accuracy of the numerical results and for providing a useful resource for future research. Moreover, according to the authors' knowledge, no such details are available in previous studies. By presenting the details of their validation studies, the authors are providing a valuable resource for future researchers. This information can be used to compare the results of new studies with previous work and to assess the accuracy of new simulations. Additionally, the figures (Figures 4–10) likely provide a visual representation of the validation results, making it easier for readers to understand and interpret the data.

For a square lid-driven cavity with mixed convection flow, the variation of the average Nusselt number with different Gr for a fixed Pr of 0.71 was studied through numerical simulations or experiments. In the case of mixed convection, as the Gr increases, the Nu_{avg} is expected to decrease. This is due to the lid-driven motion of the cavity. Details of the results are presented in Figure 4.

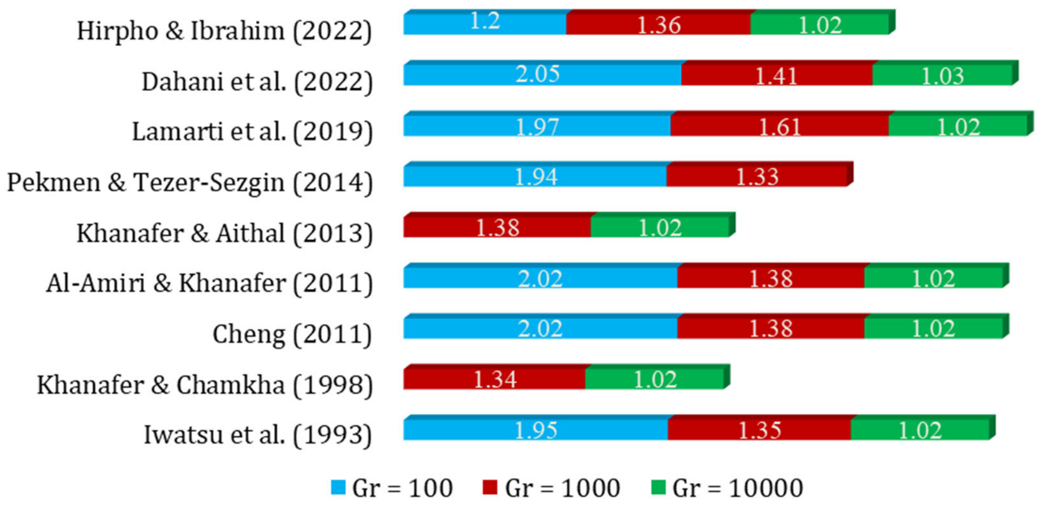

(**a**) Re = 100

Figure 4. *Cont.*

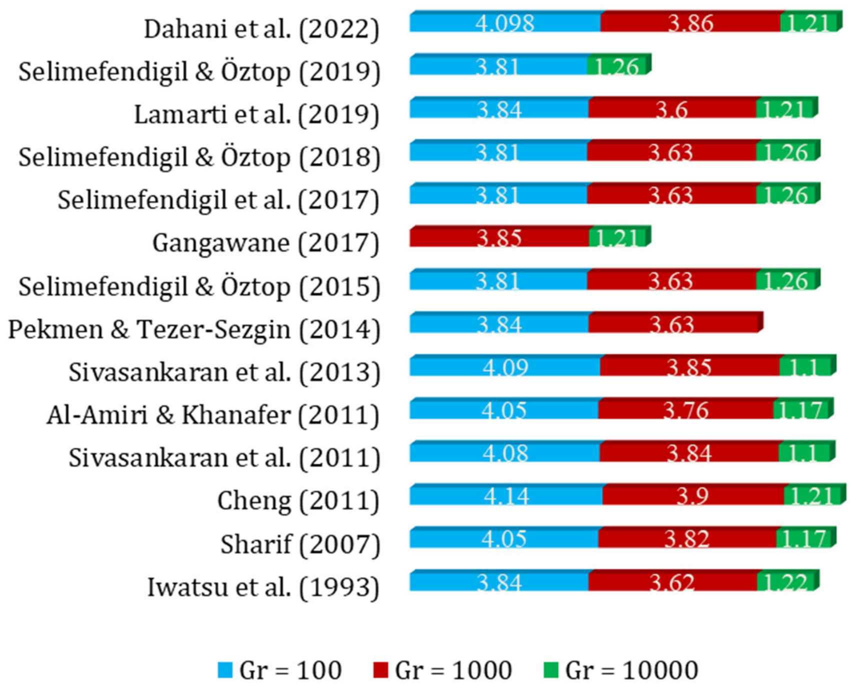

(**b**) Re = 400

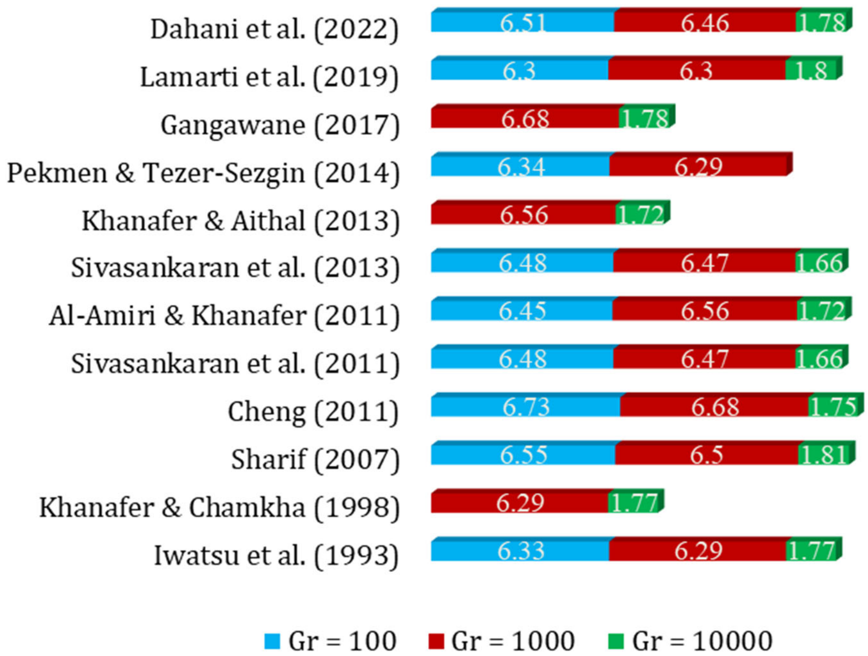

(**c**) Re = 1000

Figure 4. Variation of Nu_{avg} with different Gr for Pr = 0.71 (Case: Mixed convection flow inside a square lid-driven cavity) [31,33,34,53,55,93,105,106,124,139,142,188,189,207–211].

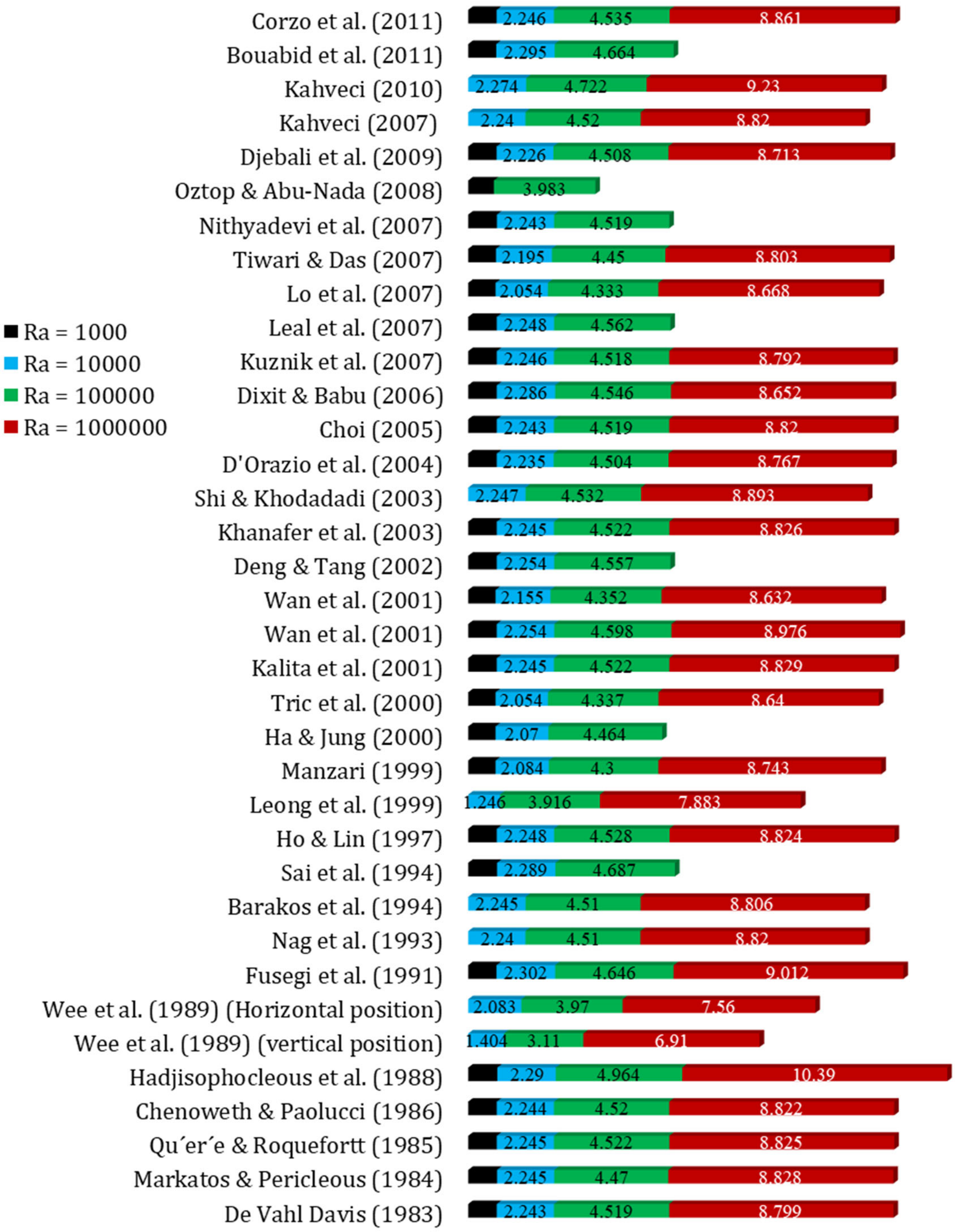

(**a**)

Figure 5. *Cont.*

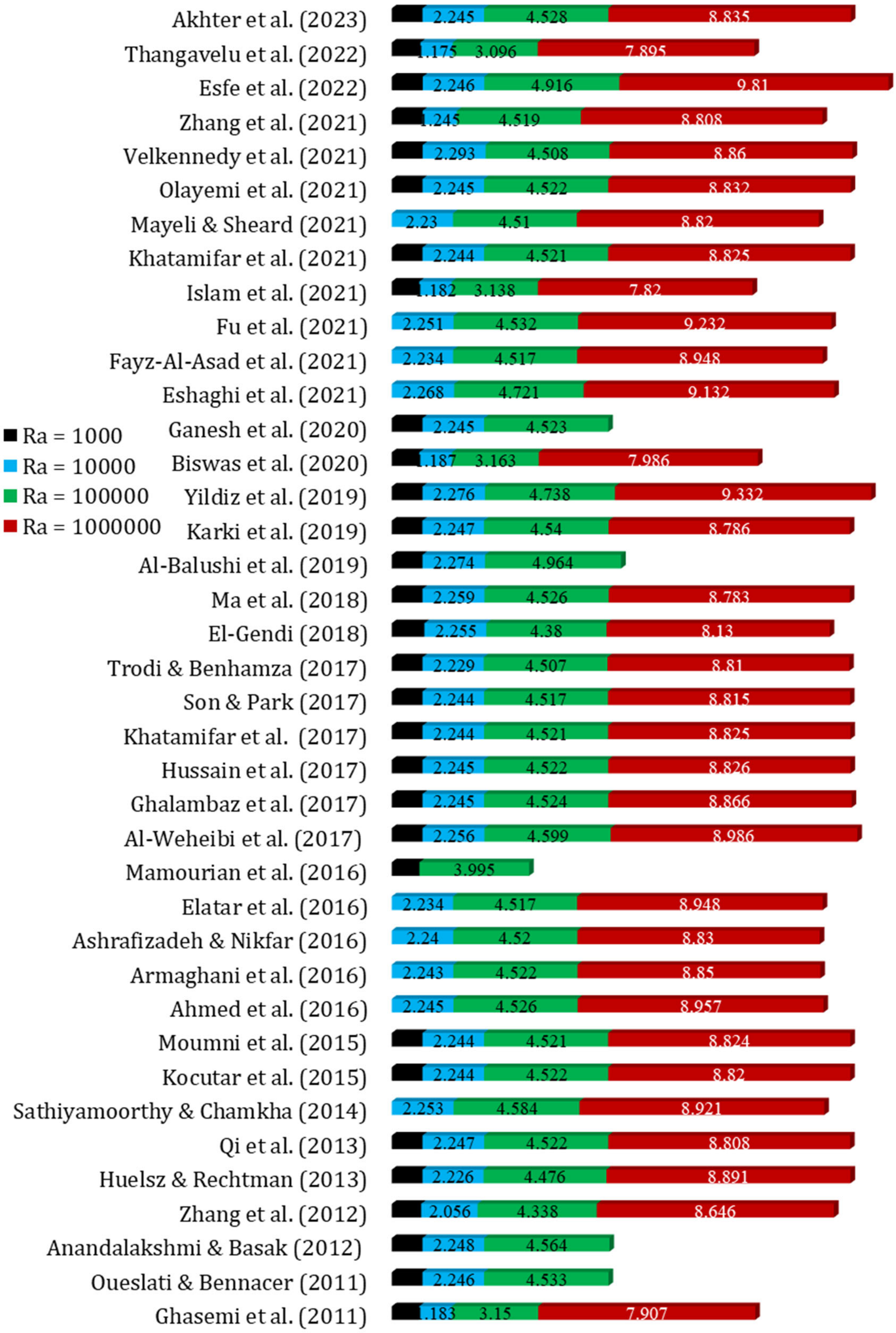

(**b**)

Figure 5. (**a**,**b**): Variation of Nu_{avg} with different Ra for Pr = 0.71 (Case: Natural convection flow in a square cavity) [2,7,9,18,52,71,75,79,89,94,99,103,149,162,163,179,212–267].

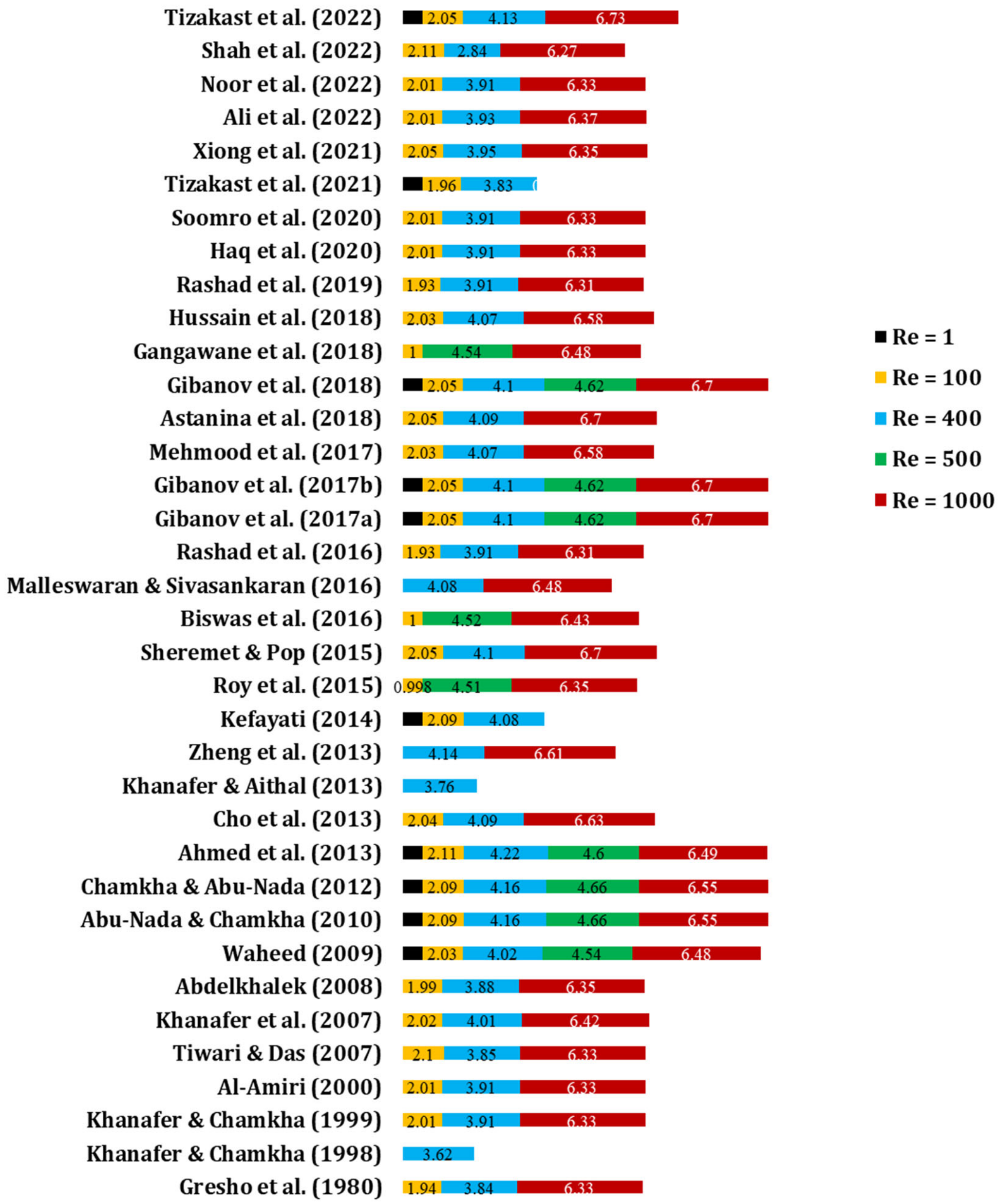

Figure 6. Variation of Nu_{avg} with different Re for Pr = 0.71 and Gr = 10^2 (Case: Mixed convection flow in a square lid-driven cavity) [12,18,42,48,50,53,73,95,96,110,115–117,150,157,178,180,183,192,198,199,208,268–278].

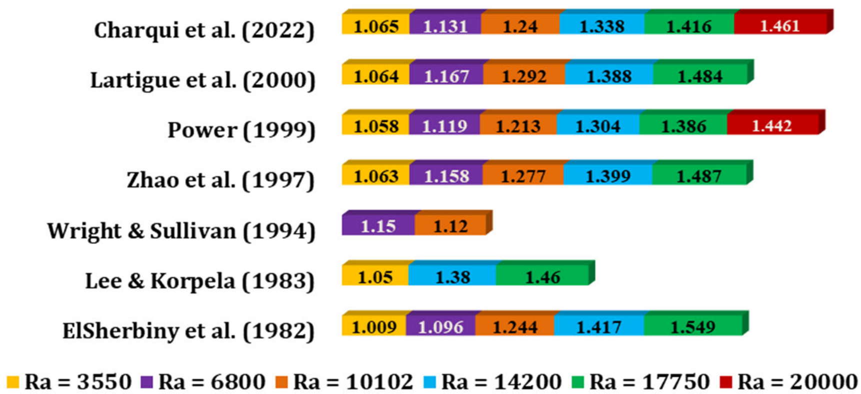

Figure 7. Variation of Nu_{avg} with different Ra for A = 40 [186,279–284].

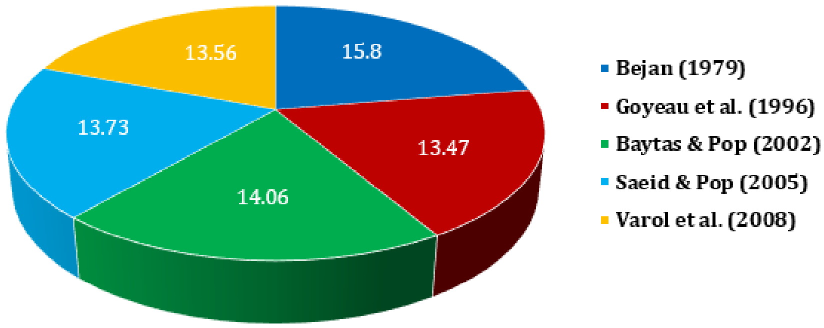

Figure 8. Variation of $\overline{Nu}$ for Ra = 10^3 (Case: Porous square cavity) [20,285–288].

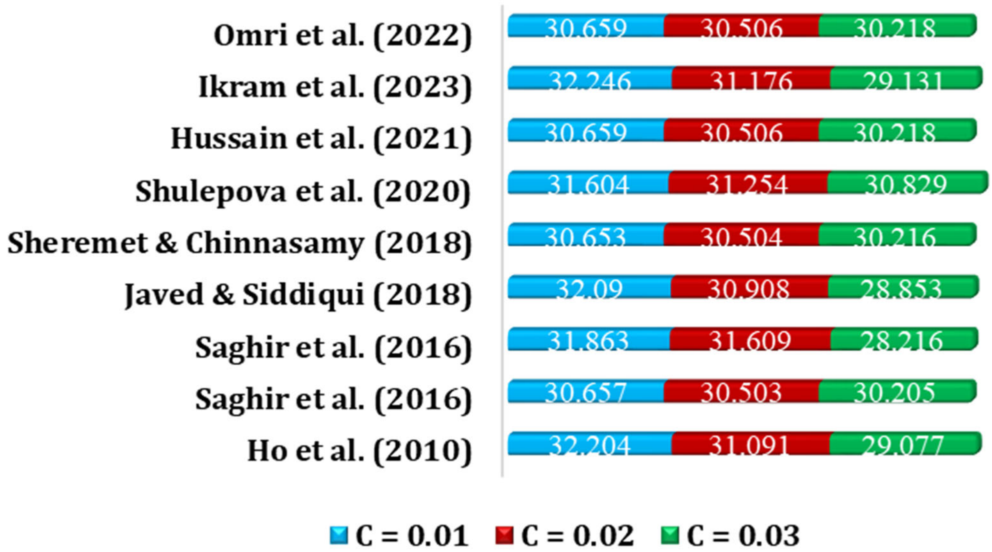

Figure 9. Variation of $\overline{Nu}$ for different nanoparticles concentration (C) of Al_2O_3 nanofluid [118,165,204,289–293].

Based on the validation data presented in Figure 4a–c, the following correlations (Equations (6)–(8)) are proposed. It is worth noting that all these correlations exhibit a maximum percentage error of less than 10%, which indicates a strong relationship between the provided data and the proposed equations.

$$\overline{Nu} = 0.97 + \frac{0.0141 * Re * Pr}{1 + \left(\frac{Gr}{756.05}\right)^{1.12}},\ 10^2 \leq \text{Gr} \leq 10^4,\ \text{Re} = 100,\ \text{Pr} = 0.71 \quad (6)$$

$$\overline{Nu} = 1.13 + \frac{0.0099 * Re * Pr}{1 + \left(\frac{Gr}{2577.39}\right)^{2.7}},\ 10^2 \leq \text{Gr} \leq 10^4,\ \text{Re} = 400,\ \text{Pr} = 0.71 \quad (7)$$

$$\overline{Nu} = 1.595 + \frac{0.068873 * Re * Pr}{1 + \left(\frac{Gr}{4971.05}\right)^{4.85}},\ 10^2 \leq \text{Gr} \leq 10^4,\ \text{Re} = 1000,\ \text{Pr} = 0.71 \quad (8)$$

In a square cavity with natural convection flow, the variation of Nu_{avg} with different Ra for a fixed Pr of 0.71 is studied throughout the literature. We know as Ra increases, the strength of natural convection increases, and the Nu_{avg} increases. However, the relationship between Nu_{avg} and Ra can be complex, as the flow pattern and heat transfer mechanisms in the cavity can vary with changing Ra. In general, for a square cavity with natural convection flow and Pr = 0.71, the variation of the Nu_{avg} with Ra can be explained by different values of Ra. For low Ra < 10^4, the heat transfer is dominated by conductive heat transfer, and Nu_{avg} is relatively constant and low. However, for intermediate Ra (10^4 < Ra < 10^8), the heat transfer is dominated by a combination of conduction and convection, and Nu_{avg} increases rapidly with Ra due to the onset of natural convection. Such findings are explained in Figure 5.

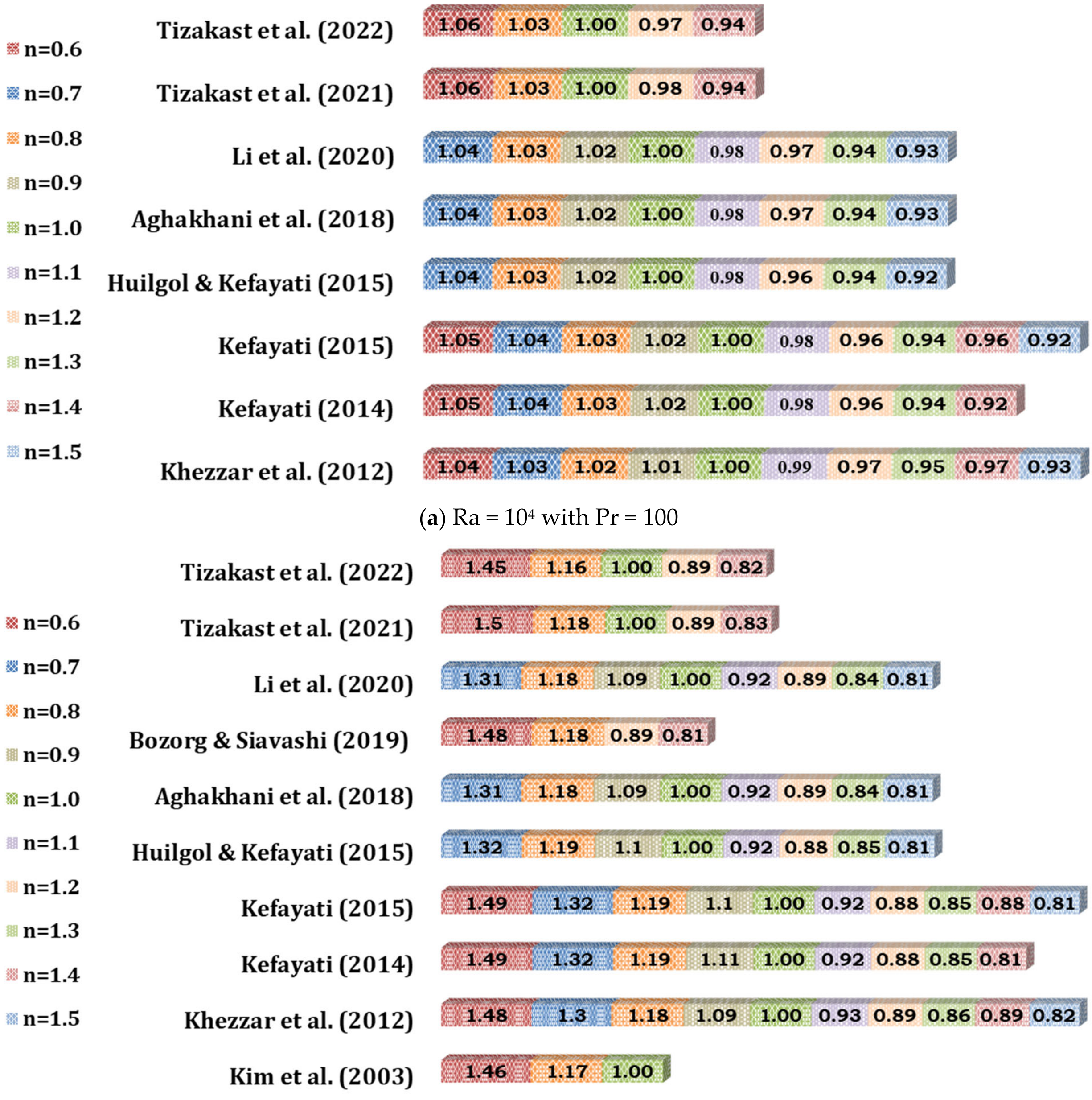

(**a**) Ra = 10^4 with Pr = 100

(**b**) Ra = 10^5 with Pr = 100

Figure 10. Variation of relative average Nusselt number for different Ra (Case: Non-Newtonian Power-law Fluids) with Pr = 100 [109,152,178,199,218,273,294–297].

Based on the results displayed in Figure 5a,b, a novel correlation is introduced for the computation of Nuavg, which is presented below. The correlation (Equation (9)) exhibits a high level of consistency with the aforementioned findings, with an error range of 1.4% to less than 10%. In a few instances, the maximum error is found to be approximately 13%, but this is attributed to the researcher's recording of low Nu_{avg} values.

$$\overline{Nu} = 0.44 + \frac{35.68 * Pr}{1 + \left(\frac{Re}{5558557.57}\right)^{-0.41}},\ 10^3 \leq \text{Ra} \leq 10^6, \text{Pr} = 0.71 \quad (9)$$

As shown in Figure 6, for a fixed Pr = 0.71 and low Gr = 100 in mixed convection flow in a square lid-driven cavity, Nu_{avg} always increases with increasing Re. This is because at low Gr, the buoyancy forces are weak, and the flow is dominated by the lid-driven motion. As Re increases, the flow becomes more vigorous, resulting in increased mixing and enhanced heat transfer.

Based on the findings depicted in Figure 6, a novel correlation for computing Nu_{avg} is introduced and presented below. The proposed correlation (Equation (10)) exhibits a strong association with the provided data, with a minimum and maximum error of 0.01% and 7.30%, respectively. However, for some of the given data, a higher percentage of error is observed, which is not attributable to the correlation, but rather is due to poorly recorded research data obtained by the researcher.

$$\overline{Nu} = 0.9969 + \frac{18.3538 * Pr}{1 + \left(\frac{Re}{1390.5345}\right)^{-0.93}},\ 1 \leq \mathrm{Ra} \leq 10^3, \mathrm{Pr} = 0.71 \quad (10)$$

We know that an increase in the aspect ratio leads to an increase in the heat transfer rate. This is because an increase in the aspect ratio leads to an increase in the surface area available for heat transfer. As a result, there is more area for the fluid to exchange heat with the solid surfaces, leading to a higher heat transfer rate. Additionally, an increase in the aspect ratio can also promote greater fluid mixing and circulation, which further enhances the heat transfer rate. We also know that Nu_{avg} increases with increasing Ra for a porous square cavity case. At low Ra, the flow is dominated by conduction, and the heat transfer is primarily governed by thermal conduction. As Ra increases, the buoyancy forces become more significant, resulting in increased flow circulation and mixing. This enhanced mixing leads to an increase in the heat transfer rate and Nu_{avg}. Such findings are presented in Figures 7 and 8, that is observed by a different researcher.

Based on the results depicted in Figure 7, a new correlation for determining Nuavg is proposed and put forward. The correlation (Equation (11)) demonstrates a high level of accuracy, with a minimum error of 0.08% and a maximum error of 9.93%. These findings suggest that the correlation has significant potential for future use.

$$\overline{Nu} = 1.04 + \frac{0.57}{1 + \left(\frac{Ra}{12499.08}\right)^{-0.76}},\ 3 \times 10^3 \leq \mathrm{Ra} \leq 2 \times 10^4 \quad (11)$$

Figure 9 presents the variation of Nu_{avg} with different nanoparticle concentrations (C) for Al_2O_3 nanofluid. It is observed that Nu_{avg} slightly decreases with the increase in C. The decrease in Nu_{avg} with increasing C may be due to several factors, such as the nanoparticles may aggregate at high concentrations, leading to a decrease in effective surface area and, thus, a decrease in convective heat transfer.

Based on the outcomes presented in Figure 9, a new correlation is suggested for computing Nu_{avg}. This correlation (Equation (12)) demonstrates a robust concurrence with the results of earlier studies, with an error range of 0.01% to a maximum of 5.41%.

$$\overline{Nu} = 27.06 + \frac{4.38}{1 + \left(\frac{C}{0.03}\right)^{4.9}}, 1\% \leq \mathrm{C} \leq 3\% \quad (12)$$

Figure 10 shows that the Nu_{avg} increases with increasing Ra for a fixed Pr = 100, which indicates an enhancement of convective heat transfer. However, the rate of increase depends on the power-law index n. It is also seen that Nu_{avg} slightly increases with the increase in n. It indicates that the non-Newtonian behavior of the fluid has a small effect on the convective heat transfer in the fluid.

Based on the data depicted in Figure 10, two correlations (Equations (13) and (14)) are proposed with minimum and maximum errors of 0.06% and 3.41%, and 0.01% and 7.69%, respectively. These correlations demonstrate excellent agreement with the provided data.

$$\overline{Nu} = \frac{0.01105 * Pr}{1 + \left(\frac{n}{4.3431}\right)^{1.5247}}, 0.1 \le n \le 2.0,\ \mathrm{Ra} = 10^4,\ \mathrm{Pr} = 100 \quad (13)$$

$$\overline{Nu} = \frac{0.061826 * Pr}{1 + \left(\frac{n}{0.1494}\right)^{0.851}}, 0.1 \le n \le 2.0,\ \mathrm{Ra} = 10^5,\ \mathrm{Pr} = 100 \quad (14)$$

5. Heat Transfer Analysis

According to the above-mentioned literature, the flow behavior inside the cavities can be classified into the following categories: effect of the applied boundary conditions to walls such as temperature difference, localized heat sources, magnetic field, or inlet flow to the cavity through a specific port(s). The other types of cavities use internal fins or cylinders to drive the flow inside the cavity. Some of the above-mentioned references (Given in Table 1) are discussed below:

5.1. Square Cavity

In the study by Abbas et al. [181], the effect of using Cu-water nanofluid on heat transfer enhancement was investigated inside a square cavity, using two circular heated obstacles and applying a constant magnetic field. They found that Nu_{avg} improved with the rise of Ra up to a certain point and then showed a negligible variation. However, for lower values of Ra, Nu decreased with Ha. Additionally, the increase in nanoparticle concentration resulted in a decrease in the heat transfer rate for each value of Ha. The study also found that the increase in magnetic field intensity led to a decrease in the rate of heat transfer because of the high sensitivity of Cu nanoparticles to the applied magnetic field. In the study by Roy et al. [197], the flow behavior inside a square cavity filled with MHD hybrid Cu-Al_2O_3/H_2O nanofluid was investigated. A cold elliptical block and a hot square block were inserted inside the cavity, and all four walls were set at the same temperature as the elliptical object. The results of the study confirmed that the local Nu increased with Ra and decreased with an applied magnetic field. Additionally, the presence of nanoparticles enhanced the heat transfer rate. The study also found that Ha had a stronger effect on local and average Nu at high values of Ra. Furthermore, high Rd led to an improvement in the rate of heat transfer. In the study by Zarei et al. [201], the flow of a Cu-H_2O nanofluid inside a square cavity with a wavy left wall and straight other walls was investigated, with a uniform heat flux applied to the left vertical wall and a constant temperature on the right vertical wall, while the other boundaries were adiabatic. They found that increasing the nanoparticles concentration and decreasing the wavelength and amplitude of the wavy wall led to an increase in Nu_{avg}. In the study by Akhter et al. [7], the flow of a hybrid nanofluid Cu-Al_2O_3/H_2O inside a square cavity was investigated. A heat-conductive circular solid was placed at the center of the cavity. The bottom and top boundaries of the cavity were partially heated and cooled, respectively. Their results confirmed that the heat transfer was enhanced with the Ra and decreased with the Ha. They also found that the thermal performance increased linearly with an increase in χ. For the nanoparticles volume fraction of 1% and 5%, there was an increase in heat transfer by 47.74% and 106.78%, respectively, as compared to the base fluid.

5.2. Rectangular Cavity

The study by Wee et al. [2] found that the rate of heat transfer in a rectangular cavity full of air is significantly higher when the cavity is in a vertical position with upwards transfer compared to a horizontal position with the downward transfer. Al-Farhany & Turan [39] found that using a rectangular porous cavity with left and right boundaries at various temperatures and insulated top and bottom walls, the flow inside the cavity was driven by buoyancy, and the results showed that the highest Nu_{avg} occurred at zero inclination for high Ra, while for low Ra, the maximum Nu_{avg} was found at 60 degrees inclination. Additionally, the results showed that as the aspect ratio and Le increase, Nu_{avg} decreases and Sh increases. Elsherbiny & Ragab [51] studied an inclined rectangular cavity with a hot spot at the bottom wall and insulated surfaces. They found that as the aspect ratio increases, Nu_{avg} decreases, and when the local heat source position was at the middle or quarter position of the bottom wall, the maximum Nu_{avg} occurred at specific aspect ratio values. Moreover, they found that Nu_{avg} increases with increasing tilt angle (φ) from 0 to 75 degrees, then starts to decrease until 150 degrees and remains constant up to 180 degrees. Elsherbiny & Ismail [69] studied an oblique rectangular cavity with two local heat sources at the bottom wall and insulated surfaces. They found that Nu_{avg} increases until φ's reaches 60 degrees and then starts to decrease until it reaches a minimum value at 180 degrees. They also found that at a tilt angle of 150 degrees, the effect of Ra on Nu_{avg} is very low, and at 180 degrees, Nu_{avg} becomes independent of Ra. Additionally, they observed that Nu_{avg} decreases by 23% when the aspect ratio reaches 10. Hatami [6] numerically investigated the free convection and flow of nanofluids in a rectangular cavity with two heated fins installed on the cold lower and upper walls while the vertical walls were insulated. They found that Nu_{avg} was higher for higher volume fractions of Al_2O_3 and similarly for lower volume fractions of TiO_2. Additionally, they observed that Nu_{avg} increases as the height of the fins increases. Yu et al. [3] studied numerically the effect of the magnetic field and electric source on the flow characteristics and heat and mass transfer of electrically conducting fluid inside a rectangular cavity. It was found that with the increase in the density of the magnetic field, the oscillatory flow became more stable, and heat transfer by convection and mass transfer was reduced. Moreover, it was also found that the magnetic field had no effect on $Nu_{avg,}$ which only varied with dimensionless heat generation or absorption coefficient, while Sh remained equal to one.

Jiang and Zhou's [4] study examined the impact of nanofluids on surface tension in a rectangular cavity. They applied a temperature difference across the vertical walls and a free surface on the upper surface. They found that for distilled water-Al_2O_3 nanofluid, a rise in nanoparticles volume fraction led to convective flow being dominated by the fluid's thermophysical properties and the surface tension temperature coefficient. For PGW-ZnO nanofluid, an increase in nanoparticle concentration resulted in convective flow being mainly controlled by the surface tension temperature coefficient. Karatas and Derbentli's [138] study investigated free convection flow in a partially heated rectangular cavity with various aspect ratios. They kept the temperature of the vertical cold boundary constant, and the temperature of the hot boundary was a time-periodic temperature. They observed that Nu_{avg} increased from 2.64 to 16.44 as the aspect ratio decreased from 6 to 1. Thiers et al. [158] explored the impact of local thermal disturbances (one on the cold side and the other on the hot side) on the flow instability in a rectangular enclosure with an aspect ratio of 4.0. They considered the left boundary as a hot boundary, while right boundary as a cold boundary, and the top and bottom walls as adiabatic. Their research showed that the highest heat transfer enhancement occurred when the local disturbance area was located at L_h= 0.7 and/or L_c = 0.3. Hasnaoui et al. [164] studied thermo-solutal convection in a rectangular cavity. They found that the flow became unstable for Sr = 0 and −0.5 and remained unstable until R = 20. They also observed that the rate of heat transfer was strongly impacted by thermo-diffusion in the range of R, leading to instabilities. Alqaed et al. [5] performed a numerical simulation to study the natural convection heat transfer and entropy generation of alumina-water nanofluid flow in a rectangular cavity. They installed two hot triangular blades on the bottom wall, and the two sidewalls were adiabatic, whereas the upper wall was set at a low temperature and the bottom wall was set at a high temperature. They found that a rise in Ra led to an increase in Nu_{avg} and entropy generation, but it decreased Be, and the increment in Ha also led to reducing Be for higher Ra. They reported that the maximum values of Nu_{avg}, entropy generation, and Be occurred at a cavity inclination of 30 degrees. Liu [191] examined the convection heat transfer behavior inside a rectangular cavity with an adiabatic fin fixed on each of the side walls. The top and bottom boundaries were adiabatic, while the left boundary was cold, and the right boundary was hot. The study found that Nu_{avg} increased by 5% for the finned cavity as compared to the non-finned one. Additionally, Nuavg for both cases increased with the angle of inclination until 5 degrees and then decreased.

Sasaguchi et al. [14] studied the heat transfer analysis numerically in a rectangular cavity containing water. All boundaries were insulated and cold (−10 °C), including the internal presence of single or double cylinder inside the cavity. The study found that the solidification speed for a single cylinder was faster than double cylinders for a temperature equal to 0 °C, while the solidification was faster for the double cylinders for a temperature higher than 4 °C. Liu & Huang [153] investigated the effect of adding thin fins to the middle of the high and low-temperature walls of a rectangular cavity, with the top and bottom walls being considered as insulated walls. They applied a linear temperature distribution to the hot and cold side walls. The study found that the effect of the adiabatic horizontal thin fin led to a change in the convective flow attached to the middle of the sidewall. Nu_{avg} correlated well with $Ra^{0.25}$ for all three thermal heating conditions examined. However, when the slope of the applied linear temperature distribution was negative to both the right and left walls, Nu_{avg} was lower than the other two heating conditions.

Joe and Perumal [169] studied the influences of rotating cylinders on the mixing and distribution of temperature within a rectangular cavity. They found that the best results were obtained when the cylinders were close to the middle line and rotated in the same direction. This resulted in improved mixing and a more uniform temperature distribution. Saha et al. [172] studied free convection flow inside a rectangular cavity with isothermally heated baffles. They concluded that the flow velocity and heat transfer interaction efficiency were highest for the case of plane baffles, where fluid was blended more effectively as the length of the baffles increased. They also found that the maximum value of Nuavg was achieved at Re = 250 for plane baffles. Additionally, they found that the heating efficiency increased with Re and Ri and decreased as the length of the baffles increased. Velkennedy et al. [179] investigated the air-flow behavior inside a ventilated rectangular cavity with two outlets and one inlet. The inlet vent was positioned on the bottom of the right wall, and the outlets were put on the top wall. Both vertical walls were considered hot walls, and the bottom wall was adiabatic. They found that the rate of heat transfer to the right wall was reduced at the upper part of the cavity due to the introduction of a cold partition. However, they also found that the heat transfer rate increased significantly with the introduction of the cold partition for lower Ra, and this difference was reduced for higher Ra. Ait-Taleb et al. [58] studied the flow behavior inside a building block that generally contains three air cavities in the horizontal orientation and two in the vertical orientation. They found that by keeping the temperatures of the upper and lower walls the cold outside and hot inside, respectively, the hollow block with two air cells deep in the vertical direction allowed for a significant reduction in heat transfer between the inside and outside of the building. Charqui et al. [186] numerically investigated the heat transfer and free convection flow inside a tall thin partitioned cavity, where the left and right parts were filled with air and water, respectively. They found that even though the partition was thin, air and water behaved differently. The temperature of the inside wall had less effect by solar flux than the heat flux through the partition. The wall opposite to sunlight was kept at 20 degrees Celsius, and the temperature of the other surface was varied between 0 degrees Celsius to 50 degrees Celsius. The other surfaces were assumed to be adiabatic.

5.3. Other Cavity Types

Alam et al. [8] investigated the effect of various types of nanofluids on thermal behavior inside a semicircular cavity that was exposed to a periodic magnetic field. They used nanoparticles such as ZnO, Fe_3O_4, Co, Al_2O_3, and Ag and base fluids such as water and kerosene. The bottom surface was exposed to non-uniform parabolic heating, while the circular surface was set at a fixed cold temperature. They found that the highest value of Nu_{avg} was obtained for Co-kerosene nanofluid by 588.197% for χ = 5%. They also found that for a specific value of χ, there was a slight rise in Nu with the augmentation of Ra. The study also revealed that the variable magnetic field and the Brownian motion of nanoparticles had a significant effect on heat transmission enhancement. Additionally, the findings indicated that a non-uniform magnetic field showed higher heat transmission than a uniform case. Acharya & Chamkha [184] studied the thermal and fluid flow behavior of Al_2O_3-H_2O nanofluid inside a hexagonal enclosure. The enclosure had three parallel fins inside, with the right and left fins being cooled and the middle one being heated. The top lid was partially heated, while the bottom boundary was fully heated, and the other boundaries were assumed to be adiabatic. The study also applied a horizontal magnetic field to the cavity. The results presented that the local Nu and Nu_{avg} increased with the increase in Ra, and the u-shaped fins gave the highest outcomes. Additionally, local Nu and Nu_{avg} decreased with Ha. The study found that the increase in the fin's height led to an increase in the rate of heat transfer, and the central position of the fins was the optimized position that gave the highest rate of heat transfer. Esfe et al. [9] studied the effect of using Al_2O_3-H_2O nanofluid in a U-shaped porous cavity on heat transfer and fluid flow. They found that Nu_{avg} reduced with the increase in Ra and χ. However, Nu_{avg} decreased when Da increased from 0 to 60, indicating that the porous structure had an impact on the heat transfer enhancement. Overall, the study provided insights into the utilization of nanofluids and porous structures to improve heat transfer in U-shaped cavities. Geridonmez & Oztop [10] studied the influence of an oblique partial periodic magnetic field on the free convection of hybrid Al_2O_3-Cu/H_2O nanofluid inside an isosceles triangular cavity. They considered three cases with different wall temperatures and magnetic field orientations and found that the heat transfer rate was reduced with an increase in Ha and that a horizontal magnetic field provided a higher rate of heat transfer than the other cases. Hirpho and Ibrahim [189] studied the mixed convection of a hybrid nanofluid (Al_2O_3-Cu/H_2O) in a trapezoidal cavity with a partially heated bottom wall, cold left and right walls, and an adiabatic top lid. They found that the local Nu number increased with the rise of χ, the Casson fluid parameter, and Ri. This indicates that the rate of heat transfer in the cavity is improved by the presence of nanoparticles, the non-Newtonian behavior of the fluid, and the buoyancy forces.

Khalil et al. [190] examined the free convection in a trapezoidal cavity with a wavy bottom wall filled with pure water and saturated metal foam as a porous medium. The top and side boundaries were kept at a cold temperature while the bottom surface was heated. The study found that Nu_{avg} increased as the number of waves and amplitude of the bottom wall's waves increased. Additionally, Nuavg improved when the cold temperature of the sides and top walls was decreased. Furthermore, an increase in Ha resulted in an increase in Nu_{avg}. Nouraei et al. [193] explored mixed convection of an H_2O-Cu nanofluid in an open semicircular cavity. The circular section was partially heated along 45 degrees at four different angles, and all other positions were insulated. The study found that the local Nu number increased from the inlet to the outlet along the curved surface for a Re of 100. Additionally, the results showed that the maximum Nu_{local} was obtained for χ = 0.06 for all cases. Prince et al. [195] investigated the conjugate natural convection inside a trapezoidal cavity with a thick base and different surface corrugations, such as flat, sinusoidal, and triangular surfaces. The base was made of different materials, such as pinewood, plexiglas, dry concrete, and glass fiber. The base was set isothermally hot while the top wall was kept isothermally cold, and the side walls were adiabatic. The study found that there was a considerable improvement in convection heat transfer for high Ra up to the value of Ra > 10^4. Moreover, the glass fiber showed the highest Nu_{avg} and the lowest dimensionless fluid temperature. For Ra $\leq 10^4$, the conduction heat transfer mode would be dominant. This suggests that the corrugated surface of the cavity base and the material of the base can significantly enhance the heat transfer rate, but the effect becomes less significant for lower Ra. Rahaman et al. [196] studied the natural convection of air inside a valley-shaped trapezoidal cavity, where the top and bottom walls were considered hot and cold, respectively, and both the side walls were adiabatic. The study found that Nu was small at the beginning for stratified air and gradually increased in the transitional phase when the stratification was broken and became fixed for Ra $\leq 10^6$. After that, Nu exhibited oscillatory behavior for Ra $\geq 10^7$.

He et al. [203] discussed the effect of a magnetic field on a phase change nanocomposite inside a cubical cavity filled with. The nanocomposites were obtained by adding Fe_3O_4 nanoparticles into paraffin. The left wall was set as a hot boundary while the other walls were insulated. The study found that, without applying a magnetic field and with a uniform distribution of the nanoparticles in the paraffin, the rate of heat transfer was increased. However, when a magnetic field was applied, the melting rate of paraffin was reduced. Ikram et al. [204] studied the heat transfer behavior inside a hexagonal enclosure equipped with different types of rotating modulators. A uniform heat flux was applied to the bottom inclined wall while the top was exposed to ambient temperature. The other two vertical walls were insulated. The results presented that the increase in Re from 100 to 1000 improved heat transfer by 57.1%. An inverse relationship between thermal storage capacity and thermal effectiveness was also observed, which means that as the thermal storage capacity increases, the thermal effectiveness decreases. Ouri et al. [205] studied the effect of convective heat transfer in an L-shaped vented cavity that contained an inner rotating cylinder. The cold fluid entered the cavity through the top lid, while the lower wall was hot, and the remaining boundaries were adiabatic. Their findings showed that Nuavg, the average Nusselt number, increased by 180% for the highest Re and 19% and 8% for cylinder rotational speeds of 1000 and −1000, respectively. In addition, the spatial Nuavg, which is the Nusselt number at different points within the cavity, showed an increase by varying the cylinder size up to 86% and 33.5% at cylinder rotational speeds of 1000 and −1000, respectively.

5.4. Lid-Driven Cavity

5.4.1. Square Cavity

In a study by Moallemi & Jang [11], the hydraulic and thermal behaviors in a square cavity were examined when a shearing force was applied by moving a glass sheet on the top wall and combined with the buoyancy force from heating the bottom wall. The results showed that the influence of buoyancy was clearer on heat transfer for higher values of Pr with constant Re and Gr. Additionally, for a minimum level of buoyancy, forced convection heat transfer was dominant and independent of Ri. The study also found that as buoyancy increased, the heat transfer mechanism transitioned from forced convection to mixed convection, with Nu_{avg} being a function of Pr. In a study by Chamkha & Abu-Nada [42], the mixed convection of a water-Al_2O_3 nanofluid flow in single and double lid-driven square cavities was examined using different nanofluid viscosity approaches. The top lid-driven wall was kept at a constant hot temperature, while the bottom lid-driven wall was set at a cold temperature. The results showed that at moderate and large Ri, the increase in χ led to an improvement in the rate of heat transfer for single and double-lid-driven cavities for both the Pak and Cho correlation and the Brinkman model. Additionally, in the single lid-driven cavity and for small Ri, Pak and Cho's correlation predicted a reduction in Nu_{avg}. However, for other conditions, an increase in Nu_{avg} was predicted by the Pak and Cho correlation, which was larger than the Brinkman model for all values of χ. In a study by Ahmed et al. [48], a numerical examination of MHD mixed convection flow in an oblique lid-driven square enclosure with an opposite temperature gradient was conducted. The sinusoidal temperature distribution was applied to the right and left walls, the top wall was considered as a moving boundary, and a zero velocity was considered for the bottom wall. The results showed that the increase in Ha had no effect on heat transfer on both vertical walls. Additionally, the rate of heat transfer enhanced with Ha and ϕ increased in the case of opposing buoyancy-driven convection. For forced convection, Nu_{local} increased on the left wall while it decreased on the right wall when the amplitude ratio of the sinusoidal temperature increased. In the study by Muthtamilselvan & Doh [63], the authors numerically investigated the heat transfer behavior of a Cu-H_2O nanofluid flowing in a lid-driven square cavity. They found that Ri had a small effect on heat transfer except for Ri = 4, where a non-linear relationship between the Nusselt number and the volumetric solid fraction was observed. They also found that for non-uniform heating, a sinusoidal behavior of local heat transfer was attained, and a maximum heat transfer occurred in the middle of the bottom wall. In the study by Pekmen & Tezer-Sezgin [209], the authors investigated the mixed convection flow behavior inside a lid-driven square cavity filled with porous media with the application of a magnetic field. The top wall was hot and moving, the bottom wall was cold and fixed, and the vertical walls were adiabatic. They found that as Ha increased, Nu_{avg} decreased due to the retarding effect of the Lorentz force. Additionally, they observed that as Da decreased, the heat transfer became more conductive even as Re increased.

In the study by Ray & Chatterjee [65], the authors discussed the influences of an external magnetic field on an electrically conducting fluid inside a lid-driven square cavity with a conducting cylindrical body inserted. The top wall was moving and fixed at a cold temperature. They found that a rise in Ri led to an enhancement in the rate of heat transfer and fluid temperature, while the presence of a magnetic field reduced the heat transfer rate. Moumni et al. [71] conducted a study on heat transfer and mixed convection flow and behavior in a square cavity with double lid-driven filled with different types of nanofluids. They found that adding nanoparticles to the fluid led to an improvement in the heat transfer rate, with copper and silver nanoparticles showing the highest heat transfer rate due to their high thermal conductivity. They also found that the rate of heat transfer raised with the increase in Ri and Re for constant nanoparticles concentration. Selimefendigil and Öztop [210] conducted a study on the effect of two rotating cylinders on mixed convection of ferrofluid flow inside a square cavity. They found that the enhancement of the Nu_{avg} was 181.5% for a negative angular speed ratio ($\Omega = -400$) and 181.6% for a positive angular speed ratio ($\Omega = 400$). They also found that the rise in the angular speed ratio caused an increase of 91.7% in Nu_{avg} and that an 88.9% enhancement in Nu_{avg} was achieved when the diameter ratio of the cylinders was changed from 2 to 0. Sheremet and Pop [73] conducted a numerical analysis on the mixed convection of a nanofluid flow inside a lid-driven square cavity where both the top and bottom walls were moving in opposite directions. The top and bottom walls were considered hot and cold walls, respectively. Their results showed that the heat transfer mechanism depends strongly on Ri and the moving parameter. They also found that Nu slightly increased with Le except in the counter-direction of moving horizontal walls, where Nu decreased with Le. Jmai et al. [76] conducted research on the effect of a partially heated wall on mixed convection Cu/H_2O nanofluid flow inside a lid-driven square cavity. Each vertical side wall contains a heat source of high temperature, and both the upper and lower boundaries can move in the same and opposite directions and are considered cold. Their results showed that for all speed ratios, Nu increased as Ri decreased. The maximum value of Nu = 54.41 was observed when the speed ratio = -2 and Ri = 0.01.

Rashad et al. [12] conducted a study on MHD mixed convection Cu–water nanofluid flow in a lid-driven square cavity. The upper and lower walls were moving opposite to each other and were considered adiabatic. The right vertical wall was partially heated, and the left wall was partially cold; the other parts of the vertical boundaries were adiabatic. Their results revealed that the highest heat transfer occurred when the size of the heat source was as small as possible and placed at the middle position of the walls. They also concluded that heat transfer decreased with the increase in Ri. The presence of a magnetic field was found to reduce the convective heat transfer, and the presence of nanoparticles led to a decrease in the Nu. Selimefendigil et al. [84] conducted a numerical analysis to study the effect of Ri, Ha, magnetic field inclination angles, and the combination of upper and lower diagonal domains on the hydraulic and thermal behavior inside a lid-driven square cavity. They found that Nu_{avg} decreased by 80.14% when Ri increased from 0.01 to 100 for inclinations angles of 90 and 0 degrees. They also found that increasing the magnetic inclination angle of the upper triangular domain led to a higher average heat transfer compared to increasing the magnetic field in the lower triangular domain. Selimefendigil & Öztop [82] studied the mixed convection inside a lid-driven square cavity with nanofluid. The cavity had elastic side walls, where the left boundary was moving upward and fixed at a constant temperature, while the right wall was a hot one. They concluded that the rate of heat transfer is increased with increasing Ri, Ha, and nanoparticles concentration. However, the rate of heat transfer is decreased with the increasing inclined angle of the magnetic field. Additionally, the study found that the influence of elasticity on the heat transfer rate is considerable, where it increased with increasing elasticity. In the study by Gangawane [93], mixed convection heat transfer was numerically explored in a top lid-driven square cavity with a triangular heated block and constant heat flux. The top wall was moving while the other walls were kept stationary, and the upper and lower boundaries were adiabatic while the vertical boundaries were at ambient temperature. Nu_{avg} increased up to a Re_{cr} between 190–220 and then began to decrease, particularly for Gr greater than 50. In the study by Gibanov et al. [95], Al_2O_3-H_2O nanofluid flow was numerically studied in a lid-driven square cavity. The upper wall was hot and moving, while the bottom wall was fixed and cold. Nu_{avg} was found to decrease with an increase in Ri and the backward step ratio.

The study by Khanafer and Aithal [102] investigated the effects of a rotating cylinder on mixed convection flow in a lid-driven square cavity. Their results demonstrated that the presence of the cylinder led to an increase in Nu_{avg} and that clockwise rotation led to an increase in $Nu_{avg,}$ while counter-clockwise rotation led to a decrease in Nu_{avg} with an increase in rotational speed. The study by Selimefendigil et al. [105] examined the effects of the magnetic field, Ri, E, Ha, nanoparticle concentration, and the presence of a flexible wall on the MHD flow of a nanofluid inside a square cavity. They found that Nu_{avg} increased with the increase in Ri and observed 74.35% of heat transfer enhancement for Ri = 5. They also found that 66.5% heat transfer enhancement was obtained for $E = 10^4$ N/m^2 as compared to the case $E = 2.5 \times 10^5$ N/m^2. Additionally, if Ha is reduced from 50 to 0, there will be an improvement in the rate of heat transfer by 54.55%. If the nanoparticles concentration increased from 0 to 0.04, there would be an improvement in heat transfer by 33.87%. The existence of a flexible wall led to an enhancement in heat transfer by 13.2%. Gibanov et al. [96] investigated mixed convection ferrofluid flow in a square cavity with a lid-driven with a moving, cold upper wall and a hot bottom wall and found that Nuavg at the heated wall increases with the increase in Ha and the thickness of porous media. Hussain et al. [99] examined the effect of an inclination angle on the heat transfer in a double lid-driven square cavity filled with Al_2O_3-H_2O nanofluid, with two fixed heat sources at the bottom wall. They confirmed that heat transfer is improved with the increase in nanoparticles concentration and Ri. Additionally, an increase in inclination angle caused an increase in Nuavg because of the left heat source, but the inverse behavior was noticed for the right heat source. Alsabery et al. [111] studied the conjugate mixed convection of H_2O-Al_2O_3 nanofluid flow inside a square cavity with a double lid driven containing a solid inner object. The top wall was kept at a constant cold temperature and moved to the right, while the bottom wall moved to the left and was kept at a fixed high temperature. The vertical walls were insulated. The study found that the presence of nanofluid enhanced the rate of heat transfer, but at low Re and high Ri, it had an inverse effect on the Nu.

Astanina et al. [110] studied mixed convection of Al_2O_3-H_2O nanofluid flow in a square cavity with a lid-driven, including two layers of porous media at the bottom with different thermal properties, permeability, and porosity. The lower wall was kept at a hot temperature, and the top moving wall was considered cold. The other walls were adiabatic. The study found that heat transfer enhanced with an increase in Ri for constant Re. It also found that Nu_{avg} reduced for different ranges of porous layer thicknesses when Ri > 1. Gangawane et al. [115] studied mixed convection flow in a square cavity containing a heated triangular block placed at the center of the cavity. The top wall was moving and insulated, while the lower wall was fixed and insulated as well, and the vertical wall was exposed to ambient temperature. The triangular block was considered isothermal and at a higher temperature than the ambient temperature. The results showed that there was a 50% increase in heat transfer when the size of the block increased from 10% to 30%. Gibanov et al. [116] studied the effect of Ri, the thickness of the lower wall, thermal conductivity ratio, and nanoparticle concentrations of Al_2O_3-H_2O nanofluid flow inside a lid-driven square cavity. The top lid was moving and hot, while the bottom wall was considered cold. The other vertical walls were insulated. The study found that the increase in thermal conductivity ratio and nanoparticle ratio led to an increase in heat transfer rate, while the increase in Ri and thickness of the bottom wall reduced heat transfer. Razera et al. [123] studied the effect of a fin on mixed convection flow inside a lid-driven square cavity. A lower wall was considered as the first position for the fin and then located on the side walls. The fin surface was considered a hot spot with high temperature, while the vertical and lower walls were set to be adiabatic. The upper moving surface was considered to be cold. The results showed that the fins on the right wall gave the highest Nusselt number while the fins on the lower wall gave an intermediate performance between the three cases. Hussain et al. [117] investigated the influence of an inclined magnetic field on the mixed convection H_2O-Al_2O_3 nanofluid flow inside a double-lid driven square cavity. The top and bottom walls were moving in opposite directions, and both walls were insulated. The left vertical wall was at a hot temperature, and the right one was considered to be cold. The results presented that Nu_{avg} increased with the increase in χ and decreased with the increase in Ri. Furthermore, Nu_{avg} reduced with the increase in Ha and the inclination angle of the magnetic field.

Taghizadeh & Asaditaheri [127] studied heat transfer by convection through an inclined lid-driven square cavity containing a circular porous cylinder placed at the center of the cavity. The lower and upper walls were considered hot and cold walls, respectively, and the vertical walls were considered adiabatic. The upper wall was moving at a steady speed, and the other walls remained fixed. They found that for all inclination angles, the increase in Da enhanced heat transfer when Ri = 0.01. For Ri $\geq$ 1, the rate of heat transfer decreased. For Ri = 5 and 10, heat transfer was more affected by the angle of inclination of the cavity, which weakens buoyancy forces and decreases the Nusselt number. Barnoon et al. [132] studied entropy generation and mixed convection of nanofluid flow in a lid-driven square cavity. The cavity was subjected to a magnetic field from the bottom wall, and a velocity was applied to the upper lid. They examined the effect of insulated and isothermal two rotating cylinders inside the cavity. They found that the increase in Ha led to reducing the heat transfer rate. The presence of an isothermal cylinder gave a higher rate of heat transfer than the existence of an insulated cylinder. However, in general, the cylinders inside the cavity-enhanced the rate of heat transfer, and the increase in angular speed of the cylinder led to a rise in the rate of heat transfer. Additionally, the fraction of nanofluid equal to 3% with a tilt angle of 0 of the cavity produces a higher rate of heat transfer. Lamarti et al. [139] explored mixed convection flow inside a square cavity with a periodically oscillating top lid. They discovered that the local Nusselt number starts high for high Re and drops rapidly. They also found that for a constant Gr, Re had a large effect on Nu_{avg} and that forced convection became dominant. Alsabery et al. [145] investigated the influence of a magnetic field on mixed convection of nanofluid flow in a square cavity with a lid driven with a thick triangular wall placed in the lower left corner. They found that the rate of heat transfer increased with the increase in Re and Ri. The maximum Nu occurred at Re = 500 and χ = 0.02. Alsabery et al. [160] studied the influence of hybrid nanofluid H_2O-Cu-Al_2O_3 flow inside a square lid-driven cavity with two vertical wavy walls containing a square block. The left wall was kept at a high temperature, the right wall was cold, and the top and bottom walls were adiabatic. They found that Nu_{avg} increased with the increase in Ri and that Nu increased with the increase in χ.

Hussain et al. [165] explored the effect of fins and inclined magnetic fields on square cavities filled with H_2O-Cu nanofluid with single and double-lid driven. The upper lid had a hot temperature, and the lower wall had a cold temperature, while the other walls were insulated. Two adiabatic vertical fins were installed on the upper wall, and an inclined magnetic field was applied to both cavities. They found that with the presence of fins, the convective heat transfer decreased with an increase in Ha and Ri. Additionally, Nu_{avg} decreased with an increase in the number of fins. Ahmed et al. [182] studied the flow and heat transfer behavior in a porous lid-driven square cavity filled with Al_2O_3-Cu/water hybrid nanofluid. The horizontal walls were moving at a constant speed, considered adiabatic, and the vertical walls were stationary. The left wall was hot, and the right one was cold. They found that the thermophoresis parameters had a very small effect on Nu_{avg}. Furthermore, Le had no effect on heat transfer enhancement, and Da had very little effect on the variation of Nu_{avg}. Ali et al. [183] examined mixed convection nanofluid flow inside a square cavity with lid-driven. The top wall was cold and moving horizontally in both directions, while the hot bottom wall was fixed and partially heated. A rotating flat plate was inserted in the cavity, and a magnetic field was subjected to the cavity. The other remaining parts of the walls were set to be adiabatic. The results confirmed that the highest rate of heat transfer occurred when the flat plate length was a quarter of the length of the cavity side (L). The improvement is more than 137.04% as compared to the case of 0.15 L, and it will be 208.89% for the case without the plate. It was also discovered that the heat transfer rate increased by 123.02% for rotational speed = 100, plate length 0.25 L, and nanoparticles concentration = 0.05, as compared with base fluid water. Batool et al. [185] studied heat and mass transfer analysis of a square cavity with lid-driven containing micropolar nanofluids under the influence of magnetic field and buoyancy force. A speed was applied to the upper wall, and the bottom wall was considered hot. The rate of heat transfer became faster at the maximum vortex viscosity parameter. Moreover, an optimized heat transfer mechanism was noticed from the bottom to the top wall, reducing the Brownian motion parameter. Dahani et al. [188] studied mixed convection and surface radiation in a square cavity with double lid-driven. One of the moving walls was considered hot, and the other was set to be cold, while the stationary walls were considered adiabatic. At Ri = 100, the contribution of radiation to the total Nu far outweighs that of convection. To minimize heat transfer, a combined effect of large Ri and angle of inclination close to 180° and non-emissive walls should be considered.

5.4.2. Rectangular Cavity

The study by Balootaki et al. [112] investigated the influence of mixed convection flow in a lid-driven rectangular cavity with a hot-moving upper surface and insulated other surfaces. The presence of a cold obstacle inside the cavity was also considered. The results demonstrated that rising the cavity inclination improves the heat transfer rate under forced convection, and the Nusselt number increases with increasing Rayleigh number for different inclination angles. The study by Louaraychi et al. [140] examined mixed convection flow in horizontal rectangular cavities with single- and double-lid driven using both numerical and analytical methods. It was found that the mixed convection parameter Ra/Pe^3 can be used to distinguish between three convection regimes: natural, mixed, and forced convection. The results showed that when forced convection is dominant, Nu_{avg} remained constant for small values of Ra and slightly increased during mixed convection heat transfer. Beyond this range, a fast linear increase in Nu_{avg} was observed for dominant natural convection heat transfer. Additionally, Nu_{avg} increased with the Peclet number (Pe) due to the shear effect. Tizakast et al. [178] conducted a numerical and analytical study on the double-diffusive mixed convection of a non-Newtonian power-law fluid in a closed rectangular cavity. The study found that the flow intensity and heat and mass transfer were insensitive to an increase in the parameter A for values of A greater than or equal to 24. The results also showed that non-Newtonian double-diffusive mixed convection is controlled by the parameters Ra_T, Pe, Le, and power-law index n. Additionally, the study found that an increase in Le had no effect on heat transfer, while a high buoyancy ratio increased both heat and mass transfer. Tizakast et al. [199] conducted a numerical and analytical study on the Rayleigh-Bénard double-diffusive mixed convection flow inside horizontal rectangular cavities subjected to uniform heat and mass fluxes along the sliding horizontal walls, with the other walls fixed and insulated. They confirmed that the heat and mass transfer and flow intensity became insensitive to the aspect ratio, A, for values of A greater than or equal to 28. For a Prandtl number greater than or equal to 10, the flow behavior became independent of Pr. The study concluded that Newtonian Rayleigh–Bénard double-diffusive mixed convection is controlled by the parameters Pe, Ra_T, Le, buoyancy ratio N, and power-law index *n*.

5.4.3. Triangular Cavity

Selimefendigil & Öztop [107] conducted research on the mixed convection of nanofluid flow in a triangular cavity with lid-driven. They found that for negative and positive x-direction motion, Nu_{avg} decreased by 41.02% and 38.77% for Ri, equal to 50 and 0.05, respectively. Additionally, Nu_{avg} decreased by 55% when Ra increased from 10^4 to 10^7. Furthermore, the study found that an enhancement of 22.95% was obtained for Nu_{avg} for the highest nanoparticle concentration. Soomro et al. [157] conducted a study on the convection heat transfer inside a lid-driven triangular cavity subjected to a horizontal constant magnetic field. The upper moving wall was set as hot, while the side inclined walls were adiabatic, and a cold temperature cylinder was placed at the center of the cavity. The study found that Nu_{avg} increased with the increase in Ri at a high flow shear rate. Additionally, Nuavg increased with the increase in Re when high viscous forces were present. Shahid et al. [175] conducted a study on the mixed convection flow inside a heated lid-driven right-angle isosceles triangular cavity. The horizontal top side of the cavity was moving horizontally and kept adiabatic, the vertical wall was hot, and the inclined wall was cold. The results of the study showed that natural convection became more dominant than forced convection as Gr increased, and this led to an increase in Nu_{avg}. Additionally, for small values of Ri, the forced convection was more dominant due to the effect of shear forces generated by the moving lid. Xiong et al. [180] studied mixed convective heat transfer of MHD fluid flow in a lid-driven triangular cavity subjected to heating by a thick triangular wall. The top wall was moving to the right with a high temperature, while the inclined sidewalls were adiabatic. Cold obstacles were placed near the side walls and along the left and right side inclined walls with a temperature lower than the top wall temperature. The results showed that the expansion of Ha led to a reduction in heat transfer. Additionally, for higher Ri, the heat transfer was enhanced due to the increase in shear rate. The study also found that for the left side obstacle, the heat transfer rate increased due to an increase in Re, while the opposite behavior was observed for Ha and Ri. For the right obstacle, the heat transfer rate was strengthened along the upper wall due to the emergence of Re, while a reverse process was followed for Ha and Ri.

5.4.4. Cubical Cavity

The study by Karbasifar et al. [119] focused on the heat transfer process of mixed convection Al_2O_3-H_2O nanofluid flow in a lid-driven cubical cavity containing a hot elliptical centric cylinder. The results showed that Nu_{avg} decreased as Ri increased for fixed χ and ϕ. Additionally, Nu_{avg} raised with the increase in χ for constant Ri and ϕ. It was also found that Nu_{avg} increased slightly when ϕ increased for constant Ri. The study also found that Nu_{avg} increased with the increase in Re and χ. In the study by Kareem & Gao [120], they explored the effect of a SiO_2-H_2O nanofluid on turbulent mixed convection inside a cubical cavity with a heated top wall and a cold bottom wall. They found that the presence of the nanofluid improved the heat transfer effectiveness, with the highest Nu_{avg} being observed for a rotational speed of -5. Additionally, the rotational velocity of the cylinder had a stronger effect on the bottom wall than on the top wall. Al-Rashed et al. [131] studied the flow of H_2O-Al_2O_3 nanofluid in an oblique lid-driven cubical cavity, including a hot elliptical centric cylinder. They found that raising the concentration of nanoparticles led to an increase in heat transfer coefficients, and Nu decreased with the increase in Ri for constant χ and inclination angle. Additionally, increasing the inclination angle slightly increased Nu for constant Ri. Alsabery et al. [146] investigated the mixed convection

H_2O-Al_2O_3 nanofluid flow inside a cubical chamber containing a heat-conducting cylinder. The right vertical wall was partially heated, the left vertical wall was considered cold, and the other walls were insulated. They found that increasing χ led to an improvement in heat transfer for a fixed Re = 10.

5.4.5. Other Types of Cavities

Abu-Nada and Chamkha [57] numerically investigated the mixed convection flow of CuO-H_2O nanofluid in a cavity with a wavy wall with a lid-driven. The top wall was hot and moving, while the cold bottom wall was wavy. They found that for all values of Ri, Nu was maximum at the left top corner of the cavity and then decreased along the heated lid until it reached zero at the middle position of the lid. After that, Nu increased slightly at the second half of the wall and then vanished at the right side of the cavity. Hatami et al. [98] investigated the behavior of nanofluid flow inside a T-shaped lid-driven porous cavity. The top moving wall was cold, while the bottom wall was hot, and the other walls were insulated. They found that both Nu_{local} and Nu_{avg} increased with the increase in Ri and Re. Additionally, they observed that increasing Da and χ led to an increase in Nu_{avg}. Selimefendigil et al. [106] studied mixed convection nanofluid flow inside a trapezoidal cavity with an adiabatic stationary cylinder. Both the left and right walls were flexible walls. The top wall was moving and considered cold, while the bottom was stationary and considered hot. The other walls were considered adiabatic. They found that heat transfer increased by 9.8% when the value of elastic modulus was raised from 10^3 to 10^5 when the elastic wall inclination was equal to 0 degrees. Additionally, they observed that Nu_{avg} increased linearly with the increase in χ, and the heat transfer was enhanced by 25.30% at the highest χ as compared to the base fluid. Cho [134] analyzed heat transfer and entropy generation of Cu-H_2O nanofluid in a lid-driven cavity and subjected it to an oblique magnetic field. The left wall was a hot moving wall, the right wavy wall was cold, and the other walls were insulated. Their results showed that Nu increased with the increase in χ or wave amplitude of the wavy surface. Additionally, during the natural convection-dominated regime, Nu had a higher value for the magnetic field inclination of 90° and 270°, while the opposite behavior was observed for the inclination of 0° and 180°. During the forced convection-dominated regime, Nu had a higher value for the magnetic field inclination of 135° and 315°, while the opposite behavior was observed for the inclination of 90° and 270°. Hadavand et al. [136] studied mixed convection H_2O-Ag nanofluid flow inside a semi-circular cavity with a lid-driven. The left side of the cavity was heated by injecting hot water, while the upper lid was cold and moving. Other surfaces were considered adiabatic. Their results showed that the best heat transfer behavior was observed for Ri = 1, χ = 0.06, and $\phi = -45°, 0°, -90°, 45°$, and 90°.

Selimefendigil and Öztop [142] conducted a study on the influence of a magnetic field on mixed convection nanofluid flow in an oblique L-shaped cavity. They found that Nu_{avg} increased by 42.2% and 39.9% for water and nanofluid, respectively, when the cavity inclination angle was changed from 180° to 150°. They also found that Nu_{avg} was reduced by 11% when an elastic wall was used instead of a solid wall at a specific Ri = 0.03. Additionally, Nu_{avg} was reduced by approximately 42% for both fluid and nanofluid for the lowest and highest Ra. Haq et al. [150] examined the heat transfer behavior in a hexagonal cavity filled with water and subjected to a magnetic field. They discovered that the heat transfer could be improved by using a cylinder with variable thermal conditions in the middle of the cavity and by increasing Ha. The Nusselt number at the heated surface decreased as Ri decreased for a specific Re = 300 and Ha = 10. Noor et al. [192] studied the forced convection of MHD flow inside a trapezoidal cavity with a circular object inside. They found that Nu decreased near the heated top lid and remained constant along the horizontal direction of the top lid. Additionally, they found that at low Ri, Nu had a higher value at the top hot-moving wall. Conversely, at high Ri, Nu decreased abruptly along the heated part of the top lid for both heated and cold conditions of the circular object. Polasanapalli and Anupindi [194] studied the mixed heat transfer behavior in an air-filled concentric annular cavity with the inner surface being hot and the outer surface being cold. They considered four different rotational conditions of cylinders: counter-rotating cylinders, co-rotating cylinders, outer rotating cylinders, and inner rotating cylinders. They found that the rate of heat transfer is lower for the differentially heated cavity, regardless of the rotational velocity of the cylinders. Shah et al. [198] studied the mixed convection flow of CuO-H_2O nanofluid in a lid-driven corrugated porous cavity with a cylindrical object inside. The object had three different surface conditions: adiabatic, cold, and hot. Internal heat generation/absorption and uniform heat were applied to the vertical wall, and the bottom was insulated. They found that Nu increased as Re increased. The highest Nu was attained for χ = 0.05. Xia et al. [200] studied the mixed convection flow of H_2O-Al_2O_3 nanofluid inside a T-shaped lid-driven cavity with a hot obstacle at different positions. The top lid was moving to the right and had a cold temperature, while all the other walls were adiabatic except the hot obstacle, which was considered hot. Their results showed that as Ri increased, the heat transfer decreased. Additionally, they found that an increase in χ helped to increase the rate of heat transfer. Furthermore, an increase in aspect ratio caused a reduction in the rate of heat transfer. Zhang et al. [202] investigated Ag-water nanofluid flow inside a semi-elliptic lid-driven cavity. The top moving lid was cold, while the curved bottom wall was hot. Their results showed that the presence of nanoparticles with high circulation led to an increase in the rate of heat transfer. Additionally, the heat transfer rate enhanced with the increase in Gr for lower Ri.

6. Conclusions

Heat transfer analysis inside cavities has been investigated by many authors. Different geometries have been adopted for the enclosed cavity in order to enhance heat transfer and improve the flow behavior inside the cavity. A high percentage of published articles worked on rectangular and square cavities, while the other geometries were triangular, trapezoidal, semi-circular, etc. Furthermore, some articles discussed the flow behavior of two adjacent rectangular domains that are used in building blocks or some types of windows. Two main hydraulic boundary conditions are applied: fixed and moving boundaries (lid-driven), while several thermal boundary conditions are applied, starting with temperature difference, heat flux, cold and hot fins, and other types of objects, etc. Moreover, the effect of sinusoidal and triangular surfaces and flexible boundaries are also considered. In addition, several articles have studied the influence of magnetic fields and different fluids types on heat transfer.

Through the review of natural convection, the findings revealed that Nu increased with the rise of Ra and nanoparticles concentration. Moreover, Nu decreased with the increase in Ha. The effect of objects inside the cavity varied with the boundary conditions applied to the surface of the object and conditions of it whether it was fixed or moving. Moreover, Nu decreased with the increase in Da considering porous material inside the cavity. The cavity with forced convection is discussed by many authors. In addition to the previous mentioned boundary conditions and types of cavities, a moving boundary is applied (lid-driven cavity). This type of condition will move the flow inside the cavity from natural convection to forced convection or mixed convection between two types.

During the lid-driven cavity, there will be an interchange relationship between forced, and natural convection depending on the applied boundary conditions and types of fluids that have been used. Some results demonstrate that buoyancy will be dominant for high values of Pr while forced convection controls the flow process inside the cavity. The influence of adding different nanoparticles led to an increase in Nu and rate of heat transfer with the rise in nanoparticles concentration. In a few cases, nanofluid had an inverse effect on Nu at low Re when Ri is high. The majority of published articles demonstrated that the increase in Ri led to a decrease in Nu and the rate of heat transfer. In the case of elastic boundaries, some results presented that the heat transfer raised with an increase in Ri. In most cases, the rate of heat transfer improved with the increase in Ha. Some articles referred to a rise in Nu with the increase in Ha, with some boundaries being elastic and the cavity being filled with porous media. The existence of some objects inside the cavity had helped to increase in heat transfer rate. For example, rotating cylinders, flat plates, triangular blocks, rectangular blades, etc., led to an increase in Nu.

Finally, this configurative systematic review focuses on the importance of heat transfer enhancement or degeneration in relation to various factors such as the shape of the cavity, the presence of fins/cylinders/blocks/blades, and the use of fluids/nanofluids/hybrid-nanofluids and/or porous media. The review also proposes future research directions based on an extensive literature review. The review includes details of the flow domain, dimensions, type of flow, parameters and their ranges, meshing, CFD methods, and algorithms, which are presented in tabular form. Additionally, the review provides extensive details on CFD validation. The authors believe that this is the first time such detailed information has been presented in a review and that it will be valuable for future researchers.

7. Future Work

In conclusion, research on heat transfer behavior in cavities has been highlighted since around 1965, and much research is still being carried out by researchers. However, several key points are not highlighted yet and can be considered as future research, and such key points are mentioned below:

- Most of the studies focused on laminar natural/mixed/forced convection flow, but very few studies considered turbulent flow regimes.
- Most recently, rotating blades or plates inside the cavity received attention from researchers. Still, no work is conducted considering the design, shape, and aerodynamic behavior of blades.
- Will it be possible to develop a general form of correlation for the average Nusselt number?
- Very little research is found considering the LES and DNS modeling in cavities for transient/turbulent flow regimes. This area should be considered a high-interest area in the future.
- The choice of turbulence models has not been highlighted yet by researchers. It can be an important study.
- Different types of shapes are considered in the literature, but more research is suggested to find an optimum design of the physical domain that can give maximum heat transfer enhancement.
- Very little or limited research work is conducted considering the presence of nanoplastic or microplastic in fluids inside a cavity. It is highly considered research for future studies.
- Study the hydraulic and thermal behavior of two immiscible fluids (for example, air and water) inside a cavity.

Author Contributions: Conceptualization, S.C.S.; methodology, G.S.; data curation, G.S. and A.A.Y.A.-W.; writing—original draft preparation, G.S. and A.A.Y.A.-W.; writing—review and editing, S.C.S. and M.C.P.; supervision, S.C.S. All authors have read and agreed to the published version of the manuscript.

Funding: This research received no external funding.

Data Availability Statement: All data are available in the manuscript.

Conflicts of Interest: The authors declare that they have no known competing interests.

Nomenclature

A	Aspect ratio
AB	Adams-Bashforth method
ADI	Alternate Direct Implicit scheme
ALE	Arbitrary-Lagrangian–Eulerian approach
Am	Amplitude
ANFIS	Adaptive Neuro-Fuzzy Interface System

b	Size of blocage (%)
B	Dimensionless magnetic induction
BGK	Bhatnagar–Gross–Krook
BiCGStab	Biconjugate gradient stabilized method
C	Concentration
CDS	Central differencing schemes
CN	Crank-Nicolson
COBYLA	Constrained Optimization BY Linear Approximations
C_p	Specific heat
DADI	Dynamic alternating direction implicit scheme
DRBEM	Dual reciprocity boundary element method
DNS	Direct numerical simulation
d_p	Nanoparticles diameter
E	Young's modulus
f	Fluid
FDM	Finite difference method
FEM	Finite element method
FVM	Finite volume method
FSI	Fluid-structure interaction
GE	Gaussian Elimination method
Gr	Grashof number
Gr_C	Mass transfer Grashof number
Gr_T	Heat transfer Grashof number
GS	Gauss-Seidel method
h	Cavity height
Ha	Hartmann number
HO-MFA	High-order mesh-free approach
IEFG–RIPM	Improved element-free Galerkin–reduced integration penalty method
J	Joul heating parameter
K	Thermal conductivity ratio
K_l	Low conductivity material
LB	lattice Boltzmann method
LES	Large Eddy Simulation
Le	Lewis number
L_h	Vertical distance between bottom of the cavity and the hot disturbance area
L_c	Vertical distance between bottom of the cavity and the cold disturbance area
M	Magnetic parameter
Ma	Mach number
MLS	Moving least squares
MRT	Multiple-Relaxation-Time
MWCNT	Multi wall carbon nanotubes
n	Flow behavior index for a power-law fluid
nf	Nanofluid
N	Buoyancy ratio
N_b	Brownian motion
N_t	Thermophoresis parameter
NR	Newton-Raphson method
Nu	Local Nusselt number
$\overline{Nu}$	Average Nusselt number (Nu_{avg})
Nu_L	Average Nusselt number based on the cavity length
Nu_{ymL}	The mean of the local Nusselt numbers
Os	Ostrogradsky number
Pe	Peclet number
PCM	Phase change material
Pr	Prandtl number
Pr_t	Turbulent Prandtl number
q	Heat generation or absorption
QUICK	Quadratic upstream interpolation for convective kinematics

R	Internal to external Rayleigh numbers ratio
Ra	Rayleigh number
Ra_T	Generalized thermal Rayleigh number
Ra_I	Internal Rayleigh number
Ra_E	External Rayleigh number
Ra_m	Magnetic Rayleigh number
Ra_L	Average Rayleigh number based on the cavity length
Ra_{yml}	The mean of the local Rayleigh numbers
Rbf-Pum	Radial basis function-based partition of unity method
RBSOR	Red and black SOR method
Rd	Radiation parameter
Re	Reynolds number
Re_w	Rotational Reynolds number
Ri	Richardson number
RK	Runge-Kutta method
RSM	Response surface methodology
s, np	Solid or nanoparticles
Sc	Schemidt number
SEM	Spectral element method
Sh	Sherwood number
SIMPLE	Semi-implicit method for pressure-linked equations
SOR	Successive over-relaxation
SUR	Successive under relaxation
Sr	Soret parameter
Ta	Taylor number
TDMA	Tri-diagonal matrix algorithm
TFM	Triangular factorization method
Tp	Partition thickness
Tr	Thermal conductivity ratio,
TS	Taylor series
UCS	Upwind compact Scheme
UDS	Upwind difference Scheme
URANS	Averaged Navier–Stokes
x	Horizontal coordinate
y	Vertical coordinate
φ	Inclination angle
χ	Nanoparticles volume fraction
ε	Emissivity
λ	Number of undulation
κ	Thermal conductivity
ϕ	Phase deviation
ρ	Density
Ω	Rotational speed
ω	Oscillation frequency
ϖ	Angular frequency
μ	Dynamic viscosity

References

1. Holman, J.P. *Heat Transfer*, 10th ed.; Mcgraw-Hill Higher Education: Boston, MA, USA, 2010; ISBN 0073529362.
2. Wee, H.K.; Keey, R.B.; Cunningam, M.J. Heat and moisture transfer by natural convection in a rectangular cavity. *Int. J. Heat Mass Transf.* **1989**, *32*, 1765–1778. [CrossRef]
3. Yu, P.X.; Xiao, Z.; Wub, S.; Tian, Z.F.; Cheng, X. High accuracy numerical investigation of double-diffusive convection in a rectangular cavity under a uniform horizontal magnetic field and heat source. *Int. J. Heat Mass Transf.* **2017**, *110*, 613–628. [CrossRef]
4. Jiang, Y.; Zhou, X. Analysis of flow and heat transfer characteristics of nanofluids surface tension driven convection in a rectangular cavity. *Int. J. Mech. Sci.* **2019**, *153–154*, 154–163. [CrossRef]

5. Alqaed, S.; Mustafa, J.; Sharifpur, M. Numerical investigation and optimization of natural convection and entropy generation of alumina/H_2O nanofluid in a rectangular cavity in the presence of a magnetic field with artificial neural networks. *Eng. Anal. Bound. Elem.* **2022**, *140*, 507–518. [CrossRef]
6. Hatami, M. Numerical study of nanofluids natural convection in a rectangular cavity including heated fins. *J. Mol. Liq.* **2017**, *233*, 1–8. [CrossRef]
7. Akhter, R.; Ali, M.M.; Alim, M.A. Entropy generation due to hydromagnetic buoyancy-driven hybrid-nanofluid flow in partially heated porous cavity containing heat conductive obstacle. *Alex. Eng. J.* **2023**, *62*, 17–45. [CrossRef]
8. Alam, M.S.; Billah, M.M.; Hossain, S.M.C.; Keya, S.S.; Haque, M.M. MHD influence on convective heat transfer in a semi-circular cavity using nonhomogeneous nanofluid model. *Int. J.* **2022**, *16*, 100197.
9. Esfe, M.H.; Rostamian, H.; Toghraie, D.; Hekmatifar, M.; Abad, A.T.K. Numerical study of heat transfer of U-shaped enclosure containing nanofluids in a porous medium using two-phase mixture method. *Case Stud. Therm. Eng.* **2022**, *38*, 102150. [CrossRef]
10. Geridonmez, B.P.; Oztop, H.F. The effect of inclined periodic magnetic field on natural convection flow of Al_2O_3-Cu/water nanofluid inside right isosceles triangular closed spaces. *Eng. Anal. Bound. Elem.* **2022**, *141*, 222–234. [CrossRef]
11. Moallemi, M.K.; Jjang, K.S. Prandtl number effects on laminar mixed convection heat transfer in a lid-driven cavity. *Int. J. Heat Mass Transf.* **1992**, *35*, 1881–1892. [CrossRef]
12. Rashad, A.M.; Ismael, M.A.; Chamkha, A.J.; Mansour, M.A. MHD mixed convection of localized heat source/sink in a nanofluid-filled lid-driven square cavity with partial slip. *J. Taiwan Inst. Chem. Eng.* **2016**, *68*, 173–186. [CrossRef]
13. Versteeg, H.K. *An Introduction to Computational Fluid Dynamics: The Finite Volume Method*, 2nd ed.; Henk, K., Malalasekera, W., Malalasekera, W., Eds.; Pearson Education Ltd.: Harlow, UK, 2007.
14. Sasaguchi, K.; Kusano, K.; Viskanta, R. A numerical analysis of solid-liquid phase change heat transfer around a single and two horizontal. vertically spaced cylinders in a rectangular cavity. *Int. J. Heat Mass Transf.* **1997**, *40*, 1349–1354. [CrossRef]
15. Al-Amiri, A.; Khanafer, K.; Bull, J.; Pop, I. Effect of sinusoidal wavy bottom surface on mixed convection heat transfer in a lid-driven cavity. *Int. J. Heat Mass Transf.* **2007**, *50*, 1771–1780. [CrossRef]
16. Saha, G.; Saha, S.; Islam, M.Q.; Akhanda, M.A.R. Natural convection in enclosure with discrete isothermal heating from below. *J. Nav. Archit. Mar. Eng.* **2007**, *4*, 1–13. [CrossRef]
17. Saha, S.C.; Lei, C.; Patterson, J.C. Effect of aspect ratio on natural convection in attics subject to periodic thermal forcing. *ANZIAM J.* **2007**, *48*, C677–C691. [CrossRef]
18. Tiwari, R.K.; Das, M.K. Heat transfer augmentation in a two-sided lid-driven differentially heated square cavity utilizing nanofluids. *Int. J. Heat Mass Transf.* **2007**, *50*, 2002–2018. [CrossRef]
19. Saha, S.; Sultana, T.; Saha, G.; Rahman, M.M. Effects of discrete isoflux heat source size and angle of inclination on natural convection heat transfer flow inside a sinusoidal corrugated enclosure. *Int. Commun. Heat Mass Transf.* **2008**, *35*, 1288–1296. [CrossRef]
20. Varol, Y.; Oztop, H.F.; Mobedi, M.; Pop, I. Visualization of natural convection heat transport using heatline method in porous non-isothermally heated triangular cavity. *Int. J. Heat Mass Transf.* **2008**, *51*, 5040–5051. [CrossRef]
21. Chen, C.-L.; Cheng, C.-H. Numerical study of the effects of lid oscillation on the periodic flow pattern and convection heat transfer in a triangular cavity. *Int. Commun. Heat Mass Transf.* **2009**, *36*, 590–596. [CrossRef]
22. Noor, D.Z.; Kanna, P.R.; Chern, M.-J. Flow and heat transfer in a driven square cavity with double-sided oscillating lids in anti-phase. *Int. J. Heat Mass Transf.* **2009**, *52*, 3009–3023. [CrossRef]
23. Ouertatani, N.; Cheikh, N.B.; Beya, B.B.; Lili, T.; Campo, A. Mixed convection in a double lid-driven cubic cavity. *Int. J. Therm. Sci.* **2009**, *48*, 1265–1272. [CrossRef]
24. Basak, T.; Roy, S.; Ramakrishna, D.; Pandey, B.D. Analysis of heat recovery and heat transfer within entrapped porous triangular cavities via heatline approach. *Int. J. Heat Mass Transf.* **2010**, *53*, 3655–3669. [CrossRef]
25. Lei, C.; O'Neill, A. Effects of adiabatic extensions on heat transfer through a differentially heated square cavity. *Int. Commun. Heat Mass Transf.* **2010**, *37*, 1221–1225. [CrossRef]
26. Saha, G. Finite element simulation of magnetoconvection inside a sinusoidal corrugated enclosure with discrete isoflux heating from below. *Int. Commun. Heat Mass Transf.* **2010**, *37*, 393–400. [CrossRef]
27. Saha, G.; Saha, S.; Hasan, M.N.; Islam, M.Q. Natural convection heat transfer within octagonal enclosure. *IJE Trans. A Basics* **2010**, *23*, 1–10.
28. Saha, S.C.; Patterson, J.C.; Lei, C. Natural convection in attics subject to instantaneous and ramp cooling boundary conditions. *Energy Build.* **2010**, *42*, 1192–1204. [CrossRef]
29. Saha, S.C.; Patterson, J.C.; Lei, C. Natural convection and heat transfer in attics subject to periodic thermal forcing. *Int. J. Therm. Sci.* **2010**, *49*, 1899–1910. [CrossRef]
30. Saha, S.C.; Patterson, J.C.; Lei, C. Natural convection in attic-shaped spaces subject to sudden and ramp heating boundary conditions. *Heat Mass Transf.* **2010**, *46*, 621–638. [CrossRef]
31. Sivasankaran, S.; Sivakumar, V.; Prakash, P. Numerical study on mixed convection in a lid-driven cavity with non-uniform heating on both sidewalls. *Int. J. Heat Mass Transf.* **2010**, *53*, 4304–4315. [CrossRef]
32. Sivakumar, V.; Sivasankaran, S.; Prakash, P.; Lee, J. Effect of heating location and size on mixed convection in lid-driven cavities. *Comput. Math. Appl.* **2010**, *59*, 3053–3065. [CrossRef]

33. Al-Amiri, A.; Khanafer, K. Fluid–structure interaction analysis of mixed convection heat transfer in a lid-driven cavity with a flexible bottom wall. *Int. J. Heat Mass Transf.* **2011**, *54*, 3826–3836. [CrossRef]
34. Cheng, T.S. Characteristics of mixed convection heat transfer in a lid-driven square cavity with various Richardson and Prandtl numbers. *Int. J. Therm. Sci.* **2011**, *50*, 197–205. [CrossRef]
35. Nasrin, R.; Parvin, S. Hydromagnetic effect on mixed convection in a lid-driven cavity with sinusoidal corrugated bottom surface. *Int. Commun. Heat Mass Transf.* **2011**, *38*, 781–789. [CrossRef]
36. Saha, S.C. Unsteady natural convection in a triangular enclosure under isothermal heating. *Energy Build.* **2011**, *43*, 695–703. [CrossRef]
37. Saha, S.C. Scaling of free convection heat transfer in a triangular cavity for Pr > 1. *Energy Build.* **2011**, *43*, 2908–2917. [CrossRef]
38. Yu, Z.-T.; Wang, W.; Xu, X.; Fan, L.-W.; Hu, Y.-C.; Cen, K.-F. A numerical investigation of transient natural convection heat transfer of aqueous nanofluids in a differentially heated square cavity. *Int. Commun. Heat Mass Transf.* **2011**, *38*, 585–589. [CrossRef]
39. Al-Farhany, K.; Turan, A. Numerical study of double-diffusive natural convective heat and mass transfer in an inclined rectangular cavity filled with porous medium. *Int. Commun. Heat Mass Transf.* **2012**, *39*, 174–181. [CrossRef]
40. Arani, A.A.A.; Sebdani, S.M.; Mahmoodi, M.; Ardeshiri, A.; Aliakbari, M. Numerical study of mixed convection flow in a lid-driven cavity with sinusoidal heating on sidewalls using nanofluid. *Superlattices Microstruct.* **2012**, *51*, 893–911. [CrossRef]
41. Basak, T.; Gunda, P.; Anandalakshmi, R. Analysis of entropy generation during natural convection in porous right-angled triangular cavities with various thermal boundary conditions. *Int. J. Heat Mass Transf.* **2012**, *55*, 4521–4535. [CrossRef]
42. Chamkha, A.J.; Abu-Nada, E. Mixed convection flow in single- and double-lid driven square cavities filled with water–Al_2O_3 nanofluid: Effect of viscosity models. *Eur. J. Mech. B Fluid.* **2012**, *36*, 82–96. [CrossRef]
43. Nasrin, R.; Parvin, S. Investigation of buoyancy-driven flow and heat transfer in a trapezoidal cavity filled with water–Cu nanofluid. *Int. Commun. Heat Mass Transf.* **2012**, *39*, 270–274. [CrossRef]
44. Raji, A.; Hasnaoui, M.; Naïmi, M.; Slimani, K.; Ouazzani, M.T. Effect of the subdivision of an obstacle on the natural convection heat transfer in a square cavity. *Comput. Fluid.* **2012**, *68*, 1–15. [CrossRef]
45. Saha, S.C.; Gu, Y.T. Free convection in a triangular enclosure with fluid-saturated porous medium and internal heat generation. *ANZIAM J.* **2012**, *53*, C127–C141. [CrossRef]
46. Saha, S.C.; Gu, Y.T. Natural convection in a triangular enclosure due to non-uniform cooling on top. *ANZIAM J.* **2012**, *53*, C53–C68. [CrossRef]
47. Teamah, M.A.; El-Maghlany, W.M. Augmentation of natural convective heat transfer in square cavity by utilizing nanofluids in the presence of magnetic field and uniform heat generation/absorption. *Int. J. Therm. Sci.* **2012**, *58*, 130–142. [CrossRef]
48. Ahmed, S.E.; Mansour, M.A.; Mahdy, A. MHD mixed convection in an inclined lid-driven cavity with opposing thermal buoyancy force: Effect of non-uniform heating on both side walls. *Nucl. Eng. Des.* **2013**, *265*, 938–948. [CrossRef]
49. Bhardwaj, S.; Dalal, A. Analysis of natural convection heat transfer and entropy generation inside porous right-angled triangular enclosure. *Int. J. Heat Mass Transf.* **2013**, *65*, 500–513. [CrossRef]
50. Cho, C.-C.; Chen, C.-L.; Chen, C.-K. Mixed convection heat transfer performance of water-based nanofluids in lid-driven cavity with wavy surfaces. *Int. J. Therm. Sci.* **2013**, *68*, 181–190. [CrossRef]
51. Elsherbiny, S.M.; Ragab, E.H. Laminar natural convection in inclined rectangular cavities with a localized heat source. *Alex. Eng. J.* **2013**, *52*, 249–257. [CrossRef]
52. Huelsz, G.; Rechtman, R. Heat transfer due to natural convection in an inclined square cavity using the lattice Boltzmann equation method. *Int. J. Therm. Sci.* **2013**, *65*, 111–119. [CrossRef]
53. Khanafer, K.; Aithal, S.M. Laminar mixed convection flow and heat transfer characteristics in a lid-driven cavity with a circular cylinder. *Int. J. Heat Mass Transf.* **2013**, *66*, 200–209. [CrossRef]
54. Ramakrishna, D.; Basak, T.; Roy, S. Analysis of heatlines and entropy generation during free convection within trapezoidal cavities. *Int. Commun. Heat Mass Transf.* **2013**, *45*, 32–40. [CrossRef]
55. Sivasankaran, S.; Sivakumar, V.; Hussein, A.K. Numerical study on mixed convection in an inclined lid-driven cavity with discrete heating. *Int. Commun. Heat Mass Transf.* **2013**, *46*, 112–125. [CrossRef]
56. Sathiyamoorthy, M.; Chamkha, J. Analysis of natural convection in a square cavity with a thin partition for linearly heated side walls. *Int. J. Numer. Method. Heat Fluid Flow* **2014**, *24*, 1057–1072. [CrossRef]
57. Abu-Nada, E.; Chamkha, A.J. Mixed convection flow of a nanofluid in a lid-driven cavity with a wavy wall. *Int. Commun. Heat Mass Transf.* **2014**, *57*, 36–47. [CrossRef]
58. Ait-Taleb, T.; Abdelbaki, A.; Zrikem, Z. Simulation of coupled heat transfers in a hollow tile with two vertical and three horizontal uniform rectangular cavities heated from below or above. *Energy Build.* **2014**, *84*, 628–632. [CrossRef]
59. Cheng, T.S.; Liu, W.-H. Effects of cavity inclination on mixed convection heat transfer in lid-driven cavity flows. *Comput. Fluid.* **2014**, *100*, 108–122. [CrossRef]
60. Cho, C.-C. Heat transfer and entropy generation of natural convection in nanofluid-filled square cavity with partially-heated wavy surface. *Int. J. Heat Mass Transf.* **2014**, *77*, 818–827. [CrossRef]
61. Kalteh, M.; Javaherdeh, K.; Toraj Azarbarzin, T. Numerical solution of nanofluid mixed convection heat transfer in a lid-driven square cavity with a triangular heat source. *Powder Technol.* **2014**, *253*, 780–788. [CrossRef]
62. Khanafer, K. Comparison of flow and heat transfer characteristics in a lid-driven cavity between flexible and modified geometry of a heated bottom wall. *Int. J. Heat Mass Transf.* **2014**, *78*, 1032–1041. [CrossRef]

63. Muthtamilselvan, M.; Doh, D.H. Mixed convection of heat generating nanofluid in a lid-driven cavity with uniform and non-uniform heating of bottom wall. *Appl. Math. Model.* **2014**, *38*, 3164–3174. [CrossRef]
64. Ramakrishna, D.; Basak, T.; Roy, S.; Momoniat, E. Analysis of thermal efficiency via analysis of heat flow and entropy generation during natural convection within porous trapezoidal cavities. *Int. J. Heat Mass Transf.* **2014**, *77*, 98–113. [CrossRef]
65. Ray, S.; Chatterjee, D. MHD mixed convection in a lid-driven cavity including heat conducting circular solid object and corner heaters with Joule heating. *Int. Commun. Heat Mass Transf.* **2014**, *57*, 200–207. [CrossRef]
66. Saha, S.C.; Gu, Y.T. Transient air flow and heat transfer in a triangular enclosure with a conducting partition. *Appl. Math. Model.* **2014**, *38*, 3879–3887. [CrossRef]
67. Xu, F.; Saha, S.C. Transition to an unsteady flow induced by a fin on the sidewall of a differentially heated air-filled square cavity and heat transfer. *Int. J. Heat Mass Transf.* **2014**, *71*, 236–244. [CrossRef]
68. Cui, H.; Xu, F.; Saha, S.C. A three-dimensional simulation of transient natural convection in a triangular cavity. *Int. J. Heat Mass Transf.* **2015**, *85*, 1012–1022. [CrossRef]
69. Elsherbiny, S.M.; Ismail, O.I. Heat transfer in inclined air rectangular cavities with two localized heat sources. *Alex. Eng. J.* **2015**, *54*, 917–927. [CrossRef]
70. Groşan, T.; Revnic, C.; Pop, I.; Ingham, D.B. Free convection heat transfer in a square cavity filled with a porous medium saturated by a nanofluid. *Int. J. Heat Mass Transf.* **2015**, *87*, 36–41. [CrossRef]
71. Moumni, H.; Welhezi, H.; Djebali, R.; Sediki, E. Accurate finite volume investigation of nanofluid mixed convection in two-sided lid-driven cavity including discrete heat sources. *Appl. Math. Model.* **2015**, *39*, 4164–4179. [CrossRef]
72. Saha, S.C.; Gu, Y.T. Natural convection in a triangular enclosure heated from below and non-uniformly cooled from top. *Int. J. Heat Mass Transf.* **2015**, *80*, 529–538. [CrossRef]
73. Sheremet, M.A.; Pop, I. Mixed convection in a lid-driven square cavity filled by a nanofluid: Buongiorno's mathematical model. *Appl. Math. Comput.* **2015**, *266*, 792–808. [CrossRef]
74. Sojoudi, A.; Saha, S.C.; Gu, Y.T. Natural convection due to differential heating of inclined walls and heat source placed on bottom wall of an attic shaped space. *Energy Build.* **2015**, *89*, 153–162. [CrossRef]
75. Armaghani, T.; Kasaeipoor, A.; Alavi, N.; Rashidi, M.M. Numerical investigation of water-alumina nanofluid natural convection heat transfer and entropy generation in a baffled L-shaped cavity. *J. Mol. Liq.* **2016**, *223*, 243–251. [CrossRef]
76. Jmai, R.; Ben-Beya, B.; Lili, T. Numerical analysis of mixed convection at various walls speed ratios in two-sided lid-driven cavity partially heated and filled with nanofluid. *J. Mol. Liq.* **2016**, *221*, 691–713. [CrossRef]
77. Kareem, A.K.; Gao, S.; Ahmed, A.Q. Unsteady simulations of mixed convection heat transfer in a 3D closed lid-driven cavity. *Int. J. Heat Mass Transf.* **2016**, *100*, 121–130. [CrossRef]
78. Kareem, A.K.; Mohammed, H.A.; Hussein, A.K.; Gao, S. Numerical investigation of mixed convection heat transfer of nanofluids in a lid-driven trapezoidal cavity. *Int. Commun. Heat Mass Transf.* **2016**, *77*, 195–205. [CrossRef]
79. Mamourian, M.; Shirvan, K.M.; Ellahi, R.; Rahimi, A.B. Optimization of mixed convection heat transfer with entropy generation in a wavy surface square lid-driven cavity by means of Taguchi approach. *Int. J. Heat Mass Transf.* **2016**, *102*, 544–554. [CrossRef]
80. Mejri, I.; Mahmoudi, A.; Abbassi, M.A.; Omri, A. LBM simulation of natural convection in an inclined triangular cavity filled with water. *Alex. Eng. J.* **2016**, *55*, 1385–1394. [CrossRef]
81. Rahmati, A.R.; Roknabadi, A.R.; Abbaszadeh, M. Numerical simulation of mixed convection heat transfer of nanofluid in a double lid-driven cavity using lattice Boltzmann method. *Alex. Eng. J.* **2016**, *55*, 3101–3114. [CrossRef]
82. Selimefendigil, F.; Öztop, H.F. Analysis of MHD mixed convection in a flexible walled and nanofluids filled lid-driven cavity with volumetric heat generation. *Int. J. Mech. Sci.* **2016**, *118*, 113–124. [CrossRef]
83. Selimefendigil, F.; Öztop, H.F. Natural convection in a flexible sided triangular cavity with internal heat generation under the effect of inclined magnetic field. *J. Magn. Magn. Mater.* **2016**, *417*, 327–337. [CrossRef]
84. Selimefendigil, F.; Öztop, H.F.; Chamkha, A.J. MHD mixed convection and entropy generation of nanofluid filled lid driven cavity under the influence of inclined magnetic fields imposed to its upper and lower diagonal triangular domains. *J. Magn. Magn. Mater.* **2016**, *406*, 266–281. [CrossRef]
85. Sojoudi, A.; Saha, S.C.; Sefidan, A.M.; Gu, Y.T. Natural convection subject to sinusoidal thermal forcing on inclined walls and heat source located on bottom wall of an attic-shaped space. *Energy Build.* **2016**, *128*, 845–866. [CrossRef]
86. Sojoudi, A.; Saha, S.C.; Xu, F.; Gu, Y.T. Transient air flow and heat transfer due to differential heating on inclined walls and heat source placed on the bottom wall in a partitioned attic shaped space. *Energy Build.* **2016**, *113*, 39–50. [CrossRef]
87. Aparna, K.; Seetharamu, K.N. Investigations on the effect of non-uniform temperature on fluid flow and heat transfer in a trapezoidal cavity filled with porous media. *Int. J. Heat Mass Transf.* **2017**, *108*, 63–78. [CrossRef]
88. Alsabery, A.I.; Chamkha, A.J.; Saleh, H.; Hashim, I. Transient natural convective heat transfer in a trapezoidal cavity filled with non-Newtonian nanofluid with sinusoidal boundary conditions on both sidewalls. *Powder Technol.* **2017**, *308*, 214–234. [CrossRef]
89. Al-Weheibi, S.M.; Rahman, M.M.; Alam, M.S.; Vajravelu, K. Numerical simulation of natural convection heat transfer in a trapezoidal enclosure filled with nanoparticles. *Int. J. Mech. Sci.* **2017**, *131–132*, 599–612. [CrossRef]
90. Balla, C.S.; Kishan, N.; Gorla, R.S.R.; Gireesha, B.J. MHD boundary layer flow and heat transfer in an inclined porous square cavity filled with nanofluids. *Ain Shams Eng. J.* **2017**, *8*, 237–254. [CrossRef]
91. Cui, H.; Xu, F.; Saha, S.C. Transition to unsteady natural convection flow in a prismatic enclosure of triangular section. *Int. J. Therm. Sci.* **2017**, *111*, 330–339. [CrossRef]

92. Das, D.; Lukose, L.; Basak, T. Role of finite element based grids and simulations on evaluation of Nusselt numbers for heatfunctions within square and triangular cavities involving multiple discrete heaters. *Int. Commun. Heat Mass Transf.* **2017**, *89*, 39–46. [CrossRef]
93. Gangawane, K.M. Computational analysis of mixed convection heat transfer characteristics in lid-driven cavity containing triangular block with constant heat flux: Effect of Prandtl and Grashof numbers. *Int. J. Heat Mass Transf.* **2017**, *105*, 34–57. [CrossRef]
94. Ghalambaz, M.; Jamesahar, E.; Ismael, M.A.; Chamkha, A.J. Fluid-structure interaction study of natural convection heat transfer over a flexible oscillating fin in a square cavity. *Int. J. Therm. Sci.* **2017**, *111*, 256–273. [CrossRef]
95. Gibanov, N.S.; Sheremet, M.A.; Oztop, H.F.; Al-Salem, K. Convective heat transfer in a lid-driven cavity with a heat-conducting solid backward step under the effect of buoyancy force. *Int. J. Heat Mass Transf.* **2017**, *112*, 158–168. [CrossRef]
96. Gibanov, N.S.; Sheremet, M.A.; Oztop, H.F.; Abu-Hamdeh, N. Effect of uniform inclined magnetic field on mixed convection in a lid-driven cavity having a horizontal porous layer saturated with a ferrofluid. *Int. J. Heat Mass Transf.* **2017**, *114*, 1086–1097. [CrossRef]
97. Hammami, F.; Souayeh, B.; Ben-Cheikh, N.; Ben-Beya, B. Computational analysis of fluid flow due to a two-sided lid driven cavity with a circular cylinder. *Comput. Fluids* **2017**, *156*, 317–328. [CrossRef]
98. Hatami, M.; Zhou, J.; Geng, J.; Song, D.; Jing, D. Optimization of a lid-driven T-shaped porous cavity to improve the nanofluids mixed convection heat transfer. *J. Mol. Liq.* **2017**, *231*, 620–631. [CrossRef]
99. Hussain, S.; Ahmad, S.; Mehmood, K.; Sagheer, M. Effects of inclination angle on mixed convective nanofluid flow in a double lid-driven cavity with discrete heat sources. *Int. J. Heat Mass Transf.* **2017**, *106*, 847–860. [CrossRef]
100. Javed, T.; Mehmood, Z.; Siddiqui, M.A.; Pop, I. Study of heat transfer in water-Cu nanofluid saturated porous medium through two entrapped trapezoidal cavities under the influence of magnetic field. *J. Mol. Liq.* **2017**, *240*, 402–411. [CrossRef]
101. Kareem, A.K.; Gao, S. Mixed convection heat transfer of turbulent flow in a three-dimensional lid-driven cavity with a rotating cylinder. *Int. J. Heat Mass Transf.* **2017**, *112*, 185–200. [CrossRef]
102. Khanafer, K.; Aithal, S.M. Mixed convection heat transfer in a lid-driven cavity with a rotating circular cylinder. *Int. Commun. Heat Mass Transf.* **2017**, *86*, 131–142. [CrossRef]
103. Khatamifar, M.; Lin, W.; Armfield, S.W.; Holmes, D.; Kirkpatrick, M.P. Conjugate natural convection heat transfer in a partitioned differentially-heated square cavity. *Int. Commun. Heat Mass Transf.* **2017**, *81*, 92–103. [CrossRef]
104. Mojumder, S.; Saha, S.; Rahman, M.R.; Rahman, M.M.; Rabbi, K.M.; Ibrahim, T.A. Numerical study on mixed convection heat transfer in a porous L-shaped cavity. *Eng. Sci. Technol. Int. J.* **2017**, *20*, 272–282. [CrossRef]
105. Selimefendigil, F.; Öztop, H.F.; Chamkha, A.J. Fluid–structure-magnetic field interaction in a nanofluid filled lid-driven cavity with flexible side wall. *Eur. J. Mech. B Fluid.* **2017**, *61*, 77–85. [CrossRef]
106. Selimefendigil, F.; Öztop, H.F.; Chamkha, A.J. Analysis of mixed convection of nanofluid in a 3D lid-driven trapezoidal cavity with flexible side surfaces and inner cylinder. *Int. Commun. Heat Mass Transf.* **2017**, *87*, 40–51. [CrossRef]
107. Selimefendigil, F.; Öztop, H.F. Mixed convection in a partially heated triangular cavity filled with nanofluid having a partially flexible wall and internal heat generation. *J. Taiwan Inst. Chem. Eng.* **2017**, *70*, 168–178. [CrossRef]
108. Sheremet, M.A.; Revnic, C.; Pop, I. Natural convective heat transfer through two entrapped triangular cavities filled with a nanofluid: Buongiorno's mathematical model. *Int. J. Mech. Sci.* **2017**, *133*, 484–494. [CrossRef]
109. Aghakhani, S.; Pordanjani, A.H.; Karimipour, A.; Abdollahi, A.; Afrand, M. Numerical investigation of heat transfer in a power-law non-Newtonian fluid in a C-Shaped cavity with magnetic field effect using finite difference lattice Boltzmann method. *Comput. Fluid.* **2018**, *176*, 51–67. [CrossRef]
110. Astanina, M.S.; Sheremet, M.A.; Oztop, H.F. MHD natural convection and entropy generation of ferrofluid in an open trapezoidal cavity partially filled with a porous medium. *Int. J. Mech. Sci.* **2018**, *48*, 326–337. [CrossRef]
111. Alsabery, A.I.; Ismael, M.A.; Chamkha, A.J.; Hashim, I. Mixed convection of Al_2O_3-water nanofluid in a double lid-driven square cavity with a solid inner insert using Buongiorno's two-phase model. *Int. J. Heat Mass Transf.* **2018**, *119*, 939–961. [CrossRef]
112. Balootaki, A.; Karimipour, A.; Toghraie, D. Nano scale lattice Boltzmann method to simulate the mixed convection heat transfer of air in a lid-driven cavity with an endothermic obstacle inside. *Phys. A Stat. Mech. Its Appl.* **2018**, *508*, 681–701.
113. Bhowmick, S.; Xu, F.; Zhang, X.; Saha, S.C. Natural convection and heat transfer in a valley shaped cavity filled with initially stratified water. *Int. J. Therm. Sci.* **2018**, *128*, 59–69. [CrossRef]
114. Cho, C.-C. Heat transfer and entropy generation of mixed convection flow in Cu-water nanofluid-filled lid-driven cavity with wavy surface. *Int. J. Heat Mass Transf.* **2018**, *119*, 163–174. [CrossRef]
115. Gangawane, K.M.; Oztop, H.F.; Abu-Hamdeh, N. Mixed convection characteristic in a lid-driven cavity containing heated triangular block: Effect of location and size of block. *Int. J. Heat Mass Transf.* **2018**, *124*, 860–875. [CrossRef]
116. Gibanov, N.S.; Sheremet, M.A.; Oztop, H.F.; Abu-Hamdeh, N. Mixed convection with entropy generation of nanofluid in a lid-driven cavity under the effects of a heat-conducting solid wall and vertical temperature gradient. *Eur. J. Mech. B Fluid.* **2018**, *70*, 148–159. [CrossRef]
117. Hussain, S.; Öztop, H.F.; Mehmood, K.; Abu-Hamdeh, N. Effects of inclined magnetic field on mixed convection in a nanofluid filled double lid-driven cavity with volumetric heat generation or absorption using finite element method. *Chin. J. Phys.* **2018**, *56*, 484–501. [CrossRef]

118. Javed, T.; Siddiqui, M.A. Effect of MHD on heat transfer through ferrofluid inside a square cavity containing obstacle/heat source. *Int. J. Therm. Sci.* **2018**, *125*, 419–427. [CrossRef]
119. Karbasifar, B.; Akbari, M.; Toghraie, D. Mixed convection of Water-Aluminum oxide nanofluid in an inclined lid-driven cavity containing a hot elliptical centric cylinder. *Int. J. Heat Mass Transf.* **2018**, *116*, 1237–1249. [CrossRef]
120. Kareem, A.K.; Gao, S. A comparison study of mixed convection heat transfer of turbulent nanofluid flow in a three-dimensional lid-driven enclosure with a clockwise versus an anticlockwise rotating cylinder. *Int. Commun. Heat Mass Transf.* **2018**, *90*, 44–55. [CrossRef]
121. Mikhailenko, S.A.; Sheremet, M.A.; Mohamad, A.A. Convective-radiative heat transfer in a rotating square cavity with a local heat-generating source. *Int. J. Mech. Sci.* **2018**, *142–143*, 530–540. [CrossRef]
122. Oglakkaya, F.S.; Bozkaya, C. Unsteady MHD mixed convection flow in a lid-driven cavity with a heated wavy wall. *Int. J. Mech. Sci.* **2018**, *148*, 231–245. [CrossRef]
123. Razera, A.L.; da Fonseca, R.J.C.; Isoldi, L.A.; dos Santos, E.D.; Rocha, L.A.O.; Biserni, C. Constructal design of a semi-elliptical fin inserted in a lid-driven square cavity with mixed convection. *Int. J. Heat Mass Transf.* **2018**, *126*, 81–94. [CrossRef]
124. Selimefendigil, F.; Öztop, H.F. Modeling and optimization of MHD mixed convection in a lid-driven trapezoidal cavity filled with alumina–water nanofluid: Effects of electrical conductivity models. *Int. J. Mech. Sci.* **2018**, *136*, 264–278. [CrossRef]
125. Sheikholeslami, M. Influence of magnetic field on Al_2O_3-H_2O nanofluid forced convection heat transfer in a porous lid-driven cavity with hot sphere obstacle by means of LBM. *J. Mol. Liq.* **2018**, *263*, 472–488. [CrossRef]
126. Sheremet, M.A.; Roşca, N.C.; Roşca, A.V.; Pop, I. Mixed convection heat transfer in a square porous cavity filled with a nanofluid with suction/injection effect. *Comput. Math. Appl.* **2018**, *76*, 2665–2677. [CrossRef]
127. Taghizadeh, S.; Asaditaheri, A. Heat transfer and entropy generation of laminar mixed convection in an inclined lid-driven enclosure with a circular porous cylinder. *Int. J. Therm. Sci.* **2018**, *134*, 242–257. [CrossRef]
128. Zhai, H.; Xu, F.; Hou, Y.; Saha, S.C. Natural Convection and Heat Transfer on a Section-Triangular Roof. *Int. Commun. Heat Mass Transf.* **2018**, *92*, 23–30. [CrossRef]
129. Zhou, W.; Yan, Y.; Liu, X.; Chen, H.; Liu, B. Lattice Boltzmann simulation of mixed convection of nanofluid with different heat sources in a double lid-driven cavity. *Int. Commun. Heat Mass Transf.* **2018**, *97*, 39–46. [CrossRef]
130. Alnaqi, A.A.; Aghakhani, S.; Pordanjani, A.H.; Bakhtiari, R.; Asadi, A.; Minh-Duc Tran, M.-D. Effects of magnetic field on the convective heat transfer rate and entropy generation of a nanofluid in an inclined square cavity equipped with a conductor fin: Considering the radiation effect. *Int. J. Heat Mass Transf.* **2019**, *133*, 256–267. [CrossRef]
131. Al-Rashed, A.A.A.A.; Shahsavar, A.; Akbari, M.; Toghraie, D.; Akbari, M.; Afrand, M. Finite Volume Simulation of mixed convection in an inclined lid-driven cavity filled with nanofluids: Effects of a hot elliptical centric cylinder cavity angle and volume fraction of nanoparticles. *Phys. A Stat. Mech. Its Appl.* **2019**, *527*, 121122.
132. Barnoon, P.; Toghraie, D.; Dehkordi, R.B.; Abed, H. MHD mixed convection and entropy generation in a lid-driven cavity with rotating cylinders filled by a nanofluid using two phase mixture model. *J. Magn. Magn. Mater.* **2019**, *483*, 224–248. [CrossRef]
133. Bhowmick, S.; Saha, S.C.; Qiao, M.; Xu, F. Transition to a chaotic flow in a V-shaped triangular cavity heated from below. *Int. J. Heat Mass Transf.* **2019**, *128*, 76–86. [CrossRef]
134. Cho, C.-C. Mixed convection heat transfer and entropy generation of Cu-water nanofluid in wavy-wall lid-driven cavity in presence of inclined magnetic field. *Int. J. Mech. Sci.* **2019**, *151*, 703–714. [CrossRef]
135. Cui, H.; Xu, F.; Saha, S.C.; Liu, Q. Transient free convection heat transfer in a section-triangular prismatic enclosure with different aspect ratios. *Int. J. Therm. Sci.* **2019**, *139*, 282–291. [CrossRef]
136. Hadavand, M.; Yousefzadeh, S.; Akbari, O.A.; Pourfattah, F.; Nguyen, H.M.; Asadi, A. A numerical investigation on the effects of mixed convection of Ag-water nanofluid inside a sim-circular lid-driven cavity on the temperature of an electronic silicon chip. *Appl. Therm. Eng.* **2019**, *162*, 114298. [CrossRef]
137. Hamid, M.; Usman, M.; Khan, Z.H.; Haq, R.U.; Wang, W. Heat transfer and flow analysis of Casson fluid enclosed in a partially heated trapezoidal cavity. *Int. Commun. Heat Mass Transf.* **2019**, *108*, 104284. [CrossRef]
138. Karatas, H.; Derbentli, T. Natural convection in differentially heated rectangular cavities with time-periodic boundary condition on one side. *Int. J. Heat Mass Transf.* **2019**, *129*, 224–237. [CrossRef]
139. Lamarti, H.; Mahdaoui, M.; Bennacer, R.; Chahboun, A. Numerical simulation of mixed convection heat transfer of fluid in a cavity driven by an oscillating lid using lattice Boltzmann method. *Int. J. Heat Mass Transf.* **2019**, *137*, 615–629. [CrossRef]
140. Louaraychi, A.; Lamsaadi, M.; Naïmi, M.; Harfi, H.E.; Kaddiri, M.; Raji, A.; Hasnaoui, M. Mixed convection heat transfer correlations in shallow rectangular cavities with single and double-lid driven boundaries. *Int. J. Heat Mass Transf.* **2019**, *132*, 394–406. [CrossRef]
141. Mohebbi, R.; Izadi, M.; Sajjadi, H.; Delouei, A.A.; Sheremet, M.A. Examining of nanofluid natural convection heat transfer in a Γ-shaped enclosure including a rectangular hot obstacle using the lattice Boltzmann method. *Phys. A Stat. Mech. Its Appl.* **2019**, *526*, 120831. [CrossRef]
142. Selimefendigil, F.; Öztop, H.F. MHD mixed convection of nanofluid in a flexible walled inclined lid-driven L-shaped cavity under the effect of internal heat generation. *Phys. A Stat. Mech. Its Appl.* **2019**, *534*, 122144. [CrossRef]
143. Abu-Hamdeh, N.H.; Oztop, H.F.; Alnefaie, K.A. A computational study on mixed convection in a porous media filled and partially heated lid-driven cavity with an open side. *Alex. Eng. J.* **2020**, *59*, 1735–1750. [CrossRef]

144. Afrand, M.; Pordanjani, A.H.; Aghakhani, S.; Oztop, H.F.; Abu-Hamdeh, N. Free convection and entropy generation of a nanofluid in a tilted triangular cavity exposed to a magnetic field with sinusoidal wall temperature distribution considering radiation effects. *Int. Commun. Heat Mass Transf.* **2020**, *112*, 104507. [CrossRef]
145. Alsabery, A.I.; Armaghani, T.; Chamkha, A.J.; Hashim, I. Two-phase nanofluid model and magnetic field effects on mixed convection in a lid-driven cavity containing heated triangular wall. *Alex. Eng. J.* **2020**, *59*, 129–148. [CrossRef]
146. Alsabery, A.I.; Sheremet, M.A.; Chamkha, A.J.; Hashim, I. Energy transport of two-phase nanofluid approach inside a three-dimensional lid-driven cubic cavity containing solid cylinder and heat source. *Chem. Eng. Process. Process Intensif.* **2020**, *154*, 108010. [CrossRef]
147. Bilal, S.; Mahmood, R.; Majeed, A.H.; Khan, I.; Nisar, K.S. Finite element method visualization about heat transfer analysis of Newtonian material in triangular cavity with square cylinder. *J. Mater. Res. Technol.* **2020**, *9*, 4904–4918. [CrossRef]
148. Cho, C.-C. Effects of porous medium and wavy surface on heat transfer and entropy generation of Cu-water nanofluid natural convection in square cavity containing partially-heated surface. *Int. Commun. Heat Mass Transf.* **2020**, *119*, 104925. [CrossRef]
149. Ganesh, N.V.; Javed, S.; Al-Mdallal, Q.M.; Kalaivanan, R.; Chamkha, A.J. Numerical study of heat generating γ Al_2O_3–H_2O nanofluid inside a square cavity with multiple obstacles of different shapes. *Heliyon* **2020**, *6*, e05752. [CrossRef]
150. Haq, R.U.; Soomro, F.A.; Wang, X.; Tlili, I. Partially heated lid-driven flow in a hexagonal cavity with inner circular obstacle via FEM. *Int. Commun. Heat Mass Transf.* **2020**, *117*, 104732. [CrossRef]
151. Khan, Z.H.; Makinde, O.D.; Hamid, M.; Haq, R.U.; Khan, W.A. Hydromagnetic flow of ferrofluid in an enclosed partially heated trapezoidal cavity filled with a porous medium. *J. Magn. Magn. Mater.* **2020**, *499*, 166241. [CrossRef]
152. Li, Z.; Shahsavar, A.; Niazi, K.; Al-Rashed, A.A.A.A.; Talebizadehsardari, P. The effects of vertical and horizontal sources on heat transfer and entropy generation in an inclined triangular enclosure filled with non-Newtonian fluid and subjected to magnetic field. *Powder Technol.* **2020**, *364*, 924–942. [CrossRef]
153. Liu, Y.; Huang, H. Effect of three modes of linear thermal forcing on convective flow and heat transfer in rectangular cavities. *Int. J. Heat Mass Transf.* **2020**, *147*, 118951. [CrossRef]
154. Rammane, M.; Mesmoudi, S.; Tri, A.; Braikat, B.; Damil, N. Solving the incompressible fluid flows by a high-order mesh-free approach. *Int. J. Numer. Method. Fluid.* **2020**, *92*, 422–435. [CrossRef]
155. Saha, S.C.; Sefidan, A.M.; Sojoudi, A. Unsteady natural convection within an attic-shaped space subject to sinusoidal heat flux on inclined walls. *Energy Eng.* **2020**, *117*, 1–17.
156. Selimefendigil, F.; Öztop, H.F. Magnetohydrodynamics forced convection of nanofluid in multi-layered U-shaped vented cavity with a porous region considering wall corrugation effects. *Int. Commun. Heat Mass Transf.* **2020**, *113*, 104551. [CrossRef]
157. Soomro, F.A.; Haq, R.U.; Algehyne, E.A.; Tlili, I. Thermal performance due to magnetohydrodynamics mixed convection flow in a triangular cavity with circular obstacle. *J. Energy Storage* **2020**, *31*, 101702. [CrossRef]
158. Thiers, N.; Gers, R.; Skurtys, O. Heat transfer enhancement by localised time varying thermal perturbations at hot and cold walls in a rectangular differentially heated cavity. *Int. J. Therm. Sci.* **2020**, *151*, 106245. [CrossRef]
159. Aljabair, S.; Ekaid, A.L.; Ibrahim, S.H.; Alesbe, I. Mixed convection in sinusoidal lid-driven cavity with non-uniform temperature distribution on the wall utilizing nanofluid. *Heliyon* **2021**, *7*, e06907. [CrossRef] [PubMed]
160. Alsabery, A.I.; Tayebi, T.; Kadhim, H.T.; Ghalambaz, M.; Hashim, I.; Chamkha, A.J. Impact of two-phase hybrid nanofluid approach on mixed convection inside wavy lid-driven cavity having localized solid block. *J. Adv. Res.* **2021**, *30*, 63–74. [CrossRef] [PubMed]
161. Çolak, E.; Ekici, O.; Öztop, H.F. Mixed convection in a lid-driven cavity with partially heated porous block. *Int. Commun. Heat Mass Transf.* **2021**, *126*, 105450. [CrossRef]
162. Eshaghi, S.; Izadpanah, F.; Dogonchi, A.S.; Chamkha, A.J.; Hamida, M.B.B.; Alhumade, H. The optimum double-diffusive natural convection heat transfer in H-Shaped cavity with a baffle inside and a corrugated wall. *Case Stud. Therm. Eng.* **2021**, *28*, 101541. [CrossRef]
163. Fayz-Al-Asad, M.; Alam, M.N.; Ahmad, H.; Sarker, M.M.A.; Alsulami, M.D.; Gepreel, K.A. Impact of a closed space rectangular heat source on natural convective flow through the triangular cavity. *Results Phys.* **2021**, *23*, 104011. [CrossRef]
164. Hasnaoui, S.; Amahmid, A.; Raji, A.; Beji, H.; Mansouri, A.E.; Hasnaoui, M. LBM simulation of stabilizing/destabilizing effects of thermodiffusion and heat generation in a rectangular cavity filled with a binary mixture. *Int. Commun. Heat Mass Transf.* **2021**, *126*, 105417. [CrossRef]
165. Hussain, S.; Jamal, M.; Geridonmez, B.P. Impact of fins and inclined magnetic field in double lid-driven cavity with Cu–water nanofluid. *Int. J. Therm. Sci.* **2021**, *61*, 106707. [CrossRef]
166. Hostos, J.C.A.; Bove, J.C.S.; Cruchaga, M.A.; Fachinotti, V.D.; Agelvis, R.A.M. Solving steady-state lid-driven square cavity flows at high Reynolds numbers via a coupled improved element-free Galerkin–reduced integration penalty method. *Comput. Math. Appl.* **2021**, *99*, 211–228. [CrossRef]
167. Ibrahim, W.; Hirpho, M. Finite element analysis of mixed convection flow in a trapezoidal cavity with non-uniform temperature. *Heliyon* **2021**, *7*, e05933. [CrossRef]
168. Ikram, M.M.; Saha, G.; Saha, S.C. Conjugate forced convection transient flow and heat transfer analysis in a hexagonal partitioned, air filled cavity with dynamic modulator. *Int. J. Heat Mass Transf.* **2021**, *167*, 120786. [CrossRef]
169. Joe, E.S.; Perumal, D.A. Computational analysis of nonhomogeneous fluid flow in a two-cylinder-driven rectangular cavity. *Appl. Eng. Sci.* **2021**, *7*, 100064. [CrossRef]

170. Mondal, P.; Mahapatra, T.R. MHD double-diffusive mixed convection and entropy generation of nanofluid in a trapezoidal cavity. *Int. J. Mech. Sci.* **2021**, *208*, 106665. [CrossRef]
171. Mebarek-Oudina, F.; Fares, R.; Aissa, A.; Lewis, R.W.; Abu-Hamdeh, N.H. Entropy and convection effect on magnetized hybrid nano-liquid flow inside a trapezoidal cavity with zigzagged wall. *Int. Commun. Heat Mass Transf.* **2021**, *125*, 105279. [CrossRef]
172. Saha, S.; Biswas, P.; Das, A.N.; Raut, S. Analysis of heat transfer characteristics through an rectangular enclosure. *Mater. Today Proc.* **2021**, *47*, 2905–2911. [CrossRef]
173. Saha, S.C.; Sefidan, A.M.; Sojoudi, A.; Molla, M.M. Transient free convection and heat transfer in a partitioned attic-shaped space under diurnal thermal forcing. *Energy Eng.* **2021**, *118*, 487–506. [CrossRef]
174. Shah, S.S.; Haq, R.U.; Al-Kouz, W. Mixed convection analysis in a split lid-driven trapezoidal cavity having elliptic shaped obstacle. *Int. Commun. Heat Mass Transf.* **2021**, *126*, 105448. [CrossRef]
175. Shahid, H.; Yaqoob, I.; Khan, W.A.; Rafique, A. Mixed convection in an isosceles right triangular lid driven cavity using multi relaxation time lattice Boltzmann method. *Int. Commun. Heat Mass Transf.* **2021**, *128*, 105552. [CrossRef]
176. Shahid, H.; Yaqoob, I.; Khan, W.A.; Aslam, M. Multi relaxation time Lattice Boltzmann analysis of lid-driven rectangular cavity subject to various obstacle configurations. *Int. Commun. Heat Mass Transf.* **2021**, *129*, 105658. [CrossRef]
177. Shekaramiz, M.; Fathi, S.; Ataabadi, H.A.; Kazemi-Varnamkhasti, H.; Toghraie, D. MHD nanofluid free convection inside the wavy triangular cavity considering periodic temperature boundary condition and velocity slip mechanisms. *Int. J. Therm. Sci.* **2021**, *170*, 107179. [CrossRef]
178. Tizakast, Y.; Kaddiri, M.; Lamsaadi, M. Double-diffusive mixed convection in rectangular cavities filled with non-Newtonian fluids. *Int. J. Mech. Sci.* **2021**, *208*, 106667. [CrossRef]
179. Velkennedy, R.; Nisrin, J.J.; Kalidasan, K.; Rajeshkanna, P. Numerical investigation of convective heat transfer in a rectangular vented cavity with two outlets and cold partitions. *Int. Commun. Heat Mass Transf.* **2021**, *129*, 105659. [CrossRef]
180. Xiong, P.-Y.; Hamid, A.; Iqbal, K.; Irfan, M.; Khan, M. Numerical simulation of mixed convection flow and heat transfer in the lid-driven triangular cavity with different obstacle configurations. *Int. Commun. Heat Mass Transf.* **2021**, *123*, 105202. [CrossRef]
181. Abbas, S.Z.; Wang, X.; Khan, W.A.; Hobiny, A.; Iqbal, K. Finite element analysis of nanofluid flow and heat transfer in a square cavity with two circular obstacles at different positions in the presence of magnetic field. *J. Energy Storage* **2022**, *51*, 104462. [CrossRef]
182. Ahmed, S.; Xu, H.; Zhou, Y.; Qiang Yu, Q. Modelling convective transport of hybrid nanofluid in a lid-driven square cavity with consideration of Brownian diffusion and thermophoresis. *Int. Commun. Heat Mass Transf.* **2022**, *137*, 106226. [CrossRef]
183. Ali, M.M.; Akhter, R.; Alim, M.A. Magneto-mixed convection in a lid driven partially heated cavity equipped with nanofluid and rotating flat plate. *Alex. Eng. J.* **2022**, *61*, 257–278. [CrossRef]
184. Acharya, N.; Chamkha, A.J. On the magnetohydrodynamic Al_2O_3-water nanofluid flow through parallel fins enclosed inside a partially heated hexagonal cavity. *Int. Commun. Heat Mass Transf.* **2022**, *132*, 105885. [CrossRef]
185. Batool, S.; Rasool, G.; Alshammari, N.; Khan, I.; Kaneez, H.; Hamadneh, N. Numerical analysis of heat and mass transfer in micropolar nanofluids flow through lid-driven cavity: Finite volume approach. *Case Stud. Therm. Eng.* **2022**, *37*, 102233. [CrossRef]
186. Charqui, Z.; Moutaouakil, L.E.; Boukendil, M.; Hidki, R. Numerical study of heat transfer in a tall, partitioned cavity confining two different fluids: Application to the water Trombe wall. *Int. J. Therm. Sci.* **2022**, *171*, 107266. [CrossRef]
187. Cui, H.; Wang, W.; Xu, F.; Saha, S.C.; Liu, Q. Transitional free convection flow and heat transfer within attics in cold climate. *Therm. Sci.* **2022**, *26*, 4699–4709. [CrossRef]
188. Dahani, Y.; Hasnaoui, M.; Amahmid, A.; Hasnaoui, S. A Multiple-Relaxation-Time lattice Boltzmann analysis of coupled mixed convection and radiation effect in a tilted two-sided lid-driven enclosure. *Chem. Phys. Lett.* **2022**, *791*, 139386. [CrossRef]
189. Hirpho, M.; Ibrahim, W. Modeling and simulation of hybrid Casson nanofluid mixed convection in a partly heated trapezoidal enclosure. *Int. J.* **2022**, *15*, 100166. [CrossRef]
190. Khalil, W.H.; Azzawi, I.D.J.; Al-damook, A. The optimisation of MHD free convection inside porous trapezoidal cavity with the wavy bottom wall using response surface method. *Int. Commun. Heat Mass Transf.* **2022**, *134*, 106035. [CrossRef]
191. Liu, Y. Free convection and heat transfer characteristics in differentially heated finned cavities with inclination. *Int. J. Therm. Sci.* **2022**, *182*, 107729. [CrossRef]
192. Noor, N.F.M.; Haq, R.U.; Wong, H.F.; Alzahrani, A.K.; Ullah, M.Z. Flow and heat transfer due to partially heated moving lid in a trapezoidal cavity with different constraints at inner circular obstacle. *Int. Commun. Heat Mass Transf.* **2022**, *135*, 106111. [CrossRef]
193. Nouraei, S.; Anvari, A.; Abed, A.M.; Akbari, O.A.; Montazerifar, F.; Baghaei, S.; Fatholahi, M. Heat transfer and entropy analysis for nanofluid flow in a semi-circular open cavity under mixed convection. *Alex. Eng. J.* **2022**, *64*, 309–334. [CrossRef]
194. Polasanapalli, S.R.G.; Anupindi, K. Mixed convection heat transfer in a two-dimensional annular cavity using an off-lattice Boltzmann method. *Int. J. Therm. Sci.* **2022**, *179*, 107677. [CrossRef]
195. Prince, H.A.; Rozin, E.H.; Sagor, M.J.H.; Saha, S. Evaluation of overall thermal performance for conjugate natural convection in a trapezoidal cavity with different surface corrugations. *Int. Commun. Heat Mass Transf.* **2022**, *130*, 105772. [CrossRef]
196. Rahaman, M.M.; Bhowmick, S.; Mondal, R.N.; Saha, S.C. Unsteady natural convection in an initially stratified air-filled trapezoidal enclosure heated from below. *Processes* **2022**, *10*, 1383. [CrossRef]

197. Roy, N.C.; Amin, R.; Ishak, A. Magnetohydrodynamic Natural Convective Hybrid Nanofluid Flow in a Square Enclosure with Different Blocks. *Iran. J. Sci. Technol. Trans. Mech. Eng.* **2022**. [CrossRef]
198. Shah, S.S.; Haq, R.U.; McCash, L.B.; Bahaidarah, H.M.S.; Aziz, T. Numerical simulation of lid driven flow in a curved corrugated porous cavity filled with CuO-water in the presence of heat generation/absorption. *Alex. Eng. J.* **2022**, *61*, 2749–2767. [CrossRef]
199. Tizakast, Y.; Kaddiri, M.; Lamsaadi, M. Rayleigh-Bénard double-diffusive mixed convection in two-dimensional rectangular cavities filled with non-Newtonian fluids. *Int. J. Mech. Sci.* **2022**, *227*, 107448. [CrossRef]
200. Xia, S.; Mostafavi, M.; Alghazali, T.; Sadi, S.; Guerrero, J.W.G.; Suksatan, W.; Toghraie, D.; Khan, A. Numerical investigation of nanofluid mixed convection in a T-shaped cavity by considering a thermal barrier. *Alex. Eng. J.* **2022**, *61*, 7393–7415. [CrossRef]
201. Zarei, M.S.; Abad, A.T.K.; Hekmatifar, M.; Toghraie, D. Heat transfer in a square cavity filled by nanofluid with sinusoidal wavy walls at different wavelengths and amplitudes. *Case Stud. Therm. Eng.* **2022**, *34*, 101970. [CrossRef]
202. Zhang, H.; Nie, X.; Bokov, D.O.; Toghraie, D.; Akbari, O.A.; Montazerifar, F.; Pourfattah, F.; Esmaeili, Y.; Khodaparast, R. Numerical study of mixed convection and entropy generation of Water-Ag nanofluid filled semi-elliptic lid-driven cavity. *Alex. Eng. J.* **2022**, *61*, 8875–8896. [CrossRef]
203. He, W.; Zhuang, Y.; Chen, Y.; Wang, C. Experimental and numerical investigations on the melting behavior of Fe_3O_4 nanoparticles composited paraffin wax in a cubic cavity under a magnetic-field. *Int. J. Therm. Sci.* **2023**, *184*, 107961. [CrossRef]
204. Ikram, M.M.; Saha, G.; Saha, S.C. Unsteady Conjugate Heat Transfer Characteristics in Hexagonal Cavity Equipped with a Multi-Blade Dynamic Modulator. *Int. J. Heat Mass Transf.* **2023**, *200C*, 123527. [CrossRef]
205. Ouri, H.; Selimefendigil, F.; Bouterra, M.; Omri, M.; Alshammari, B.M.; Kolsi, L. MHD hybrid nanofluid convection and phase change process in an L-shaped vented cavity equipped with an inner rotating cylinder and PCM-packed bed system. *Alex. Eng. J.* **2023**, *63*, 563–582. [CrossRef]
206. Sayed, M.A.; Hadžiabdić, M.; Dehbi, A.; Ničeno, B.; Mikityuk, K. Simulation of flow and heat transfer in a differentially heated cubical cavity using coarse Large Eddy Simulation. *Int. J. Therm. Sci.* **2023**, *183*, 107892. [CrossRef]
207. Iwatsu, R.; Hyun, J.M.; Kuwahara, K. Mixed convection in a driven cavity with a stable vertical temperature gradient. *Int. J. Heat Mass Transf.* **1993**, *36*, 1601–1608. [CrossRef]
208. Khanafer, K.M.; Chamkha, A.J. Mixed convection flow in a lid-driven enclosure filled with a fluid-saturated porous medium. *Int. J. Heat Mass Transf.* **1999**, *42*, 2465–2481. [CrossRef]
209. Pekmen, B.; Tezer-Sezgin, M. MHD flow and heat transfer in a lid-driven porous enclosure. *Comput. Fluid.* **2014**, *89*, 191–199. [CrossRef]
210. Selimefendigil, F.; Öztop, H.F. Mixed convection of ferrofluids in a lid driven cavity with two rotating cylinders. *Eng. Sci. Technol. Int. J.* **2015**, *18*, 439–451. [CrossRef]
211. Sharif, M.A.R. Laminar mixed convection in shallow inclined driven cavities with hot moving lid on top and cooled from bottom. *Appl. Therm. Eng.* **2007**, *27*, 1036–1042. [CrossRef]
212. Al-Balushi, L.M.; Uddin, M.J.; Rahman, M.M. Natural convective heat transfer in a square enclosure utilizing magnetic nanoparticles. *Propuls. Power Res.* **2019**, *8*, 194–209. [CrossRef]
213. Anandalakshmi, R.; Basak, T. Heat flow visualization for natural convection in rhombic enclosures due to isothermal and non-isothermal heating at the bottom wall. *Int. J. Heat Mass Transf.* **2012**, *55*, 1325–1342. [CrossRef]
214. Ashrafizadeh, A.; Nikfar, M. On the numerical solution of generalized convection heat transfer problems via the method of proper closure equations–Part II: Application to test problems. *Numerical Heat Transfer. Part B* **2016**, *70*, 204–222. [CrossRef]
215. Barakos, G.; Mitsoulis, E.; Assimacopoulos, D. Natural convection flow in a square cavity revisited: Laminar and turbulent models with wall functions. *Numer. Method. Fluid.* **1994**, *18*, 695–719. [CrossRef]
216. Biswas, N.; Chamkha, A.J.; Manna, N.K. Energy-saving method of heat transfer enhancement during magneto-thermal convection in typical thermal cavities adopting aspiration. *SN Appl. Sci.* **2020**, *2*, 1911. [CrossRef]
217. Bouabid, M.; Hidouri, N.; Magherbi, M.; Brahim, A.B. Analysis of the magnetic field effect on entropy generation at thermosolutal convection in a square cavity. *Entropy* **2011**, *13*, 1034–1054. [CrossRef]
218. Choi, Y.J. A Numerical Study on a Lumped-Parameter Model and a CFD Code Coupling for the Analysis of the Loss of Coolant Accident in a Reactor Containment. Ph.D. Thesis, Universit'e de Marne-la-Vall´ee, Paris, France, 2005.
219. Chenoweth, D.R.; Paolucci, S. Natural convection in an enclosed vertical air layer with large horizontal temperature differences. *J. Fluid Mech.* **1986**, *169*, 173–210. [CrossRef]
220. Corzo, S.F.; Damian, S.M.; Ramajo, D.; Nigro, N.M. Numerical simulation of natural convection phenomena. *Mec. Comput.* **2011**, *30*, 277–296.
221. Deng, Q.H.; Tang, G.F. Numerical visualization of mass and heat transport for conjugate natural convection/heat conduction by streamline and heatline. *Int. J. Heat Mass Transf.* **2002**, *45*, 2373–2385. [CrossRef]
222. de Vahl Davis, G. Natural convection of air in a square cavity: A benchmark numerical solutions. *Int. J. Numer. Method. Fluid.* **1983**, *3*, 249–264. [CrossRef]
223. D'Orazio, A.; Corcione, M.; Celata, G.P. Application to natural convection enclosed flows of a lattice Boltzmann BGK model coupled with a general purpose thermal boundary condition. *Int. J. Therm. Sci.* **2004**, *43*, 575–586. [CrossRef]
224. Dixit, H.N.; Babu, V. Simulation of high Rayleigh number natural convection in a square cavity using the lattice Boltzmann method. *Int. J. Heat Mass Transf.* **2006**, *49*, 727–739. [CrossRef]

225. Djebali, R.; Ganaoui, M.E.l.; Sammouda, H.; Bennacer, R. Some benchmarks of a side wall heated cavity using Lattice Boltzmann approach. *Fluid Dyn. Mater. Process.* **2009**, *5*, 261–282.
226. Elatar, A.; Teamah, M.A.; Hassab, M.A. Numerical study of laminar natural convection inside square enclosure with single horizontal fin. *Int. J. Therm. Sci.* **2016**, *99*, 41–51. [CrossRef]
227. El-Gendi, M.M. Numerical simulation of unsteady natural convection flow inside a pattern of connected open square cavities. *Int. J. Therm. Sci.* **2018**, *127*, 373–383. [CrossRef]
228. Fu, C.; Rahmani, A.; Suksatan, W.; Alizadeh, S.M.; Zarringhalam, M.; Chupradit, S.; Toghraie, D. Comprehensive investigations of mixed convection of Fe–ethylene-glycol nanofluid inside an enclosure with different obstacles using lattice Boltzmann method. *Sci. Rep.* **2021**, *11*, 20710. [CrossRef] [PubMed]
229. Fusegi, T.; Kuwahara, K.; Farouk, B. A numerical study of three-dimensional natural convection in a differentially heated cubic enclosure. *Int. J. Heat Mass Transf.* **1991**, *34*, 1543–1557. [CrossRef]
230. Ghasemi, B.; Aminossadati, S.M.; Raisi, A. Magnetic field effect on natural convection in a nanofluid-filled square enclosure. *Int. J. Therm. Sci.* **2011**, *50*, 1748–1756. [CrossRef]
231. Ha, M.Y.; Jung, M.J. A numerical study of three-dimensional conjugate heat transfer of natural convection and conduction in a differentially heated cubic enclosure with a heat-generating cubic conducting body. *Int. J. Heat Mass Transf.* **2000**, *43*, 4229–4248. [CrossRef]
232. Hadjisophocleous, G.V.; Sousa, A.C.M.; Venart, J.E.S. Prediction of the transient natural convection in enclosures of arbitrary geometry using a nonorthogonal numerical model. *Numer. Heat Transf. Part A* **1988**, *13*, 373–392.
233. Ho, C.J.; Lin, F.H. Simulation of natural convection in a vertical enclosure by using a new incompressible flow formulation-pseudovorticity-velocity formulation. *Numer. Heat Transf. Part A Appl.* **1997**, *31*, 881–896. [CrossRef]
234. Islam, T.; Alam, M.N.; Asjad, M.I.; Parveen, N.; Chu, Y.-M. Heatline visualization of MHD natural convection heat transfer of nanofluid in a prismatic enclosure. *Sci. Rep.* **2021**, *11*, 10972. [CrossRef] [PubMed]
235. Kalita, J.C.; Dalal, D.C.; Dass, A.K. Fully compact higher-order computation of steady-state natural convection in a square cavity. *Phys. Rev. E* **2001**, *64*, 066703. [CrossRef]
236. Karki, P.; Yadav, A.K.; Perumal, D.A. Study of adiabatic obstacles on natural convection in a square cavity using Lattice Boltzmann method. *J. Therm. Sci. Eng. Appl.* **2019**, *11*, 034502. [CrossRef]
237. Kahveci, K. A differential quadrature solution of natural convection in an enclosure with a finite-thickness partition. *Numer. Heat Transf. Part A Appl.* **2007**, *51*, 979–1002. [CrossRef]
238. Kahveci, K. Buoyancy driven heat transfer of nanofluids in a tilted enclosure. *ASME J. Heat Transf.* **2010**, *132*, 062501. [CrossRef]
239. Khanafer, K.; Vafai, K.; Lightstone, M. Buoyancy-driven heat transfer enhancement in a two-dimensional enclosure utilizing nanofluids. *Int. J. Heat Mass Transf.* **2003**, *46*, 3639–3653. [CrossRef]
240. Khatamifar, M.; Lin, W.W.; Dong, L. Transient conjugate natural convection heat transfer in a differentially-heated square cavity with a partition of finite thickness and thermal conductivity. *Case Stud. Therm. Eng.* **2021**, *25*, 100952. [CrossRef]
241. Kocutar, P.; Skerget, L.; Ravnik, J. Hybrid les/urans simulation of turbulent natural convection by bem. *Eng. Anal. Bound. Elem.* **2015**, *61*, 16–26. [CrossRef]
242. Kuznik, F.; Vareilles, J.; Rusaouen, G.; Krauss, G. A double-population lattice Boltzmann method with non-uniform mesh for the simulation of natural convection in a square cavity. *Int. J. Heat Fluid Flow* **2007**, *28*, 862–870. [CrossRef]
243. Leal, M.A.; Machado, H.A.; Cotta, R.M. Integral transform solutions of transient natural convection in enclosures with variable fluid properties. *Int. J. Heat Mass Transf.* **2007**, *43*, 3977–3990. [CrossRef]
244. Leong, W.H.; Hollands, K.G.T.; Brunger, A.P. Experimental Nusselt numbers for a cubical-cavity benchmark problem in natural convection. *Int. J. Heat Mass Transf.* **1999**, *42*, 1979–1989. [CrossRef]
245. Lo, D.C.; Young, D.L.; Murugesan, K.; Tsai, C.C.; Gou, M.H. Velocity-vorticity Formulation for 3-D Natural Convection in an Inclined Cavity by DQ Method. *Int. J. Heat Mass Transf.* **2007**, *50*, 479–491. [CrossRef]
246. Ma, Y.; Mohebbi, R.; Rashidi, M.M.; Yang, Z. Simulation of nanofluid natural convection in a U-shaped cavity equipped by a heating obstacle: Effect of cavity's aspect ratio. *J. Taiwan Inst. Chem. Eng.* **2018**, *93*, 263–276. [CrossRef]
247. Mamourian, M.; Shirvan, K.M.; Pop, I. Sensitivity analysis for MHD effects and inclination angles on natural convection heat transfer and entropy generation of Al_2O_3-water nanofluid in square cavity by Response Surface Methodology. *Int. Commun. Heat Mass Transf.* **2016**, *79*, 46–57. [CrossRef]
248. Manzari, M.T. An explicit finite element algorithm for convection heat transfer problems. *Int. J. Numer. Method. Heat Fluid Flow* **1999**, *9*, 860–877. [CrossRef]
249. Markatos, N.C.; Pericleous, K.A. Laminar and turbulent natural convection in an enclosed cavity. *Int. J. Heat Mass Transf.* **1984**, *27*, 755–772. [CrossRef]
250. Mayeli, P.; Sheard, G.J. Natural convection and entropy generation in square and skew cavities due to large temperature differences: A Gay–Lussac-type vorticity stream-function approach. *Int. J. Numer. Method. Fluid.* **2021**, *93*, 2396–2420. [CrossRef]
251. Nag, A.; Sarkar, A.; Sastri, V.M.K. Natural convection in a differentially heated square cavity with a horizontal partition plate on the hot wall. *Comput. Methods Appl. Mech. Eng.* **1993**, *110*, 143–156. [CrossRef]
252. Nithyadevi, N.; Sivasankaran, S.; Kandaswamy, P. Buoyancy-driven convection of water near its density maximum with time-periodic partially active vertical walls. *Meccanica* **2007**, *42*, 503–510. [CrossRef]

253. Olayemi, O.A.; Khaled, A.-F.; Temitope, O.J.; Victor, O.O.; Odetunde, C.B.; Adegun, I.K. Parametric study of natural convection heat transfer from an inclined rectangular cylinder embedded in a square enclosure. *Aust. J. Mech. Eng.* **2021**, 1–14. [CrossRef]
254. Oueslati, F.S.; Bennacer, R. Heterogeneous nanofluids: Natural convection heat transfer enhancement. *Nanoscale Res. Lett.* **2011**, *6*, 222. [CrossRef]
255. Oztop, H.; Abu-Nada, E. Numerical study of natural convection in partially heated rectangular enclosures filled with nanofluids. *Int. J. Heat Fluid Flow* **2008**, *29*, 1326–1336. [CrossRef]
256. Qi, C.; He, Y.; Yan, S.; Tian, F.; Hu, Y. Numerical simulation of natural convection in a square enclosure filled with nanofluid using the two-phase Lattice Boltzmann method. *Nanoscale Res. Lett.* **2013**, *8*, 1–16. [CrossRef] [PubMed]
257. Qu´er´e, P.L.; Roquefortt, T.A.D. Computation of natural convection in two- dimensional cavities with Chebyshev polynomials. *J. Comput. Phys.* **1985**, *57*, 210–228. [CrossRef]
258. Sai, B.V.K.S.; Seetharamu, K.N.; Narayana, P.A.A. Solution of transient laminar natural convection in a square cavity by an explicit finite element scheme. *Numer. Heat Transf. Part A Appl.* **1994**, *25*, 412–422.
259. Shi, X.; Khodadadi, J.M. Laminar natural convection heat transfer in a differentially heated square cavity due to a thin fin on the hot wall. *J. Heat Transf.* **2003**, *125*, 624–634. [CrossRef]
260. Son, J.H.; Park, I.S. Numerical study of MHD natural convection in a rectangular enclosure with an insulated block. *Numer. Heat Transf. Part A Appl.* **2017**, *71*, 1004–1022. [CrossRef]
261. Thangavelu, M.; Nagarajan, N.; Yang, R.-J. Magnetohydrodynamic effect on thermal transport by silver nanofluid flow in enclosure with central and lower heat sources. *Heat Transf. Eng.* **2022**, *43*, 1755–1768. [CrossRef]
262. Tric, E.; Labrosse, G.; Betrouni, M. A First Incursion into the 3-D Structure of Natural Convection of Air in a Differentially Heated Cubic Cavity from Accurate Numerical Solutions. *Int. J. Heat Mass Transf.* **2000**, *43*, 4043–4056. [CrossRef]
263. Trodi, A.; Benhamza, M.E.H.B. Particle shape and aspect ratio effect of Al_2O_3–water nanofluid on natural convective heat transfer enhancement in differentially heated square enclosures. *Chem. Eng. Commun.* **2017**, *204*, 158–167. [CrossRef]
264. Wan, C.; Patnaik, B.S.V.; Wei, D.G.W. A new benchmark quality solution for the buoyancy-driven cavity by discrete singular convolution. *Numer. Heat Transf. Part B Fundam.* **2001**, *40*, 199–228.
265. Yıldız, C.; Arıcı, M.; Karabay, H. Comparison of a theoretical and experimental thermal conductivity model on the heat transfer performance of Al_2O_3-SiO_2/water hybrid-nanofluid. *Int. J. Heat Mass Transf.* **2019**, *140*, 598–605. [CrossRef]
266. Zhang, W.; Huang, Z.; Zhang, C.; Xi, G. Conjugate wall conduction-fluid natural convection in a three-dimensional inclined enclosure. *Numer. Heat Transf. Part A Appl.* **2012**, *61*, 122–141. [CrossRef]
267. Zhang, X.H.; Saeed, T.; Algehyne, E.A.; El-Shorbagy, M.A.; El-Refaey, A.M.; Ibrahim, M. Effect of L-shaped heat source and magnetic field on heat transfer and irreversibilities in nanofluid-filled oblique complex enclosure. *Sci. Rep.* **2021**, *11*, 16458. [CrossRef]
268. Abdelkhalek, M.M. Mixed convection in a square cavity by a perturbation technique. *Comput. Mater. Sci.* **2008**, *42*, 212–219. [CrossRef]
269. Abu-Nada, E.; Chamkha, A.J. Mixed convection flow in a lid-driven inclined square enclosure filled with a nanofluid. *Eur. J. Mech. B Fluid.* **2010**, *29*, 472–482. [CrossRef]
270. Al-Amiri, A.M. Analysis of momentum and energy transfer in a lid-driven cavity filled with a porous medium. *Int. J. Heat Mass Transf.* **2000**, *43*, 3513–3527. [CrossRef]
271. Biswas, N.; Manna, N.K.; Mahapatra, P.S. Enhanced thermal energy transport using adiabatic block inside lid-driven cavity. *Int. J. Heat Mass Transf.* **2016**, *100*, 407–427. [CrossRef]
272. Gresho, P.M.; Lee, R.L.; Sani, R.L. On the time-dependent solution of the incompressible Navier–Stokes equations in two and three dimensions. In *Recent Adv. Numerical Methods in Fluids*; Pineridge: Swansea, UK, 1980.
273. Kefayati, G.R. Double-diffusive mixed convection of pseudoplastic fluids in a two-sided lid-driven cavity using FDLBM. *J. Taiwan Inst. Chem. Eng.* **2014**, *45*, 2122–2139. [CrossRef]
274. Khanafer, K.M.; Al-Amiri, A.M.; Pop, I. Numerical simulation of unsteady mixed convection in a driven cavity. Using an externally excited sliding lid. *Eur. J. Mech. B Fluid.* **2007**, *26*, 669–687. [CrossRef]
275. Mehmood, K.; Hussain, S.; Sagheer, M. Mixed convection in alumina-water nanofluid filled lid driven square cavity with an isothermally heated square blockage inside with magnetic field effect. *Int. J. Heat Mass Transf.* **2017**, *109*, 397–409. [CrossRef]
276. Rashad, A.M.; Mansour, M.A.; Armaghani, T.; Chamkha, A.J. MHD mixed convection and entropy generation of nanofluid in a lid-driven U-shaped cavity with internal heat and partial slip. *Phys. Fluid.* **2019**, *31*, 042006. [CrossRef]
277. Roy, M.; Roy, S.; Basak, T. Role of various moving walls on energy transfer rates via heat flow visualization during mixed convection in square cavities. *Energy* **2015**, *82*, 1–22. [CrossRef]
278. Waheed, M.A. Mixed convective heat transfer in rectangular enclosures driven by a continuously moving horizontal plate. *Int. J. Heat Mass Transf.* **2009**, *52*, 5055–5063. [CrossRef]
279. ElSherbiny, S.M.; Raithby, G.D.; Hollands, K.G.T. Heat transfer by natural convection across vertical and inclined air layers. *J. Heat Transf. Trans. ASME* **1982**, *104*, 96–102. [CrossRef]
280. Lartigue, B.; Lorente, S.; Bourret, B. Multicellular natural convection in a high aspect ratio cavity: Experimental and numerical results. *Int. J. Heat Mass Transf.* **2000**, *43*, 3157–3170. [CrossRef]
281. Lee, Y.; Korpela, S.A. Multicellular natural convection in a vertical slot. *J. Fluid Mech.* **1983**, *126*, 91–121. [CrossRef]

282. Power, J.P. Finite Element Model of Turbulent Flow and Heat Transfer in a Fenestration System. Ph.D. Thesis, The University of Massachusetts Amherst, Amherst, MA, USA, 1999.
283. Wright, J.L.; Sullivan, H.F. A two-dimensional numerical model for natural convection in a vertical. rectangular window cavity. *ASHRAE Trans.* **1994**, *100*, 1193–1206.
284. Zhao, Y.; Goss, W.P.; Curcija, D. Prediction of the multicellular flow regime of natural convection in fenestration glazing cavities. *ASHRAE Trans.* **1997**, *10*, 1–12.
285. Baytas, A.C.; Pop, I. Free convection in a square porous cavity using a thermal non-equilibrium model. *Int. J. Therm. Sci.* **2002**, *41*, 861–870. [CrossRef]
286. Bejan, A. On the boundary layer regime in a vertical enclosure filled with a porous medium. *Lett. Heat Mass Transf.* **1979**, *6*, 93–102. [CrossRef]
287. Goyeau, B.; Songbe, J.P.; Gobin, D. Numerical study of double-diffusive natural convection in a porous cavity using the Darcy-Brinkman formulation. *Int. J. Heat Mass Transf.* **1996**, *39*, 1363–1378. [CrossRef]
288. Saeid, N.H.; Pop, I. Natural convection from a discrete heater in a square cavity filled with a porous medium. *J. Porous Media* **2005**, *8*, 55–63. [CrossRef]
289. Ho, C.J.; Liu, W.K.; Chang, Y.S.; Lin, C.C. Natural convection heat transfer of alumina-water nanofluid in vertical square enclosures: An experimental study. *Int. J. Therm. Sci.* **2010**, *49*, 1345–1353. [CrossRef]
290. Omri, M.; Jamal, M.; Hussain, S.; Kolsi, L.; Maatki, C. Conjugate natural convection of a hybrid nanofluid in a cavity filled with porous and non-newtonian layers: The impact of the power law index. *Mathematics* **2022**, *10*, 2044. [CrossRef]
291. Saghir, M.Z.; Ahadi, A.; Mohamad, A.; Srinivasan, S. Water aluminum oxide nanofluid benchmark model. *Int. J. Therm. Sci.* **2016**, *109*, 148–158. [CrossRef]
292. Sheremet, M.; Chinnasamy, S. Convective–radiative heat transfer in a cavity filled with a nanofluid under the effect of a nonuniformly heated plate. *Int. J. Numer. Method. Heat Fluid Flow* **2018**, *28*, 1392–1409. [CrossRef]
293. Shulepova, E.V.; Sheremet, M.A.; Oztop, H.F.; Abu-Hamdeh, N. Mixed convection of Al_2O_3–H_2O nanoliquid in a square chamber with complicated fin. *Int. J. Mech. Sci.* **2020**, *165*, 105192. [CrossRef]
294. Huilgol, R.R.; Kefayati, G.H.R. Natural convection problem in a Bingham fluid using the operator-splitting method. *J. Non Newton. Fluid Mech.* **2015**, *220*, 22–32. [CrossRef]
295. Kefayati, G.R. Mesoscopic simulation of magnetic field effect on natural convection of power-law fluids in a partially heated cavity. *Chem. Eng. Res. Des.* **2015**, *94*, 337–354. [CrossRef]
296. Khezzar, L.; Siginer, D.; Vinogradov, I. Natural convection of power law fluids in inclined cavities. *Int. J. Therm. Sci.* **2012**, *53*, 8–17. [CrossRef]
297. Kim, G.B.; Hyun, J.M.; Kwak, H.S. Transient buoyant convection of a power-law non-Newtonian fluid in an enclosure. *Int. J. Heat Mass Transf.* **2003**, *46*, 3605–3617.